Fall 2020

Modeling, Simulation, and Testing of Sweeping Convection

Amir Kiaee
Southern Methodist University, akiaee@smu.edu

MODELING, SIMULATION, AND TESTING OF

SWEEPING CONVECTION

Approved by

_____

Dr. José L. Lage

_____

Dr. Ali Beskok

_____

Dr. David Willis

_____

Dr. Usama El Shamy

_____

Dr. Silvio Junqueira

MODELING, SIMULATION, AND TESTING OF SWEEPING CONVECTION

A Dissertation Presented to the Graduate Faculty of

Lyle School of Engineering

Southern Methodist University

in

Partial Fulfillment of the Requirements

for the Degree of

Doctor of Philosophy

with a

Major in Mechanical Engineering

by

Amir Kiaee

(B.S., Amirkabir University of Technology, Iran, 2006)
(M.S., Amirkabir University of Technology, Iran, 2009)

December 19, 2020

ACKNOWLEDGMENTS

I would express my sincere gratitude to my honorable advisor, Prof. José Lage, for his continuous guidance, encouragement and precious advice throughout my research. His insights and suggestions contributed to the progress of my research from beginning to end.

Many thanks to Prof. Ali Beskok, Dr. David Willis, Dr. Usama El Shamy and Dr. Silvio Junqueira for their efforts and valuable comments as members of my Ph.D. advisory committee. It has been an honor for me to interact with them in such capacity. I am greatly thankful to all of my friends at SMU for their support. Last not by least, I am very grateful for the loving support of my beloved family. This work has been financially supported by NSF Grant No. CBET-1404017. Any opinions, findings, and conclusions or recommendations expressed in this material are those of the author and do not necessarily reflect the views of the National Science Foundation.

DEDICATION

I would like to dedicate my dissertation to the people from whom I have received the most support and love, my beloved wife (Parisa) and daughter (Doreen), my dearest father and my precious mother.

Kiaee, Amir B.S., Amirkabir University of Technology, Iran, 2006
M.S., Amirkabir University of Technology, Iran, 2009

Modeling, Simulation, and Testing of Sweeping Convection

Advisor: Professor Jose Lage

Doctor of Philosophy awarded: December 19, 2020
Dissertation completed: December 2, 2020

In this study, the new convection heat transfer concept of sweeping convection, using large particles flowing with a fluid in a channel, is considered. This novel concept is inspired by the gas exchange process in alveolar capillaries, where red blood cells (RBCs) flow with blood plasma, yielding very high gas transfer efficiency. An important characteristic of alveolar capillary blood flow, believed to be related to the high efficiency of the lungs, is the snug fitting of the RBCs into the capillaries. This tight fitting sets the RBCs (particles) acting like pistons as they flow downstream with the plasma (fluid), facilitating mass transfer by disrupting the velocity and concentration boundary layers that otherwise develop along the channel. The analogy between mass and heat transfer supports the expectation this effect would be presented also under heat convection. Hence, the sweeping of the boundary layers by solid particles, and the resulting increased mixing, is expected to yield higher convection heat transfer coefficients, as compared to the heat transfer coefficient achieved when a fluid clear of particles is flowing through a heated (or cooled) channel. Therefore, results of a computational and analytical investigation are presented here, followed by some experimental testing of sweeping heat convection.

The primary system considered here consists of a regular, straight channel through which a Newtonian liquid (water, with uniform and constant properties) flows with or without spherical solid particles (constant and uniform properties) immersed in it.

Simulations were performed for the fluid-particle flow beginning from a quiescent state (named "startup flow") through a heated channel, either with a constant and uniform surface temperature or with a constant and uniform surface heat flux condition. An additional group of simulations were performed considering the flow to begin from a fully developed clear fluid state in which particles were included starting to flow in the channel prior to the heated section. The simulations took place under the laminar flow regime ($27 < Re < 564$). Two Fluid Structure Interaction (FSI) methods were utilized to simulate the flowing of the particle with the fluid, namely: Moving Mesh and Immersed Solid. The numerical model and the corresponding CFD code were developed using ANSYS CFX software as basis. The results reveal the particle effect on the convection process to be localized and yet very significant, with the surface-averaged Nu number increasing by up to 60% at a specific time in the process and up to 35% when time averaged during the entire process; and with negligible pressure drop effect across the channel. A focused analysis of the flow at the gap between the moving particle and the channel surfaces yielded an analytical prediction of the fluid and particle velocities, which was validated by the numerical results. The results also show the three essential effects of the particle as it sweeps the fluid in the channel, namely: stretching the flow upstream (dragging additional cold fluid into the channel), compressing it downstream (pushing hot fluid out of the channel), and accelerating it through the gap (stronger surface convection). The somewhat unexpected result of high heat transfer coefficient with negligible pressure drop increase reinforces the expectation of sweeping convection being a very effective new convection mechanism with tremendous practical potential, particularly for its inherently low pressure drop penalty.

In the experimental effort of this work, a new particulate flow circulation system is introduced, not only to provide a tool to verify numerical simulation and analytical results but also to study the practical aspects of implementing sweeping convection in a convection heat transfer system. The novel experimental apparatus, designed as a flow loop, uses a vortex-based pumping effect created by an impeller to set the fluid (liquid) and particles in motion inside a container that then feeds the flow through a tube linked to a heated pipe for testing. The vortex-based pumping system performs very well, alleviating three major draw backs of fluid-particle flows, namely pumping without damaging the particles, and particle agglomeration (clogging) and settling in the flow system. For the heat transfer investigation, the testing tube section was fitted with a uniform surface heater and instrumented with several thermocouples for fluid and surface temperature monitoring. Two types of experimental procedures were then performed: (1) a Local Effect Study (LES), which focuses on a single or only a few particles circulating in the test section at a time; and, (2) the Overall Effect Study (OES), which investigates the effect of a large number of particles placed in the circulation system. Results from the LES procedure shows the same flow and heat transfer characteristics as observed in the numerical simulations, particularly the local channel surface temperature drop and recovery upon the passing of a particle. The OES procedure results indicated the average surface temperature of the locations near the outlet in particle flow to be significantly lower than the temperature achieved under clear flow for the same flow conditions. The results of the conducted experimental tests support qualitatively the findings of the numerical simulations, and provide venues for expanding this study.

KEY WORDS: Sweeping convection, Convective heat transfer, Particle flow

TABLE OF CONTENTS

LIST OF FIGURES

NOMENCLATURE

U_i	Velocity at the channel inlet (m/s)
U_{ave}	Average velocity in the channel (m/s)
t	Time (s)
L	Channel length (m)
H	Channel width (m)
$\dot{q}$	Heat transferred per unit time (W)
q”	Heat flux (W/m^2)
h	Convective heat transfer coefficient (W/m^2K)
C_P	Specific heat (J/kg ºC)
T_w	Channel surface temperature (K)
T_b	Bulk temperature (K)
Re	Reynold Number
Pr	Prandtl Number
T_∞	Surrounding temperature (K)
Nu	Nusselt number
HF	Average heat flux over the channel length (W/m^2)
k	Thermal conductivity of the fluid (W/m K)

Greek symbols

η_{Nu}	Heat transfer improvement based on Nusselt curves (%)
η_{HF}	Heat transfer improvement based on heat flux curves (%)
δ	Thickness of boundary layer (m)
ν	Kinematic viscosity (m^2/s)
α	Thermal diffusivity (m^2/s)

Chapter 1

INTRODUCTION

1.1. Motivation

Thermal engineers continuously look for ways to increase heat transfer in heat exchangers with minimum cost. There are several active and passive techniques one can pursue for achieving high heat transfer coefficient in channel flows, including the use of actuators, geometric changes, surface roughness and solid obstacles to induce mixing and disrupt the boundary layers that otherwise form along the channel. Actuators induce mixing by producing and sending vortices along the channel [1]. Geometric changes involve modifications in the shape of the channel, usually from straight (regular) to a more complicated form, also intended to cause mixing [2]. Increasing the roughness of the channel surfaces, or even attaching small obstacles along the internal surfaces of the channel, is another alternative to increase the heat transfer coefficient via better mixing [3]. All these methods have one thing in common: the action to improve the heat transfer is based on causing flow mixing, which leads to an undesired by-product, i.e., the increase in the pressure drop along the channel. The increase in pressure drop, in turn, yields the need for more energy to maintain the fluid flowing.

A more modern distinct alternative to obtain higher heat transfer efficiency is based on particulate flows, a class of multiphase (solid-fluid) flows with a very large number of very small particles, small in relation to the channel cross section dimensions, all disperse in the fluid medium forming a slurry. This alternative presents tremendous practical challenges, such as agglomeration of the solid particles, settling, and increased pressure drop (pumping power).

There is, however, one naturally occurring particulate flow that differs from the slurry flow and is observed in the flow of blood through alveolar capillaries, shown in figure 1.1. Observe the main characteristic of this flow is the dimension of the particles (the red cells) being similar to the channel cross-section dimension.

Fig. 1.1 Red blood cells flowing with plasma through a capillary with similar dimension [4]

Focusing on this main characteristic, consider the flow of a single solid particle in a fluid flowing through a channel, with the channel cross-section dimension being only slightly larger than the dimension of the particle. In this case, the particle would have a snug fit to the channel, and the flow can be split into two regions. The first would be the region upstream of the flowing particle, where the flowing particle would drag inlet fluid deep into the channel, "slowing down" the growth of the boundary layers along the channel surfaces. This is akin of having the boundary layers stretched along the channel surfaces. The second region is downstream of the particle, formed by the fluid being pushed forward by the particle, with the particle then essentially squeezing the boundary layers against the channel surfaces. Conceivably, the solid particle acts like a piston, sweeping along the channel surface, mixing ("breaking") the boundary layers, reducing the transport resistance (heat or mass transfer from the surfaces), and enhancing the convection process. These two effects combined, namely the stretching and the squeezing of the convection boundary layers, is what we term the sweeping flow effect.

Prior preliminary modelling and numerical simulations of a steady-periodic capillary system were performed [5], considering a square cross section channel mimicking an alveolar capillary, heated uniformly at the top and bottom surfaces, and filled with liquid water flowing with discrete, phase-change filled particles. Spherical particles with diameter slightly smaller than the channel diameter were chosen. A similar configuration was considered, [6-8], for studying only the flow of ice and water through a circular pipe in a train-like fashion.

1.2. Research Objectives

The overall objective of the present research is to study numerically and experimentally a specific type of convective heat transfer due to a particle flow in narrow circular channels where the diameter of the particles is very close to the channel diameter. This novel concept is inspired by the gas exchange process in alveolar capillaries, where red blood cells flow with blood plasma, yielding very high gas transfer efficiency. An important characteristic of alveolar capillary blood flow, believed to be related to the high efficiency of the lungs, is the snug fitting of the RBCs into the capillaries [9].

From a heat transfer point-of-view, the tight fitting between particles and the channel walls sets the particles acting like pistons as they flow downstream with the fluid, disrupting the velocity and temperature profiles that characterize the developed boundary layers in a heated straight, and long enough, channel. The sweeping of the boundary layers is expected to yield higher heat transfer coefficients, as compared to the heat transfer coefficient achieved in steady fully developed regime.

1.3. Content of dissertation

The dissertation contains 5 chapters. Chapter 1 includes introduction, motivation and objectives of the research. In chapter 2, some important concepts of fluid mechanics and heat transfer, which are used in this study, are briefly reviewed. This review includes: boundary layer theory, convective heat transfer, internal flow, fully developed flow, Nusselt number, particle flow and fluid-structure interaction. All numerical study and simulations are presented in chapter 3 in the form of separate case studies with the focus on heat transfer improvement achieved in particulate flow over the clear (of particles) flow under the same flow conditions. While the focus of this study was on numerical analysis,

an experimental setup was developed for two reasons, namely: to compare with the results from the numerical simulations and to test the engineering design practicality of the sweeping convection idea for circular tubes. Chapter 4 contains the experimental study, where the experimental design, set-up of the apparatus and the results are presented and discussed. Finally, some conclusions and future research are discussed in the last chapter of this dissertation, i.e. chapter 5.

Chapter 2

BRIEF REVIEW OF HEAT TRANSFER AND FLUID MECHANICS CONCEPTS

2.1. Introduction

This chapter contains a brief review of heat transfer and fluid mechanics concepts which are related to this study. In fact, the focus of this research is on a specific internal flow class with consideration to heat transfer. Furthermore, in most cases considered in the current study, the flow is two-phase due to the presence of solid particles in conjunction with the fluid. The study of the interaction between solid particles and the fluid flowing together through a channel requires the use of an advanced concept in fluid mechanics termed Fluid-Structure Interaction (FSI). The concepts briefly reviewed here include: boundary layer theory, convective heat transfer, Newton's law of cooling, internal flow, flow entrance region, fully developed flow region, heat transfer in fully developed flow, Nusselt number, particle flow, and FSI.

2.2. Boundary layer theory

The fundamental concept of the momentum boundary layer was suggested by Ludwig Prandtl, in 1904, at the International Mathematical Congress in Heidelberg, through a lecture entitled “On fluid flow with very little friction” [10]. He explained that

the viscosity of a fluid plays a role in a thin layer adjacent to the surface, which he called "boundary layer" [11]. A momentum boundary layer is an imaginary layer of viscous fluid, close to a solid surface in contact with a stream moving in relation to the surface, in which the flow speed tangent to the surface varies from the wall speed (i.e., zero, if the wall is stationary), where the flow sticks to the wall because of its viscosity, up to a certain speed u_0 which corresponds to the free stream velocity measured far from the surface. The determination of the momentum boundary layer thickness δ is somewhat arbitrary because the speed evolution from the value at the surface to the free stream value is asymptotic.

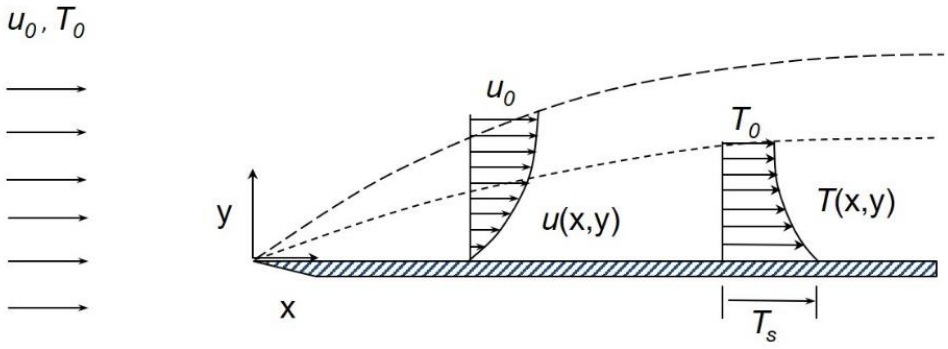

Fig. 2.1 Schematic drawing depicting heated fluid flow over a flat plate [12]

The thermal boundary layer formed in a fluid moving along a surface at a different temperature is similar, in several ways, to the description of the momentum boundary layer introduced by Prandtl. The temperature of the fluid also gradually changes from the temperature at the solid surface to the free stream temperature. Similarly to the momentum boundary layer, the definition of a precise location at which the fluid temperature becomes the free stream temperature is also somewhat arbitrary as the evolution from the surface is asymptotic. Nevertheless, these two layers can have a well-defined characteristic thickness. Figure 2.1. depicts the two boundary layers along a heated flat plate, for a fluid with Prandtl

number greater than unity. A thermal and a momentum boundary layer are formed as the fluid moves along the plate. Boundary layers in internal flows will be discussed later in this chapter.

2.3. Convective heat transfer

Convective heat transfer, or simply convection, is the transfer of heat across a solid-fluid interface when the fluid and solid have relative speeds and different temperatures. Convection is usually the dominant form of heat transfer when liquids and gases are involved. Although often discussed as a distinct method of heat transfer, convective heat transfer involves the combined processes of conduction (i.e., heat diffusion) and advection (i.e., thermal energy transferred by bulk fluid flow). Convection is classified as natural and forced depending on how the fluid motion is initiated and maintained. In natural convection, any fluid motion is caused by natural means such as the buoyancy effect (i.e. the rise of a fluid warmer and lighter, or the fall of a fluid cooler and heavier than the surrounding fluid). Whereas in forced convection the fluid is forced to flow over a surface or in a tube by external means such as a pump or a fan. The bulk fluid temperature, which is a fluid-speed weighted cross-section average fluid temperature, is not only a convenient reference for evaluating properties related to convective heat transfer, but also represents the thermodynamics temperature at the cross-section, being useful in internal flows, particularly in pipes and ducts [13].

Another convection classification can be made depending on the smoothness and undulations of the solid surfaces bounding the flow. Wavy irregular surfaces are commonly encountered in heat transfer devices, which include solar collectors, regenerative heat exchangers and underground energy storage systems. These surfaces

play a significant role in the heat transfer processes in these devices, adding a geometric complexity due to their undulations. Hence, the convection along these surfaces behave differently from the convection along straight surfaces [14], requiring elegant mathematical simplification techniques to be tackled analytically.

2.4. Newton's law of cooling

Based on Newton's cooling law the rate of convective heat flux to/from a moving body is proportional to the difference in temperatures between the body and its surroundings [14]. The constant of proportionality is called the heat transfer coefficient. This law is applicable when the coefficient (h) is independent, or relatively independent, of the temperature difference between the body and the surrounding. This law is usually written as:

$$\dot{q} = hA(T - T_{\infty}) \tag{2.1}$$

where $\dot{q}$ is the heat transferred per unit time across the body-fluid interface of area A (the area of the body through which heat is transferred), h is the heat transfer coefficient, T is the body's surface temperature and T_{∞} is the surrounding temperature – i.e., fluid temperature measured far away from the solid. The convective heat transfer coefficient is usually dependent upon the physical properties of the fluid and the physical configuration (e.g., geometry, flow type).

2.5. Internal flow

An internal flow is a flow configuration where the flowing substance is guided in the periphery of its flow direction by solid surfaces. This configuration represents a convenient geometry for heating and cooling fluids used in chemical processing,

environmental control, and energy conversion technologies, for instance. Streams that flow through ducts are primary examples of internal flows. This class of fluid flow and convection phenomena distinguishes itself from the class of an external flow convection phenomena where the fluid flow can be considered as having its direction bounded only partially by solid surfaces (e.g., when a solid object is surrounded by the flow).

There are two basic questions in the design of an internal flow configuration. The first question is the friction between the moving fluid (stream) and the solid surfaces, and the second is the heat transfer rate, or the thermal resistance between the stream and the surfaces [15]. The fluid friction part of the problem leads to the calculation of the pressure drop experienced by the stream over a finite length in the flow direction. This calculation is essential in practice for the determination of the flow energy requirement, such as pump power needed to maintain the flow. The heat transfer question is usually supplementary, as the internal flow will transfer energy if a temperature difference exits between the fluid and the surrounding surfaces. To calculate the heat transfer rate and the temperature distribution through the fluid in forced convection, one must know the flow velocity distribution. When the variation of temperature over the flow field is sufficiently weak, the fluid density and viscosity are adequately considered as independent of temperature. In this case, the calculation of the velocity field and pressure drop become independent of the fluid temperature field and heat transfer. This is the case in all the configurations and results in this dissertation.

2.6. Flow entrance region

The flow development in a parallel plates channel is shown, for a Newtonian fluid, in figure 2.2. Beyond the entrance (inlet) region, the viscosity effect extends over the entire cross section and the flow is said to be fully developed.

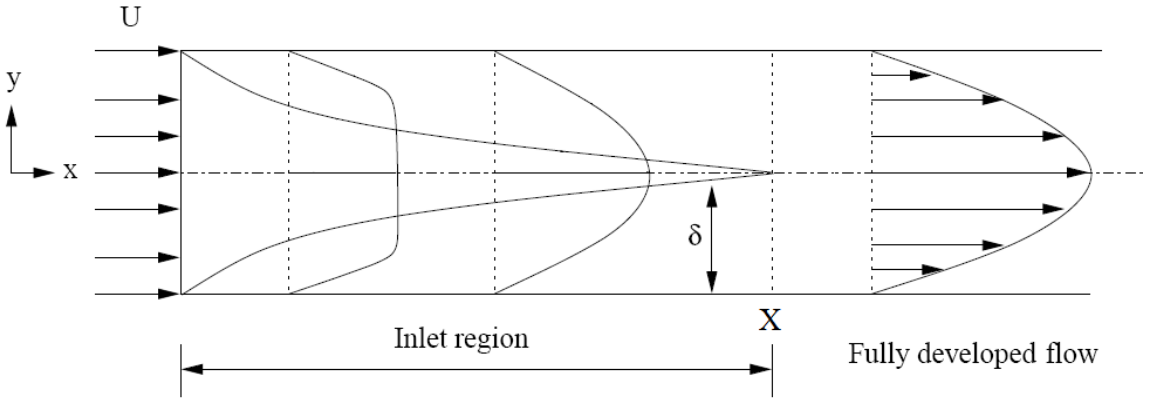

Fig. 2.2 Flow development in a parallel plate channel

The flow velocity in the inlet cross section (i.e. $x = 0$) is assumed uniform (U). Mass conservation means that U is also the mean velocity at any position x downstream of the inlet. The momentum boundary layers grow along the channel surfaces until they meet at the distance X downstream from the entrance. The length X is called hydrodynamic entrance length, indicated in figure 2.2. In the entrance length region, the boundary layers coexist with a core in which the velocity is uniform (U_c). Mass conservation and the fact that the fluid slows down in the boundary layers requires that U_c grow bigger than U as the fluid moves downstream. The length X divides the duct flow into an entrance region ($0 < x \leq X$) and a fully developed flow region ($x \geq X$) [16]. The flow friction and heat transfer characteristics of the entrance region are similar to those of unbounded boundary layer

flows. Observe that X is not a precise measure, for the same reason the thickness of a boundary layer (δ) is difficult to precise.

2.7. Fully developed flow region

Considering figure 2.2, the key feature of the flow in the region downstream of $x \sim X$ is that the horizontal component of the velocity (u), does not change in the x direction anymore. Due to continuity, the variation of the transverse velocity component with y must equal zero, and since this velocity is zero at the solid (impermeable) surfaces it follows the transverse speed must be zero everywhere in the cross section. This feature is a consequence of the geometric constraint beyond X where the boundary layers cannot continue to grow. Another consequence of the full development of the flow is that the pressure is uniform in each constant-x cross section (i.e., $\partial P/\partial y = 0$). This feature is derived by substituting the transverse velocity component $v = 0$ into the momentum equation for the y direction.

2.8. Heat transfer in fully developed flow

By analogy with the developing velocity profile described in connection with figure 2.2, there is a thermal entrance region of length X_T. In this region the thermal boundary layers grow causing changes in the distribution of temperature over the duct cross section. Downstream from $x \sim X_T$ the thermal boundary layers merge and the shape of the temperature profile across the duct either no longer varies, for the case of surfaces with uniform heat flow, or it changes continuously until the fluid reaches the temperature of the surfaces, for the case of isothermal surfaces.

In heat transfer, the bulk temperature, known as mean temperature, is related to the bundle of mini-streams of enthalpy that make up the bulk enthalpy stream. The definition

of T_m involves a u-weighted average of the temperature distribution over the flow cross section. In internal convection, the heat transfer coefficient ($h = q''/\Delta T$) is based on the difference between the surface temperature (T_0) and the mean temperature T_m. In the fully developed region of a duct flow with uniform and constant wall heat flux, T_w and T_m would change linearly along the channel and at the same rate. Hence, temperatures T_w and T_m would show as two straight and parallel lines in a temperature versus location graph [15]. This fact is very useful for the validation of numerical simulation results.

2.9. Nusselt number

In heat transfer, the Nusselt number (*Nu*) can be considered, in scaling sense, as the ratio of convective to conductive heat transfer, such as along a surface-fluid interface where the two heat flows are perpendicular to the interface. Observe at the interface the conductive heat equals the heat convection because of the nonslip condition. Named after Wilhelm Nusselt, the Nusselt number is a dimensionless number. A similar non-dimensional parameter is the Biot number, with the difference that the conduction heat is considered at the solid surface side of the interface, and not the fluid side.

The Nusselt number is important because it contains the heat transfer coefficient information. Indeed, one interpretation of Nusselt number is simply that of a dimensionless heat transfer coefficient. Mathematically Nu is defined as:

$$Nu = \frac{hL}{k} \sim \frac{Convective \text{ heat transfer}}{\text{Conductive heat transfer}} \tag{2.2}$$

where h is the convective heat transfer coefficient of the flow, L is a characteristic length and k is the thermal conductivity of the fluid. Selection of the characteristic length should be in the direction of growth (or thickness) of the boundary layer for channel flow. For

complex shapes, the characteristic length may be defined as the volume of the fluid body divided by the surface area. The thermal conductivity of the fluid is typically evaluated at the film temperature, which for engineering purposes may be calculated as the mean-average of the bulk fluid temperature and surface temperature [17].

2.10. Particle flow

In classical thermodynamics, a phase is defined as a gas, a liquid, or a solid. Multiphase flow is the simultaneous flow of more than one phase. Particle flow refers to a class of two-phase fluid flow, in which one of the phases (the fluid) is continuously connected and referred to as the continuous or carrier phase, and the other phase is made up of small and typically dilute particles referred to as the dispersed or particle phase. Fine aerosol particles in air is an example of a particle flow, with the aerosols being the dispersed phase and the air being the carrier phase. Other examples include fluidized beds in chemical reactions, fuel-injection system in internal combustion engines and blood flow in mammals.

The modeling of two-phase flows has a tremendous variety of engineering and scientific applications: pollution dispersion in the atmosphere, fluidization in combustion processes, and aerosol deposition in spray medication, along with many others. The presence of a second phase in the flow can affect the transport of other entities by the flow (e.g., momentum and energy), enhancing or hindering the transport. The use of small size particles, in relation to the flow channel dimensions, in large quantities forms a slurry, which, when flowing, yields another example of a two-phase flow. Slurries were considered a potential alternative for enhancing convection heat transfer, except by one

important disadvantage as they require a high pump-power to circulate through a flow system.

Understanding the motion of particles in narrow channels has become more important with the recent advent of microfluidic devices used for many cell-based assays. This problem has its roots in the related problem of the motion of a particle near a single wall [18]. A number of fundamental experimental and numerical studies on particle dynamics in channels with parallel planar walls particles have been published [19-22].

2.11. Fluid-structure interaction

Fluid-structure interaction (FSI) is a multi-physics coupling between the laws that describe fluid dynamics and structural mechanics. The phenomenon resulting from fluid and structure interactions is characterized by a deformable or moving structure and a surrounding or internal fluid flow. When a fluid encounters a solid structure along the flow, the fluid exerts stresses causing strains on the solid that lead to deformations. These deformations can be quite large or very small, depending on the pressure and velocity of the flow and the material properties of the fluid and structure [23].

FSI can be broadly categorized as one-way or two-way coupled. In one-way FSI, the deformations of the structure are quite small and the variations in time are also relatively slow, so the fluid behavior will not be greatly affected by the structure deformation, and only the resultant stresses in the solid needs to be considered. A pipe carrying hot flow is an example of this category. In this case, significant thermal stresses in the solid are induced by thermal gradients in the flow field. However, since the resulting deformation of the solid is small, the flow field is not greatly affected by it. This allows fluid numerical simulations (via CFD) and solid numerical simulations (via FEA) to be run

independently, with loads transferred in only one direction, i.e., from the fluid to the structure. Another example is non-deformable particles flowing with a fluid. For being non-deformable, the particles do not affect the fluid through their deformation. Keep in mind the presence of the solid phase affects the flow field, even when the solid deformation does not.

On the other hand, in two-way FSI the deformations of the structure are large, the velocity and pressure fields of the fluid are then affected as a result, and the problem needs to be treated as a bidirectionally coupled multi-physics analysis, where the fluid flow and pressure fields affect the structural deformations, and the structural deformations then affect the flow and pressure fields. Industrial examples of such flows include aerodynamic flutter of wings, buffeting of car hoods, transient wind loads on buildings and bridges, and biomedical flows involving compliant blood vessels and valves. In two-way FSI, both Structural and Fluid solvers must be run with loads transferred between them [24].

In the modeling and numerical efforts presented in the following chapter, the one-way FSI is used primarily because the solid deformation is very small under the conditions investigated.

Chapter 3

NUMERICAL SIMULATION

3.1. Introduction

The numerical simulations conducted in this project are detailed in this chapter. The numerical model and the corresponding CFD code were developed using ANSYS CFX software as basis. The strategy behind the numerical simulation part of this research was to begin with the simplest configuration possible, develop the corresponding numerical model, overcome programming difficulties and obtain reliable simulations to then pursue more complicated configurations. This strategy helped to progressively build a better understanding of the physical problem by increasing the level of detailed information obtained through the simulations, particularly on velocity and temperature fields. The increased complexity resulting from the more complicated configurations was dealt with progressively toward achieving a working numerical model in line with the desire to obtain a good balance between mimicking practical configurations and obtaining accurate results with reasonable numerical effort.

Consequently, each advanced configuration study was developed considering the results from prior configuration studies, by adding new features and/or removing simplifying assumptions from it. With one exception, all models discussed here are dimensional and the dimensions used in the models follow reasonable actual dimensions one would expect in practice. This choice was made to expedite the verification of the numerical results against existing physical expectation. The exception is a nondimensional model done to validate the simulation results against some available analytical solutions.

The first model considered here is for the configuration of a single non-deformable, neutrally buoyant and adiabatic particle moving along a straight isothermal channel. A moving mesh method, together with a one-way FSI approach, was used for this model. As mentioned previously, additional configurations were developed based on the results from the first configurations, considering several parameters, including inlet flow velocity, particle size, channel surface heating condition (isoflux vs isothermal), and number of particles. In all cases the focus was on the heat transfer achieved by the particulate flow as compared to the heat transfer obtained with the clear (of particle) flow under the same flow conditions. The topics discussed in this chapter evolve as follows:

- Start-up sweeping convection effects of a single particle in a straight isothermal channel with uniform inlet velocity condition
- Start-up sweeping convection effects of a single particle in a straight isoflux channel with fully developed inlet velocity condition
- Sweeping convection effects of two particles in a straight isothermal channel with fully developed inlet velocity condition and the effects of varying the distance between particles

- A model with partially heated channel and initialization based on steady state results
- Velocity profile in particle flow
- Non-dimensional study of the sweeping convection

3.2. Start-up sweeping convection effects of a single particle in straight isothermal channels with uniform inlet velocity condition

Results of a preliminary numerical study are presented in this section, considering the transient start-up flow of an originally quiescent liquid (water) and a solid (impermeable), neutrally buoyant, adiabatic spherical particle through a straight channel. The surfaces of the channel are heated isothermally and maintained at a temperature different from the initial and inlet flowing fluid and particle temperatures. Particles with distinct diameters are tested as to determine their effects on the sweeping of the thermal boundary layer that forms along the channel surfaces as the fluid and particle flow downstream. Flow speed is also varied for each particle diameter as to check the diffusion-convection competing effect within the channel. The particles are considered adiabatic in the present case, allowing the isolation of the sweeping heat transfer effect from the particle heat capacity effect. The results quantify the convection effects of a single particle flowing with the fluid through direct comparison with the results obtained for the clear (of particles) fluid flow case. Some important results are observed, such as the small effect of the particle when the particle diameter is small in comparison to the channel size, even though the particle moves at a higher speed (because more of it is located at the center of the channel, where the fluid speed is greater) than when the particle diameter is larger. This observation is at the core of the fundamental sweeping effect caused by the particle.

3.2.1. Problem description and modeling

The basic configuration, figure 3.1, is a straight, finite length channel filled with an isothermal stationary fluid and a solid, neutrally buoyant, adiabatic particle centered in it, positioned near the inlet. At a certain time, the surfaces of the channel are set at a temperature higher than the fluid and particle initial temperatures, and the fluid (and particle) are set to move by imposing a constant and uniform fluid speed at the channel inlet. Numerical simulation results for the transient convection process that follows are obtained by solving the balance equations for the fluid and solid particle, with coupling conditions at their interfaces. The basic continuity, momentum and energy equations for a Newtonian fluid with constant and uniform properties are:

$$\nabla . \mathbf{u} = 0 \tag{3.1}$$

$$\frac{\partial \mathbf{u}}{\partial t} + (\mathbf{u} . \nabla)\, \mathbf{u} = -\frac{1}{\rho}\nabla P + \nu \nabla^2 \mathbf{u} \tag{3.2}$$

$$\frac{\partial \mathrm{T}}{\partial t} + (\mathbf{u} . \nabla)\, \mathrm{T} = \alpha \nabla^2 \mathrm{T} \tag{3.3}$$

The momentum balance equation for the solid particle, assumed neutrally buoyant rigid and non-deformable, is the Newton second law, $\boldsymbol{F}=m\mathbf{a}$, where F is the force imposed by the flowing liquid. The momentum equations for fluid and particle are solved using the simplified one-way FSI procedure in which fluid forces are external load to the particle while no particle force is feed backed to the fluid.

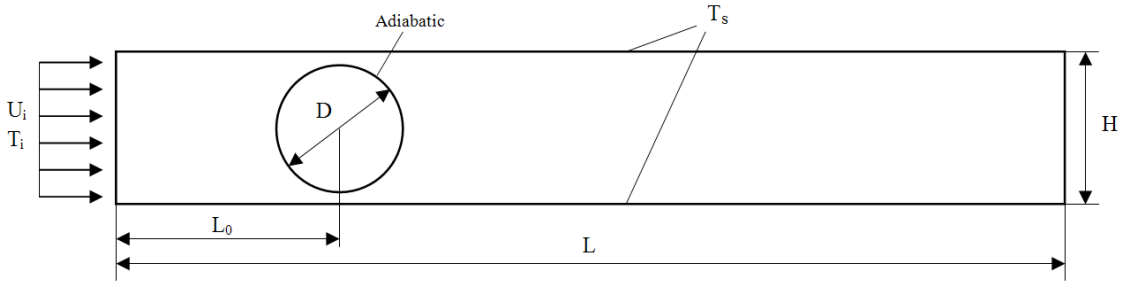

Fig. 3.1 Schematic view of the test channel with isothermally heated top and bottom surfaces cooled by flowing fluid having a discrete spherical solid particle flowing with it

In this initial configuration, numerical results are presented for a total channel length L = 200 mm, initial particle distance from inlet L_0 = 12 mm, channel height H = 4.8 mm, and several inlet fluid speeds, namely U_i = 2.5, 5, 10, 17, and 26 mm/s. The inlet and initial temperature conditions for the fluid and particle is T_i = 300 K. Considering water as the flowing fluid, the corresponding range of Reynolds number, defined in respect to the channel height H and inlet speed U_i, and Prandtl number would be $27 \leq Re \leq 280$, and Pr = 6.13, respectively. The Re range was chosen as to provide a relatively (in respect to the channel length) short developing length for the flow, in which case the sweeping effect of the particle is more likely to affect the convection process. At the channel outlet, the static pressure is set as P = 0 while the thermal boundary condition is set as zero gradient condition ($\partial T/\partial x = 0$). The channel surface temperature at time zero of the simulation is T_w = 340 K (constant and uniform surface temperature). Finally, simulations for two distinct particle diameters are reported, namely for D = 4 and 2 mm. Observe the large diameter allows for only 0.4 mm gap spacing between the surface of the centered particle and the channel surfaces.

3.2.2. Results

Results for the large and small particle cases with inlet speed 26 mm/s (Re = 280) are shown in figure 3.2. From top to bottom the figure shows the time evolution of the convection effect. The effect of the large particle as it sweeps the boundary layer is clearly seen when compared to the small particle and the clear (no particle) fluid cases. Also interesting is the imperceptible effect of the small particle on the convection process, contrasting with the observable effects of the large particle results, namely the clear accumulation of warm fluid downstream of the particle as time goes by, and the pulling (dragging) of cold inlet fluid further into the channel. Observe also how the small particle flows further downstream of the channel than the large particle at the same time increment. This is because, as both particles are centered in the channel, the small particle moves faster for being surrounded by fluid moving at faster speed, on average, than the large particle.

The speed of a particle flowing with the fluid in the channel can be calculated using the position versus time plot. An example is shown in figure 3.3, where the position of both large and small particles in the channel is plotted versus time. Observe in both cases U_i = 0.026 m/s. The observed linear relations between position and time suggest the terminal constant speeds for both, large and small particles, have been achieved. The slopes indicate the large and small particle speeds to be 0.029 m/s and 0.0358 m/s, respectively. For the large particle, the analytical prediction presented previously yields a particle speed of 0.028 m/s, which compares very well again with the numerical results. It worth recalling in fully developed flow between parallel plates, maximum velocity occurs at the center of the channel and is equal to 1.5 U_i. In figure 3.2, with average speed U_i =

0.026 m/s, U_{max} = 0.039 m/s. Observe the smaller particle has a speed close to the maximum velocity, as expected.

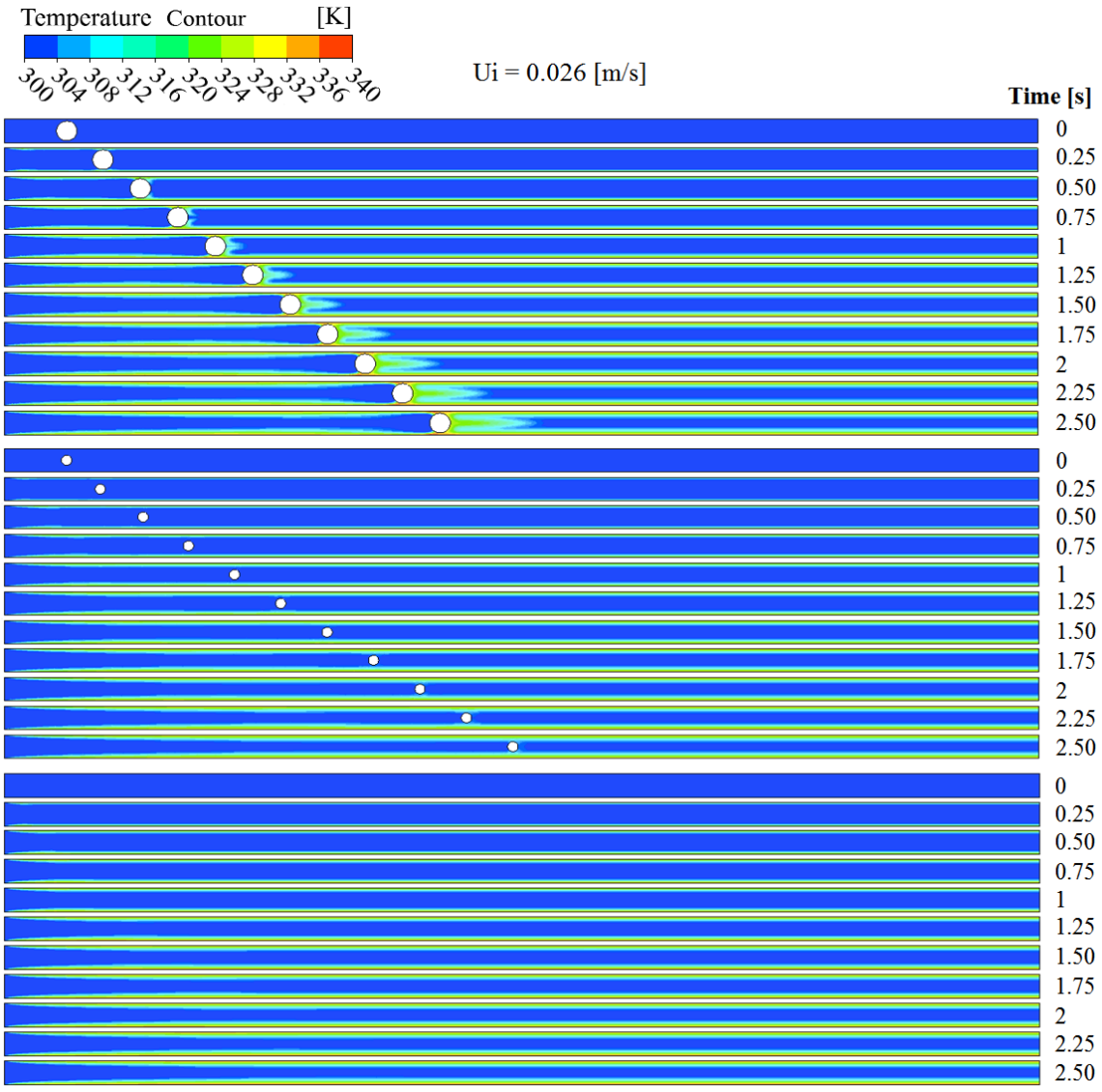

Fig. 3.2 Time evolution of convection by fluid with large particle (top), fluid with small particle (middle) and a clear fluid (bottom), from start-up with inlet velocity of 26 mm/s

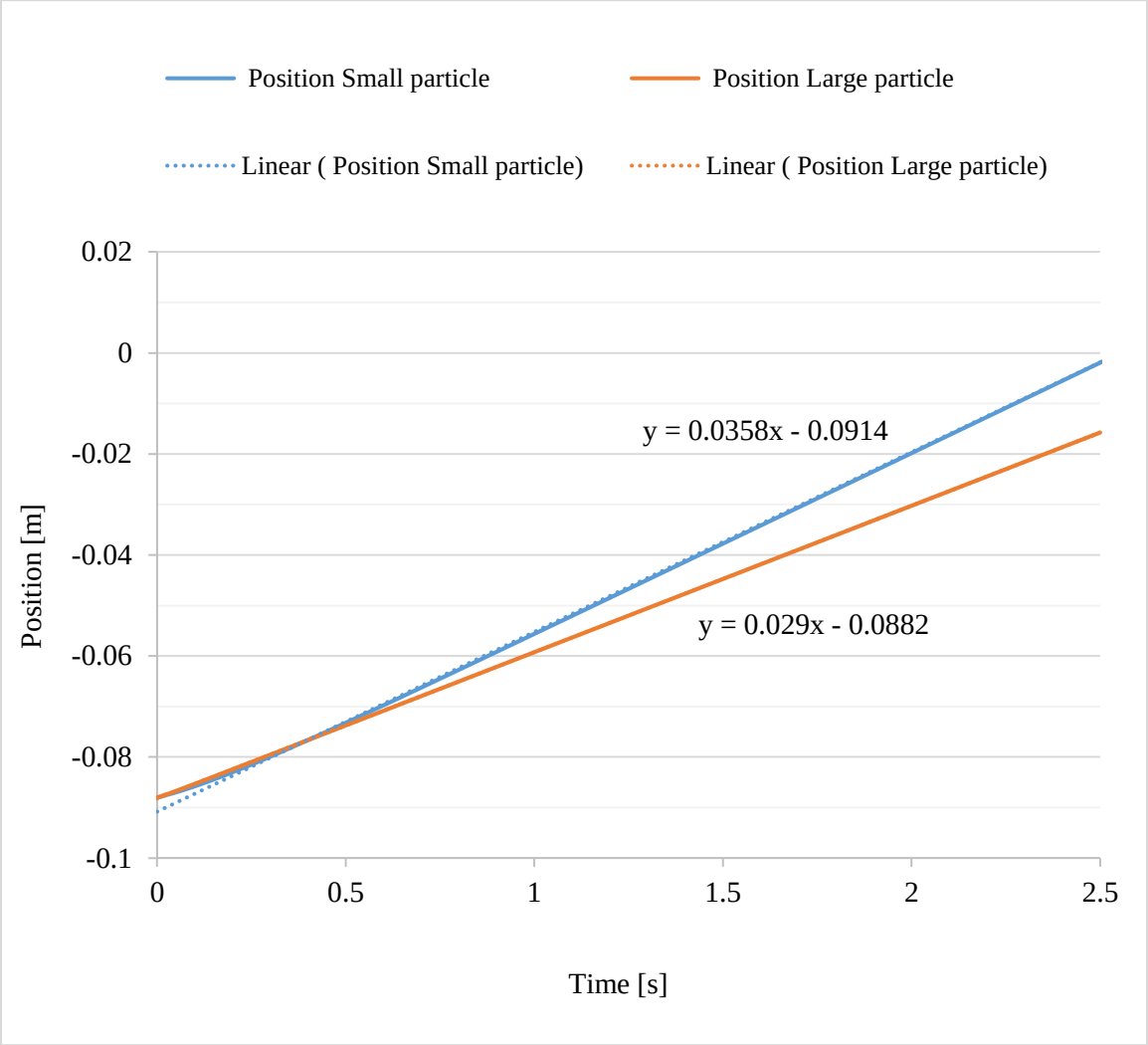

Fig. 3.3 Position of small and large particles versus time with inlet velocity of 26 mm/s

Figure 3.4 shows Results for the large and small particle cases with inlet speed 2.5 mm/s (Re = 27). The average temperature of the fluid in the channel is higher in this case, than the temperature observed in the flow shown in figure 3.2, because the flow rate is smaller, as expected. The boundary sweeping effect of the large particle can be observed considering also the accumulation of warmer fluid in front of the particle as the particle flows downstream.

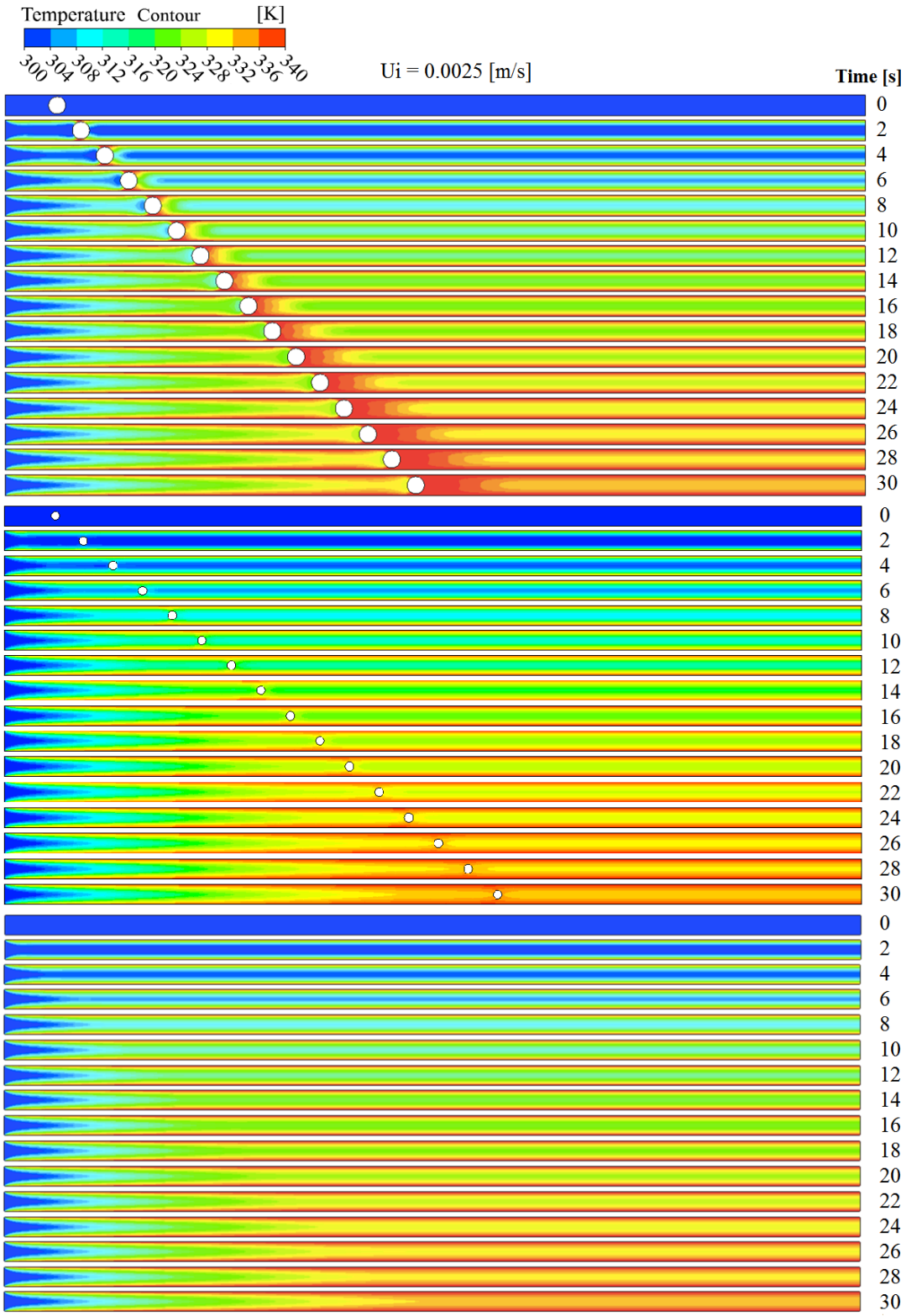

Fig. 3.4 Time evolution of convection by a fluid and large particle (top), small particle (middle) and clear fluid (bottom), from start-up with inlet velocity of 2.5 mm/s

Figure 3.5 compares temperature contours of three similar cases (same particles) at the same location along the channel with flows having different inlet velocities, from low (top) to high (bottom). Of course, for each case the resulting flow and heat transfer was captured at a specific time so that all three have the particle at the same position in the channel. The top channel result, for the case of smallest inlet flow speed, shows the shortest developing length of all three cases, with the fluid immediately downstream of the particle already reaching the channel surface temperature within the entire channel cross section. This is due to the thick thermal boundary layer, developed at low flow rate, which is swept by the flowing particle.

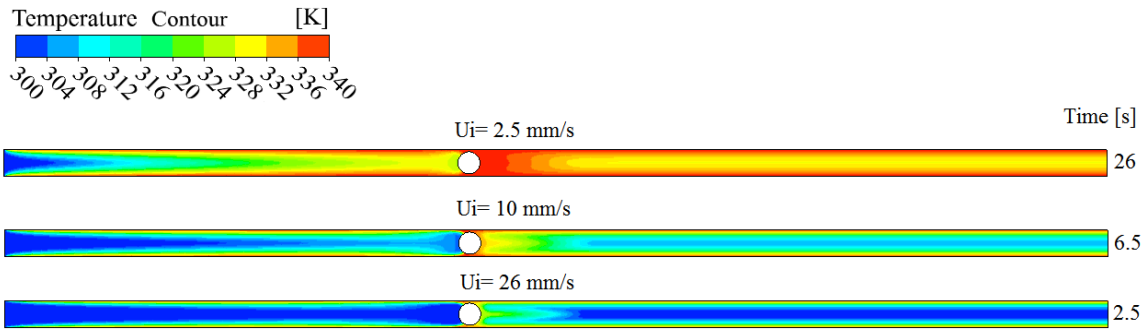

Fig. 3.5 Temperature contours for cases with different velocities captured for the same particle location

Notice also for the low speed case the fluid isotherms downstream of the particle have a concave pattern with higher temperature near the surface. This would yield a hindered heat transfer process at the channel surface in this region. As the inlet speed increases (from top to bottom channels in figure 3.5), however, the isotherms concavity switches to a convex pattern, with the warm fluid pushed toward the center of the channel. The cooler fluid then near the channel surface would lead to a higher convection heat transfer there.

At the upstream (left side) of the particle, no matter how high the inlet velocity is, there is always a relatively low temperature fluid bulk trailing the particle, which causes lower mean temperature and increases the heat transfer from the channel surfaces. Hence, the presence of the particle causes two different effects on the two sides of it: downstream of the particle the concentration of warm fluid may increase or decrease heat transfer (depending on temperature profile – concavity); and, upstream of the particle the dragged cold fluid should always increase locally the convection heat transfer from the channel surfaces. The overall improvement depends on these two effects.

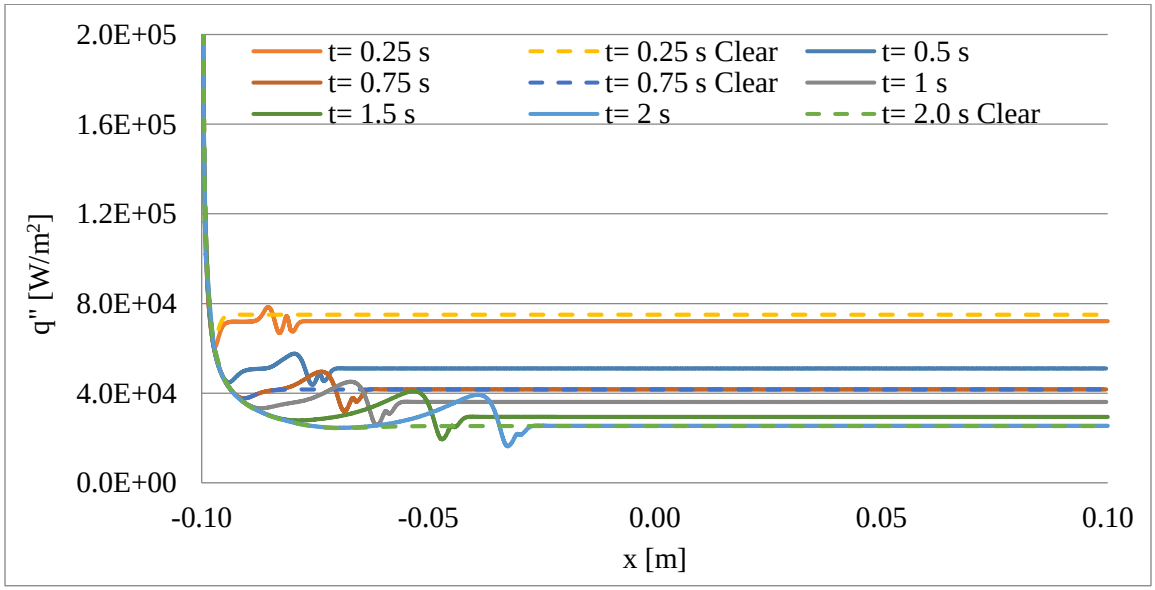

Fig. 3.6 Variation of heat flux along the channel for clear fluid (no particle, dashed lines) and particle (continuous lines) cases, with large particle and inlet speed of 26 mm/s

The results presented so far clearly indicate the heat transfer improvement by the particle sweeping effect depends on particle size and flow velocity. The results of figures 3.2 and 3.4 anticipate a very small flow and heat transfer effect when using particles with small diameter (relative to the channel size); hence the focus now turns to the large particle

case. The local, instantaneous effect of the flowing particle is better identified in figure 3.6, where the calculated heat flux flowing from the channel surfaces to the fluid are plotted along the channel surface at 6 different times for the large particle with inlet fluid speed of 26 mm/s. Notice the dashed lines show the resulting heat flux for the clear fluid case, for reference. The wall heat transfer is computed using the heat flux formulation of Fourier's law of heat conduction ($q" = -\mathrm{k}\frac{\partial \mathrm{T}}{\partial \mathrm{y}}$).

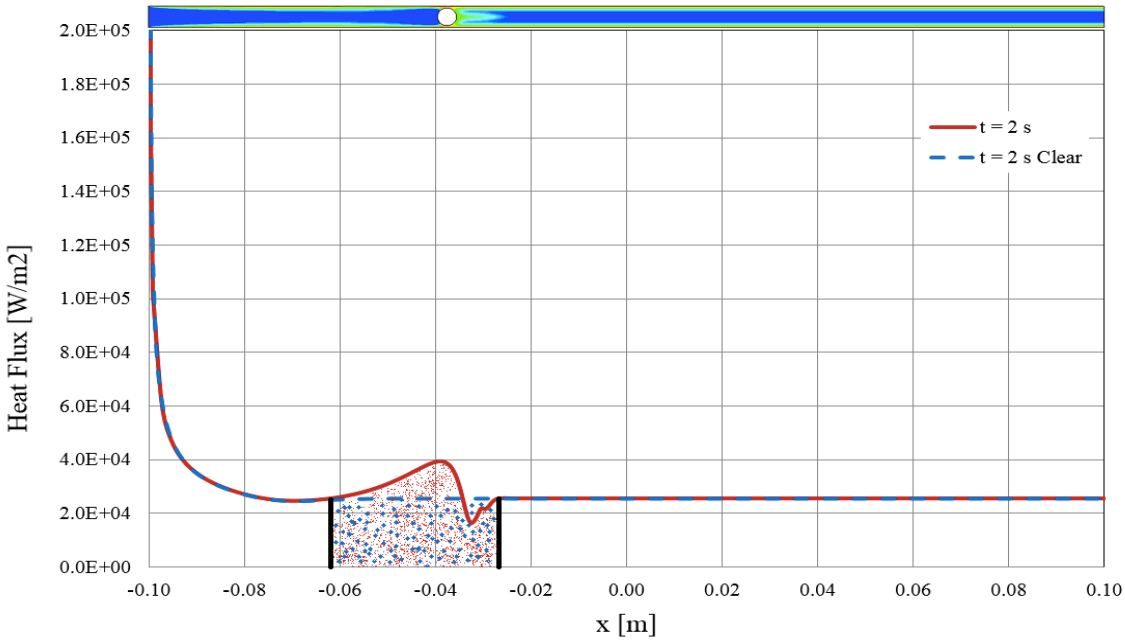

Fig. 3.7 Local difference between heat flux along the channel for clear fluid and particle cases at time 2 s, with large particle and inlet speed of 26 mm/s

Interestingly, the particle effect is constrained within a region 1-2 particle diameter downstream of the particle and about 8-10 particle diameters upstream of it. Obviously, this region of influence around the particle increases during the particle flow. The overall particle effect on the heat transfer process is quantitatively determined by integrating the heat flux curve along the entire channel. The difference in the total energy transfer

between the clear fluid and the particle cases is the shaded areas shown under each curve in figure 3.7 (notice the heat fluxes match precisely everywhere else within the channel) limited by the two solid vertical lines included in the figure for clarity. Figure 3.7 shows the local difference between heat flux along the channel for clear fluid and particle cases at time 2 s, with large particle and inlet speed of 26 mm/s. The average of these curves for the regions without overlapping can be calculated using numerical integration. Let HF_P and HF_C be the averaging results for the fluid with particle and the clear fluid cases respectively. A quantitative comparison of the single particle case is done using a figure-of-merit parameter defined as η_{HF}, for heat flux, in relation of the clear fluid case, defined as:

$$\eta_{HF} = \frac{HF_P - HF_C}{HF_C} \times 100 \tag{3.4}$$

where η_{HF} is the percent variation of HF_P and HF_C, varying in time as shown in the top graph of figure 3.8. For higher inlet velocities, the curves presented in the bottom graph of figure 3.8 clearly show very large and increasing enhancing effect on the convection heat transfer by the presence of the particle. Keep in mind in the bottom chart the horizontal axis has been changed from *time* to a *scaled time* using a factor of $U_i/(U_{max})$ to better compare cases with different inlet velocities on the same plot. It can be observed in the case with the lowest speed of 2.5 mm/s (Re = 27), there is no improvement in heat transfer due to collection of warm fluid with temperature almost as same as surface temperature, in front of the particle which reduces heat transfer downstream of it. This suggests for a certain channel width, gap size and thermal conditions, there should be a minimum inlet velocity for particle flow to yield a heat transfer improvement. In the present case this inlet

speed seems to be around 10 mm/s. A general pattern for all cases is for η_{HF} to increase to a maximum value and then decrease with a slower rate through the time. With higher inlet speed, the efficiency curves have higher peaks and the peaks tend to occur in later scaled times, as one would expect.

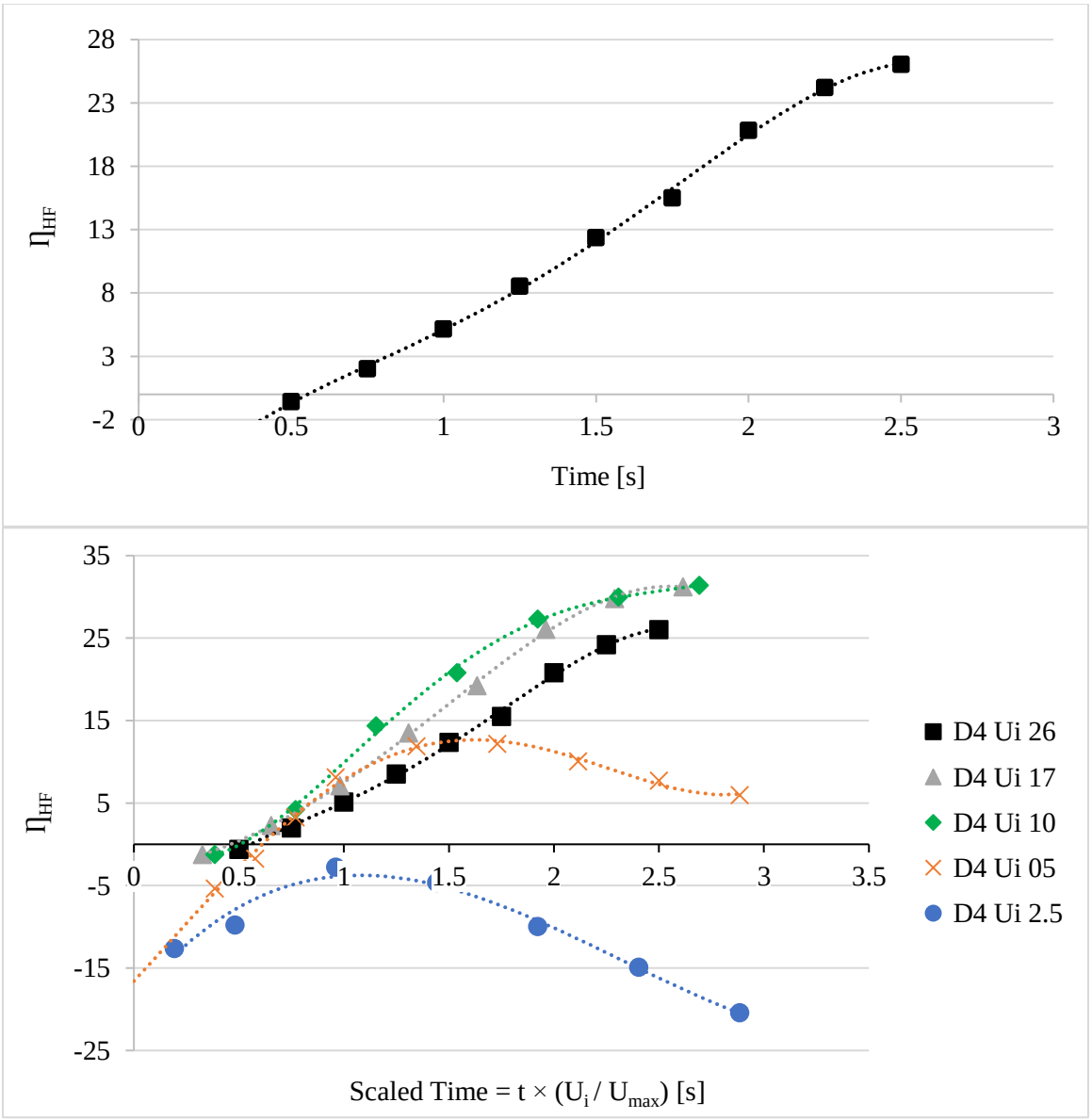

Fig. 3.8 Time variation of percentage heat flux difference between the particle and clear fluid cases for large particle (D = 4 mm) and inlet speed U_i = 26 mm/s (top), and comparison between cases with different inlet velocities using a scaled time (bottom)

3.2.3. Summary and conclusions

Results are obtained via numerical simulations of flow of water along a straight isothermal channel with and without a single solid, adiabatic, neutrally buoyant particle flowing with the fluid. Different fluid speeds and two particle diameters are considered. The results indicate a strong effect on the convection heat transfer process when the particle is present, with enhanced heat transfer upstream the particle location and hindering heat transfer downstream of the particle location as compared to the result obtained for the clear fluid case. Although the effect is limited to a flow region around the particle, it is nevertheless substantial, particularly for the case of large diameter particle. The results confirm the existence of the sweeping convection effect by flowing solid particles with large dimension during the start-up of a convection process.

The results from this initial study provide several valuable insights about the sweeping convection concept. For instance, observing the nonsignificant effect of the small particle led the study to focus on large particles. Another issue is the effect of the entrance length on the sweeping convection: with the velocity profile at the inlet as uniform, the flow would develop at the beginning of the channel with momentum boundary layers from top and bottom growing till they meet at a location somewhere downstream in the channel, with the flow becoming fully developed beyond that location. Similarly, the thermal boundary layer also develops from the inlet. Heat transfer improvement is negligible in the region of flow developing when the boundary layers are thin and restricted to a region close to the channel surfaces. This effect is more pronounced for higher inlet velocities because of the longer entrance length they yield. Hence, the imposing of uniform

velocity inlet condition hinders the sweeping effect. This hindrance was investigated further in subsequent simulations by replacing the uniform inlet velocity profile with a fully developed one.

Another potential issue that the initial study highlights is the need for an appropriate tool to quantitatively compare different cases when the channel surfaces are isoflux, as opposed to isothermal. Although isothermal contour plots depict the effect on heat transfer of a particulate flow over the clear flow in the isothermal case, they no longer provide a quantitative measure of the effect in the isoflux surface case. When isothermal condition is considered for the channel surfaces, as in the initial study previously considered, then the resulting heat flux through the surfaces is an appropriate parameter to quantitatively compare different cases. For the isoflux condition however, the surface heat flux is useless for comparison purposes because its value is imposed as a constant for all cases. Although the resulting surface temperature along the channel could be used for comparison, the integration of surface temperature along the channel does not provide a useful physical quantity, as the heat flux does in the isothermal case. The solution for this issue is considered in detail in the following section.

3.3. Start-up sweeping convection effects of a single particle in a straight isoflux channel with fully developed inlet condition

Numerical simulation results of the transient start-up flow of a liquid (water) and a solid spherical particle through a straight, isoflux heated channel is reported here. The convection process begins with the quiescent fluid and particle in the channel at a set

uniform temperature. The inlet fluid velocity and temperature are kept constant throughout the simulations, being respectively, fully developed and uniform. The study aims at determining the effects of the particle on the sweeping of the boundary layers that forms along the channel surfaces, now under isoflux condition. The particle is considered adiabatic, allowing for the isolation of the sweeping effect from the particle heat capacity effect on the convection process, and neutrally buoyant. Similar to the previous study, results reported here compare the convection effects of a single particle flowing with the fluid to the results obtained for the clear fluid flow case.

3.3.1. Problem description and modeling

The basic configuration considered here is like the previous case with a few differences, as shown in figure 3.9. At a certain time, a constant and uniform heat flux is imposed at the surfaces of the channel while the fluid is set to move by the imposed constant and fully developed inlet velocity. Observe the fluid inlet velocity is set as uniform in the previous configuration, which resulted in a momentum developing region along part of the channel. The now imposed fully developed inlet velocity profile eliminates the momentum developing region. Numerical simulation results are obtained by solving the balance equations for the fluid and solid particle, with coupling conditions at their interface. The basic continuity, momentum and energy equations for a Newtonian fluid with constant and uniform properties, are the same as the ones listed earlier, in equations 3.1-3.3.

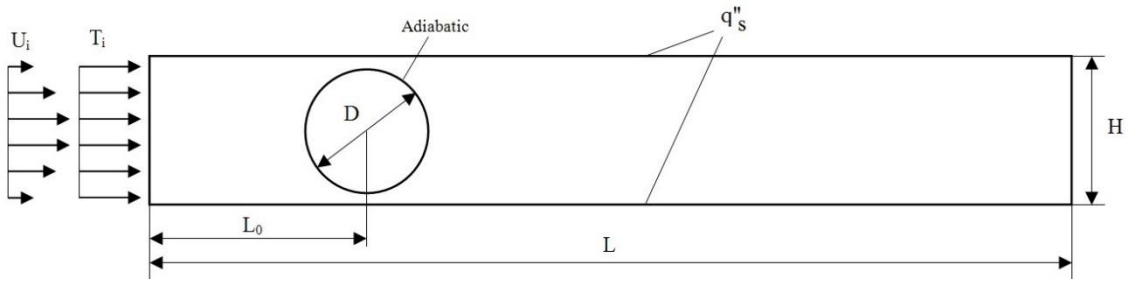

Fig. 3.9 Schematic view of the test channel with isoflux top and bottom surfaces, cooled by a flowing fluid having a discrete spherical solid particle flowing with it

The momentum balance equation for the solid particle, assumed rigid and non-deformable, is the Newton second law as described in the modeling discussion of the previous configuration. Like the previous configuration, the balance equations for fluid and particle are solved using a second-order accurate finite volume method, with cell vertex (finite element) domain discretization, and the simplified one-way FSI procedure for the momentum equations. The particle is not allowed to rotate or oscillate, and is considered rigid and neutrally buoyant, imposing an obstruction to the flowing fluid in the form of viscous and form resistance, which then drives the particle via action-reaction effect. Hexahedral moving mesh with 30,000 cells for the clear case and about 40,000 cells for particle case are used, for being determined to offer a good compromise between required computational time for convergence and numerical accuracy (grid independence) of the results. Time step size was selected as 0.01 s based on time step independency studies run concurrently with the grid independency tests.

Numerical results are presented for a total channel length L = 200 mm, initial particle distance from inlet L_0 = 12 mm, channel height H = 4.8 mm, and averaged inlet fluid speed U_{ave} = 26 mm/s, all mimicking the previous configuration. The inlet and initial

temperature conditions for fluid and particle are T_i = 300 K. Considering water as the flowing fluid, the corresponding Reynolds number, defined in respect to the channel height H and average speed U_{ave}, and Prandtl number would be Re = 280, and Pr = 6.13. The static pressure at the flow outlet is set as P = 0, and longitudinal temperature gradient is zero, while the heat flux applied along the channel top and bottom surfaces is fixed as q''_s = 4 kW/m^2. The particle diameter is chosen as D = 4 mm - note this diameter allows for only 0.4 mm spacing between the centered particle and the channel surfaces (the effect of particle diameter was investigated in the previous configuration, with the indication that particles with diameter less than 50 % the dimension of the channel have negligible sweeping effect on the convection process).

3.3.2. Results

The time evolution of the temperature contours, as the particle moves along the channel, is shown in figure 3.10 (top) by a sequence of equally spaced time-shots. Results for the clear fluid case, for the same times, are included in figure 3.10 (bottom) for comparison. The effect of the particle as it sweeps the boundary layer is clearly seen when comparing the two sets of shots. Notice in the first three shots, from t = 0 to t = 1.0 s, not much difference between the two cases is noticed. However, from t = 1.5 s, the region downstream the particle is clearly different, with an accumulation of hot fluid in front of the particle as the particle moves downstream of the channel. Also noticeable is the trailing effect upstream of the particle – see for instance t = 4 s – with a bulged blue region near the left side of the particle. This results from the particle pulling inlet (cold) fluid much deeper into the channel than the case for clear fluid can do. This is the stretching effect the

particle has on the boundary layer that develops along the channel surfaces, and is like what has been verified in the isothermal channel surfaces case analyzed previously.

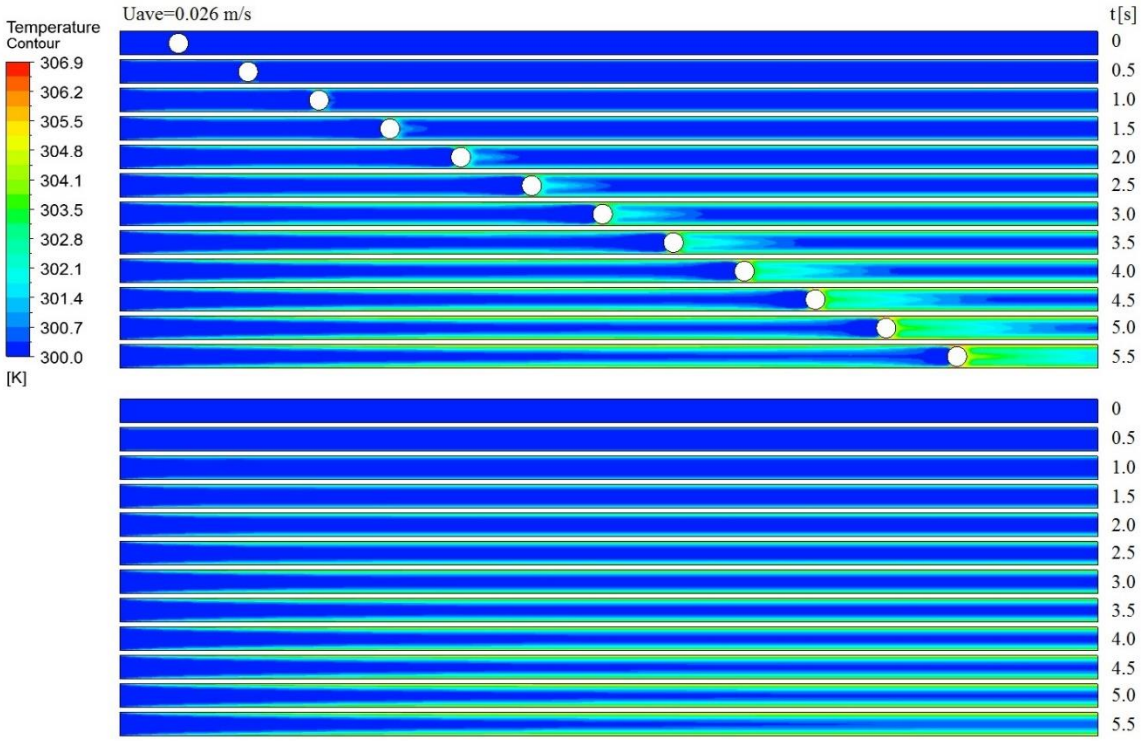

Fig. 3.10 Temperature time evolution of flow in a heated channel by a fluid and particle (top), and a clear fluid (bottom), from start-up.

The local, instantaneous effect of the flowing particle is identified in more detail in figure 3.11, where the temperatures along the channel surface (top or bottom, are the same due to symmetry) are plotted with continuous lines, each for a different time. Notice the results for the clear fluid case at t = 1, 3, and 5 s are also plotted in the same graph using dashed lines. Plotting results of both (particle and clear fluid) cases in the same graph is advantageous: observe that any deviation of the full line in relation to the dashed line for any time is a direct result of the particle effect. Interestingly, the particle effect on the channel surfaces is again (like the isothermal surfaces case) constrained in space within a region

roughly 1 to 2 particle diameters downstream of the particle and to within about 8 to 10 particle diameters upstream of it, with the effect upstream of the particle growing more than the downstream one as the particle moves along the channel.

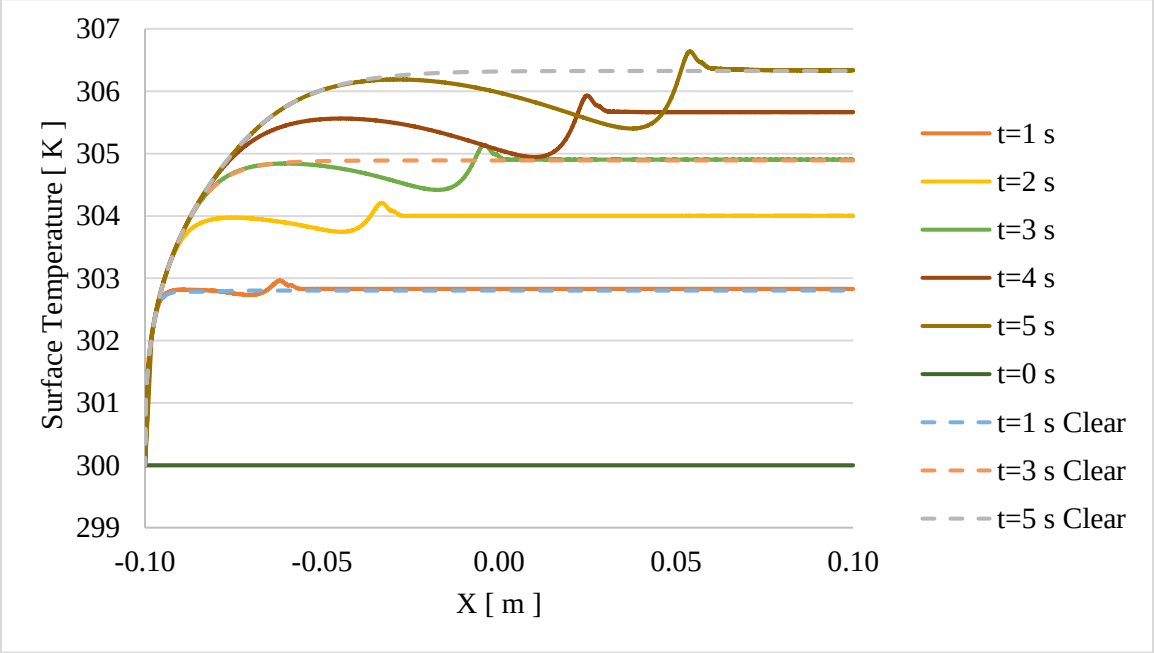

Fig. 3.11 Local variation of surface temperature along the channel for particle (continuous line) and clear fluid (no particle, dashed line), with average speed of 26 mm/s

Observe the surface temperature upstream of the particle being lower than the temperature without particle results from the particle pulling the inlet cold fluid with it as it moves along the channel (the stretching effect of the particle). Recalling the uniform heat flux condition at the channel surfaces, a smaller channel surface temperature means a smaller temperature difference between channel surface and fluid, and by consequence a higher convection heat transfer coefficient when the particle is included in the flow. Now, figure 3.11 shows the surface temperature is increased downstream of the particle as compared to the clear fluid case, even if within a small region. This is evidence of the particle sweeping the hot fluid that accumulates along the surfaces downstream of the channel (the squeezing

effect of the particle). The accumulation of hot fluid in front of the particle makes the surface temperature increase slightly but continuously as time goes by (and the particle flows downstream the channel), yielding a smaller heat transfer coefficient within this region.

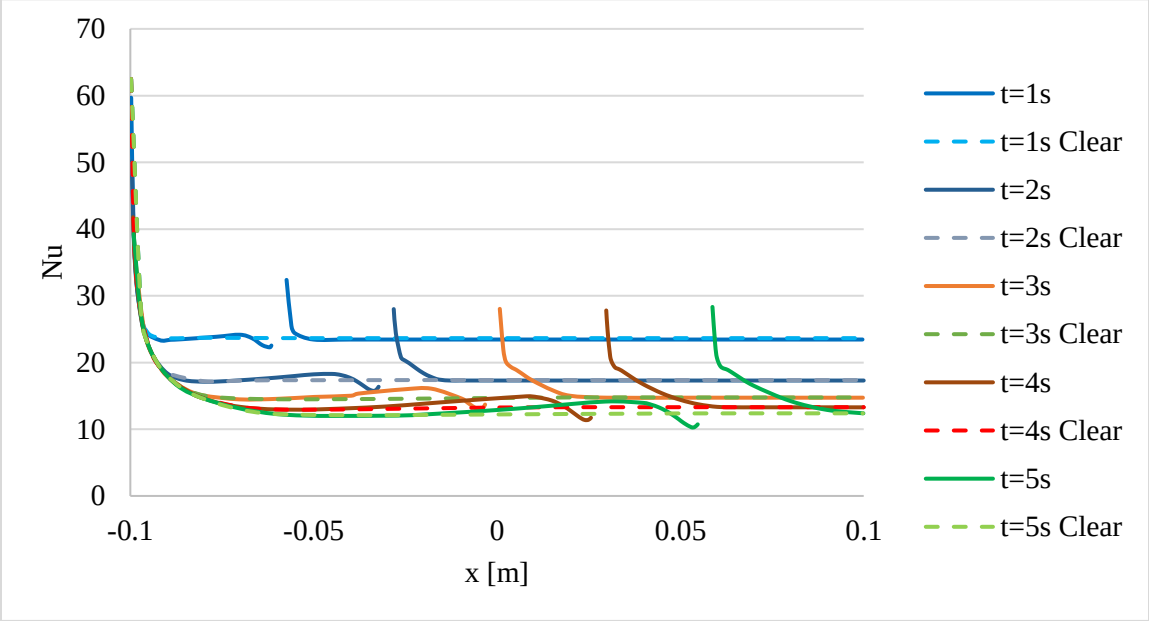

Fig. 3.12 Local variation of Nu along the channel for clear fluid (no particle, dashed line) and particle (continuous line) cases, with average speed of 26 mm/s

It is important to quantify the resulting particle effect on the heat transfer process. This is done in figure 3.12 via the Nusselt number, Nu, along the entire channel, defined as the local heat transfer coefficient, which is the ratio of the heat flux (uniform in the present configuration) and the difference between the local channel surface and the fluid bulk temperatures. Hence, the Nusselt number, for evaluating the convection performance, was calculated along the channel using:

$$T_b = \frac{\int uT\, dA}{\int u\, dA} \tag{3.5}$$

$$Nu = \frac{q''2H}{k(T_w - T_b)} \tag{3.6}$$

where T_b is the fluid bulk temperature, u and T are the local horizontal fluid speed and temperature, respectively, A is the cross-section area of the channel, q″ is the heat flux across the channel surface, H is the channel height, k is the fluid thermal conductivity, and T_w is the local wall temperature. A significant difference between the Nu curves for the clear fluid (dashed lines) and the particle (continuous line) cases can be observed in the vicinity of the particle. However, these two curves match precisely within the channel far enough from the particle, showing again the local character of the particle effects.

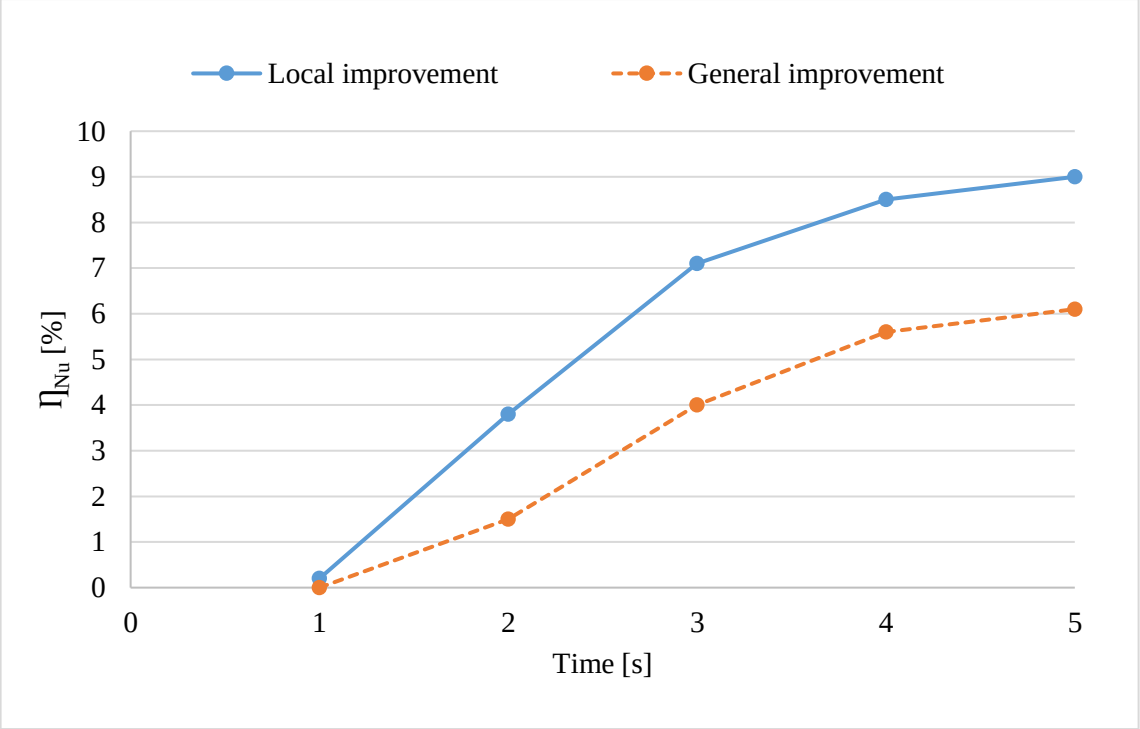

Fig. 3.13 Overall heat transfer improvement in time with large particle and inlet average speed 26 mm/s

Observe in figure 3.13 the Nu curves are not continuous because they are not plotted along the region occupied by the particle. In this area, T_b is calculated based on a small

amount of fluid within the gap between the particle and the channel wall where the fluid temperature is very close to the wall temperature. This leads to a very large Nu to be calculated due to a very small difference between T_b and T_w. Although this result is realistic, for being restricted to a small flow area and for affecting the readability (graph scaling) of the Nu values around and away the particle a decision was made to remove it from the graph.

Comparable to the isothermal case, a quantitative comparison of the particle and the clear fluid cases is done using a figure-of-merit parameter defined as η_{Nu}, for Nusselt number in relation of the clear fluid case, defined as:

$$\eta_{Nu} = \frac{(Nu_P - Nu_C)}{Nu_C} \times 100 \tag{3.7}$$

where Nu_p and Nu_c are surface-average Nu for the particle (P) case and the clear (C) case, respectively. Figure 3.13 presents two curves for η_{Nu} versus time. The dashed curve is built with η_{Nu} values obtained when using the entire channel length for the integration of Nu, while the solid curve is obtained with integration only along the section along which Nu_p does not match Nu_c. Notice the dashed curve falls lower than the solid curve because integrating along the entire channel provides a global result, smoothing out (or diluting) the local variations. This leads to a very small η_{Nu} value anytime the two Nu results (for the particle case and clear case) match – which happens along most of the channel (see t = 1 s curve in figure 3.12). These curves show, as time goes by (i.e., particle moving forward), the heat transfer efficiency increases. From the solid curve one could find a maximum of 9 % improvement in the heat transfer process for this particular case.

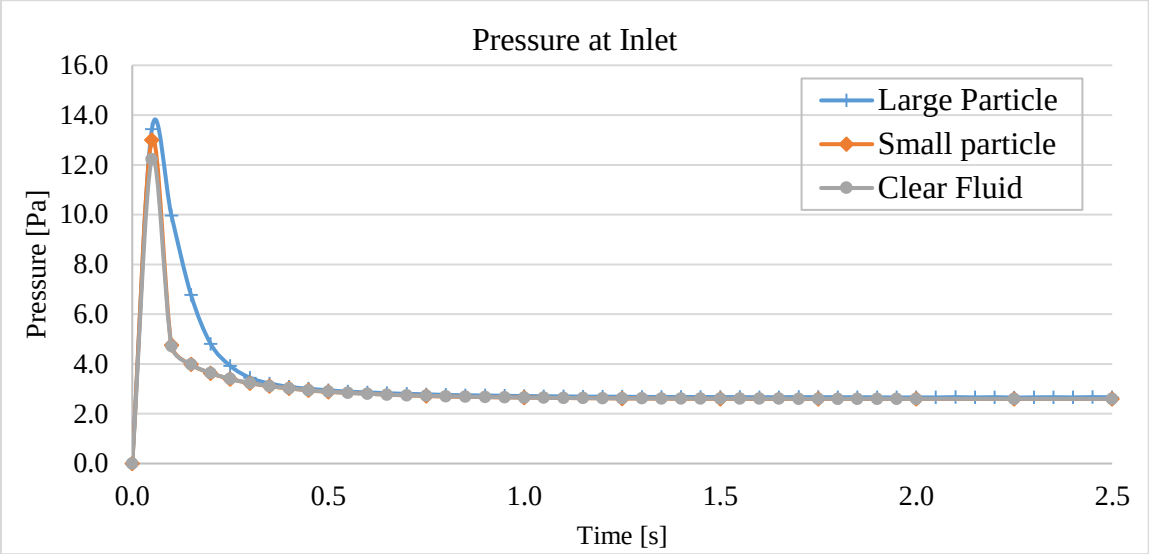

Fig. 3.14 Time variation of static pressure at inlet in the case with U_{ave} = 26 mm/s

One important effect of all convection heat transfer enhancements is the potential increase in pressure drop along the channel, which leads to an increase in pumping power (cost) for the process to take place. Figure 3.14 shows the time variation of the inlet flow pressure for the small (D = 2 mm) and large (D = 4 mm) particles and the clear fluid cases (notice the outlet pressure is the same – equal to zero - in all cases). Interestingly, the pressure variation in the case of the small particle is practically identical to the pressure variation of the clear fluid case, as if the particle did not affect the flow pressure. Even in the large particle case, when one could expect strong pressure effect due to the very narrow gap between the particle and the channel surfaces, the pressure variation is higher than for the clear fluid case in the beginning (acceleration) phase of the flow, but then the difference drops to less than 2.5 % when the pressure evolution reaches a plateau. In conclusion: the pressure effect in both cases with the particle is very small. This aspect places the sweeping convection method at the forefront of existing convection enhancement alternatives when it comes to avoiding a substantial increase in pressure drop (i.e., pump power).

3.3.3. Summary and conclusions

In this section, results obtained via numerical simulations of flow of water along a straight isoflux heated channel with and without a single solid spherical particle flowing with the fluid are presented. Two solid particles, one small and one large, are considered, the large one with diameter slightly smaller than the channel cross section dimension being the most effective in enhancing the convection process. The results (of the large particle) reveal the particle effect on the convection process to be localized and yet very significant, with the surface-averaged Nu number (introduced for quantifying the sweeping heat transfer effect for the isoflux case) increasing by up to 9%, and with negligible pressure drop effect across the channel. This result supports the expectation of sweeping convection being a very effective new convection mechanism with tremendous practical potential. The results also indicate enhanced heat transfer upstream the particle location and hindered heat transfer downstream of the particle location, as compared to the results obtained for the clear fluid case. The net effect, however, is a considerable gain in heat transfer efficiency. Although the effect is limited to a flow region around the particle, it is nevertheless substantial considering only one particle is present in the flow at all times. The results then confirm the existence of the sweeping convection effect by a flowing solid particle during the start-up convection process in a channel.

3.4. Sweeping convection effects of two particles in a straight isothermal channel with fully developed inlet velocity condition and the effects of varying the distance between them

The two configuration cases mentioned in this chapter so far were solved numerically using a Moving Mesh method. This method re-meshes the domain every time the particle changes location along the channel. Remeshing can be programed to be done

automatically during the solution of the equations when the geometry of the configuration simulated is simple enough. Although the geometry of the current problem is relatively simple, generating a high-fidelity mesh around the particle - particularly in the very small gap region between the particle and the channel surfaces - requires lots of extra steps in the meshing subroutine, which makes the automatic mesh generation impractical. Manual remeshing is then the option here, which means exporting the new geometry of the domain (the one resulting from the particle changing its location in the channel) for a new mesh to be generated and sent back to the solver for simulating another time in the process.

An alternative to the Moving Mesh method is the Immersed Solid method, which does not require remeshing the domain during the simulation. This method enables one to model transient simulations involving rigid solid objects that move through a fluid domain by using an immersed solid domain placed inside the fluid domain. As the numerical simulation proceeds, the solver applies a source of momentum to the fluid inside the immersed solid domain forcing it to move like the solid [25]. The Immersed Solid method may not be as accurate as the Moving Mesh method, but it requires much less time for the numerical set-up and for running a simulation in comparison to the Moving Mesh method. Therefore, the remaining configurations presented here have results obtained by using the Immersed Solid method.

In this section the effect of two particles in transient, start-up flow of water through a straight heated channel, and the effects of varying their starting distances, is considered using numerical simulations. Similar to the previous configurations, the simulation starts with the stationary fluid and two particles in the channel at a uniform temperature while upper and lower channel surfaces are maintained at a different isothermal condition. The

study aims at determining not only the effects of having two particles in the channel, but also the effects of the distance between the two particles on the sweeping of the thermal boundary layers that forms along the channel surfaces as the fluid and particles move. Results reported here compare the convection effects of the two particles, with different initial distances, to the convection obtained for the clear fluid flow case.

3.4.1. Problem description and modeling

The present configuration expands on the previous two by investigating the effect of adding an additional particle to the flow in the channel and considering the effect the distance between the two particles has on the convection process. The basic configuration considered here is that of a straight, finite length channel filled with an initially isothermal and stationary fluid. There are two solid particles within the fluid, positioned at distances L_1 and L_2 from the channel inlet, figure. 3.15. At a certain time, the surfaces of the channel are set as isothermal with temperature higher than the fluid initial temperature, and the fluid is set to move by imposing a fully developed velocity profile and a uniform temperature at the channel inlet.

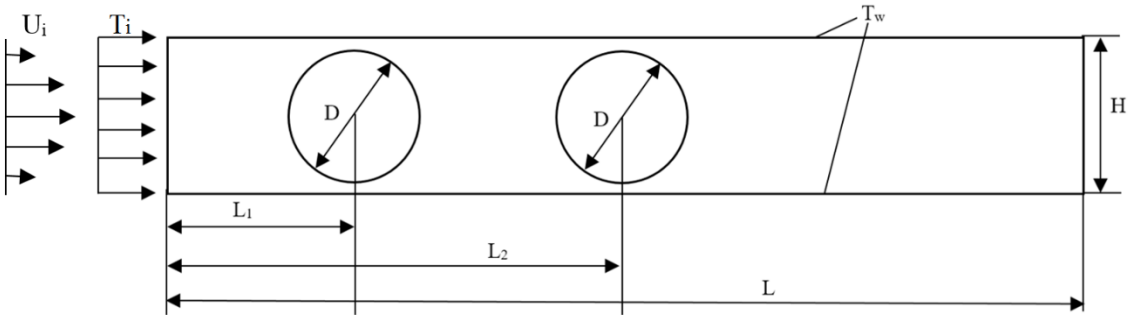

Fig. 3.15 Schematic view of the test channel with isothermal surfaces, cooled by a flowing fluid having two discrete spherical solid particles flowing with it

Numerical simulation of the ensuing flow and heat transfer process within the channel is performed by using the balance equations for the fluid flow and heat transfer. The basic continuity, momentum and energy equations for a Newtonian fluid with constant and uniform properties are already mention in equations 3.1 through 3.3, and the energy equation for the particle is:

$$\frac{\partial \mathrm{T}}{\partial t} = \alpha \nabla^2 \mathrm{T} \tag{3.8}$$

Notice here the particles are assumed participating in the thermal process. In equation (3.8) the thermal diffusivity of the particles, α, equals that of the flowing fluid used in equation (3.3). This is done deliberately to isolate the sweeping convection effect from the possible effect resulting from different solid/fluid thermal properties.

The Immersed Solids method is used here to model the transient simulations involving rigid solid particles moving through the channel. The model involves the use of two immersed solid domains placed inside the fluid domain. The balance equations for fluid and particles are solved using a second-order accurate finite volume method, with cell vertex domain discretization, and the simplified one-way FSI procedure for the momentum equation (note the particle is not allowed to rotate or oscillate, and is considered rigid, neutrally buoyant, imposing an obstruction to the flowing fluid in the form of viscous and form resistance, which then drives the particle via action-reaction effect). The heat transfer interaction between solid particles and the surrounding fluid is done by imposing compatibility conditions along the fluid-solid interface, namely continuity of temperate and heat flow across the interfaces. A clear (of particles) case, in which particles are absent from the channel flow, is also simulated numerically for comparison, being the base-line

case to which the performance of the particles is compared. Hexahedral stationary mesh with 152,000 fluid cells for the clear case and about 19,200 cells for each particle are used, for being determined to offer a good compromise between the required computational time for convergence and grid independence. Time step size was chosen to be 0.01 s based on time step independency studies.

Numerical results are presented for a total channel length L = 200 mm, initial first particle distance from inlet L_1 = 12 mm, initial second particle distance from inlet varying as L_2 = 18 mm, 24 mm, 36 mm, 48 mm, and 60 mm, channel height H = 4.8 mm, and averaged inlet fluid speed U_{ave} = 10 mm/s (this speed yielded best results for the isothermal single particle case, previously considered). The inlet and initial temperature conditions for fluid and particle are T_i = 300 K. Considering water as the flowing fluid, the corresponding Reynolds number, defined in respect to the channel height H and average speed U_{ave}, would be Re = 108, and the Prandtl number Pr = 6.13. The static pressure at the flow outlet is set as P = 0, while the wall temperature applied along the channel top and bottom surfaces is T_w = 340 K. The particle diameter is chosen as D = 4 mm - note this diameter allows for only 0.4 mm spacing gap between the centered particle and the channel surfaces.

The Nusselt number, for evaluating the convection performance, was calculated along the channel using equations 3.5 and 3.6. Finally, the resulting effects on the convection process by the two particles at varying distances are compared to the single particle and to the clear (of particle) flow cases.

3.4.2. Results

Temperature contours along the channel at time 10 s are presented in figure 3.16. From top to bottom, the first distribution is for clear flow, and the second is for a single particle. Then follows five distributions with two particles and different initial distances L_2, and one distribution with different L_1 and maximum L_2. For simplicity, the two particle cases will be referred to by numbers representing the distance between the centers of the particles in multiples of the particle diameter, namely D = 4 mm. Hence, the case with L_1 = 12 and L_2 = 18 mm, when the distance between the center particles is 6 mm, will be referred to as 1.5D case, and so on.

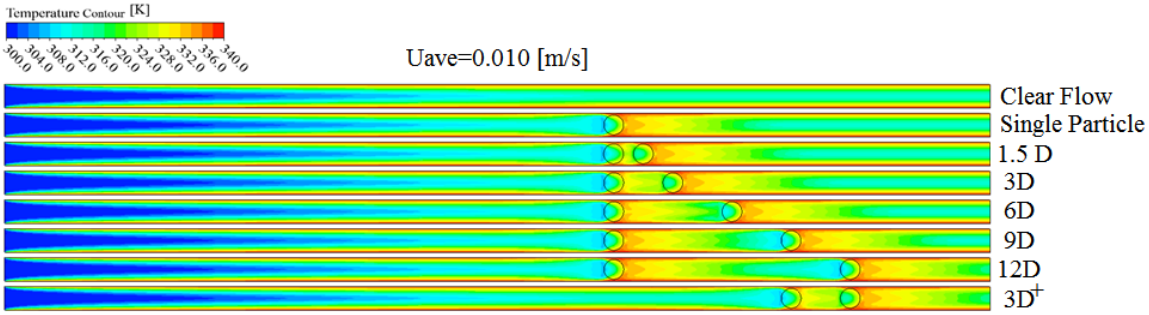

Fig. 3.16 Temperature contours sample within the heated channel with clear fluid, single particle, and two particles, at 10 s

Observe in figure 3.16 the temperature distribution within the first half of the channel seems identical to the clear case even when particles are present, because after 10 s the particles effect in that region is no longer identifiable. The dragging effect by the particles, however, is still noticeable right upstream of the leftmost particle in all particle cases. This is shown by the temperature distribution distortion seen around the back of the particles. This is also observable in the region upstream of the right particle, particularly

for the cases 6D, 9D and 12D, with the dragging effect becoming more pronounced as the distance between the two particles increases.

Also, in the two particle cases, the channel region between the two particles is affected by the squeezing effect (hindering convection) of the upstream particle and the dragging effect (enhancing convection) of the downstream particle. These two effects tend to counteract each other, particularly when the particles are close together, such as the 1.5D and 3D cases. The temperature of the fluid in this region for these cases tend to be high, hindering the heat transfer process in it. However, when the particle distance increases, say cases 9D and 12D, the squeezing effect of the left particle still has enough room to evolve without interfering much with the dragging effect of the right particle. The resulting effect is a lower temperature in the in-between particle's region, for an overall better heat transfer process. These results show the particles can interact when near each other, and this interaction tend to be detrimental to the convection process. Case $3D^+$ with $L_1 = 48$ mm and $L_2 = 60$ mm, a different 3D case with same particle-to-particle distance as the case $L_1 = 12$ mm and $L_2 = 24$ mm, seems to indicate the particles initial location in the channel to have no other effect on the heat transfer process caused by the particles inside the channel besides moving the local effect of the particles a little downstream of the channel.

The local Nusselt number along the channel is shown in figure 3.17 for the clear fluid, 3D, 6D, and 12D cases. Observe all curves merge from x = 0, until the location of the first particle, at around x = 0.12 m. The dragging effect caused by the first (leftmost) particle results in a spike in Nu upstream of the first particle, as observed for x (distance from the inlet) a little less than 0.12 m. The Nu then drops, where the particle is, then it increases again due to the squeezing effect downstream of the particle. This evolution

before and after the particle is a characteristic of each particle, resulting from the local sweeping effect of the particle, and it is observable in all cases shown in figure 3.16.

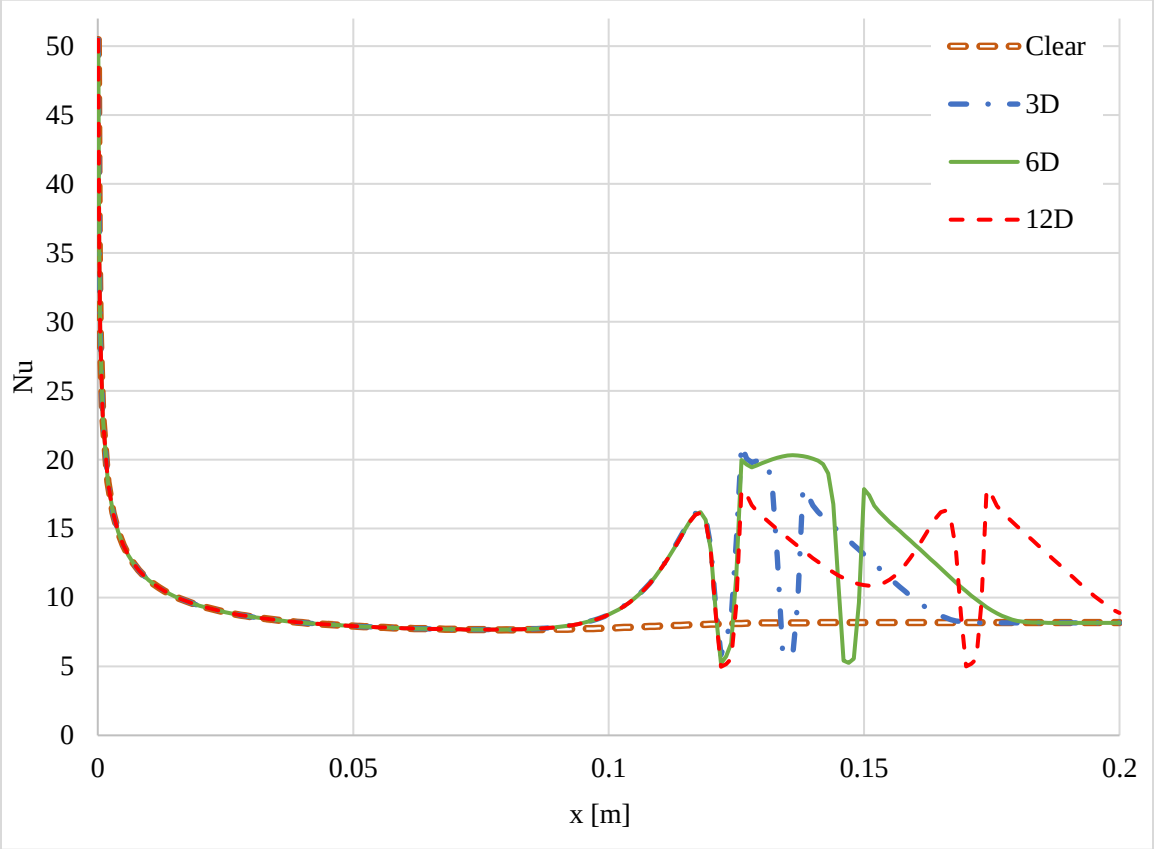

Fig. 3.17 Nusselt number along the channel length at 10 s for clear and two-particle cases

The first difference between the curves appears when comparing the 3D and 6D cases with the 12D case. The Nu for the first two cases reaches a higher value than the Nu for the 12D case. The proximity of the second particle in the cases 3D and 6D keeps Nu high due to the dragging effect of the downstream particle. The Nu for the 12D case, however, indicates a drop in Nu after the first particle, and then a recovery as the second particle location is approached. Notice this drop between the particles is not enough to reach the clear fluid case Nu value – this would eventually happen if the two particles were further apart from each other, in which case their effects would be identical to the effects

of two individual noninteracting particles flowing in the channel far enough from each other. The Nu curves then follow the same evolution for the second particle as the evolution for the first particle, with a smooth increase upstream of the particle, a drop around the particle location and another spike downstream of the particle.

The overall effect of the particles can be related to the surface averaged Nu, obtained by integrating Nu along the channel length. That is, the overall effect is proportional to the area under the Nu curves of figure 3.17. It seems clear from this figure that the Nu evolution in between the two particles determine which case is most effective. The computation indicates the case 6D to be the most effective, although the 12D case is a close second.

The heat flux, bulk temperature, and Nusselt number values across the entire channel length for the 6D case at time equal to 10 s are shown in figure 3.18. Comparing these graphs to the temperature contour of figure 3.16 shows exactly how the heat flux and bulk temperature relate. Anywhere the bulk temperature drops the heat flux increases. This inverse relationship causes dramatic changes in the Nusselt curve. An increase in heat flux also causes an increase in Nusselt number which shows an overall increase in the convective effects of the particle. In this case, it shows that the area between the particles achieves the highest heat transfer throughout the channel.

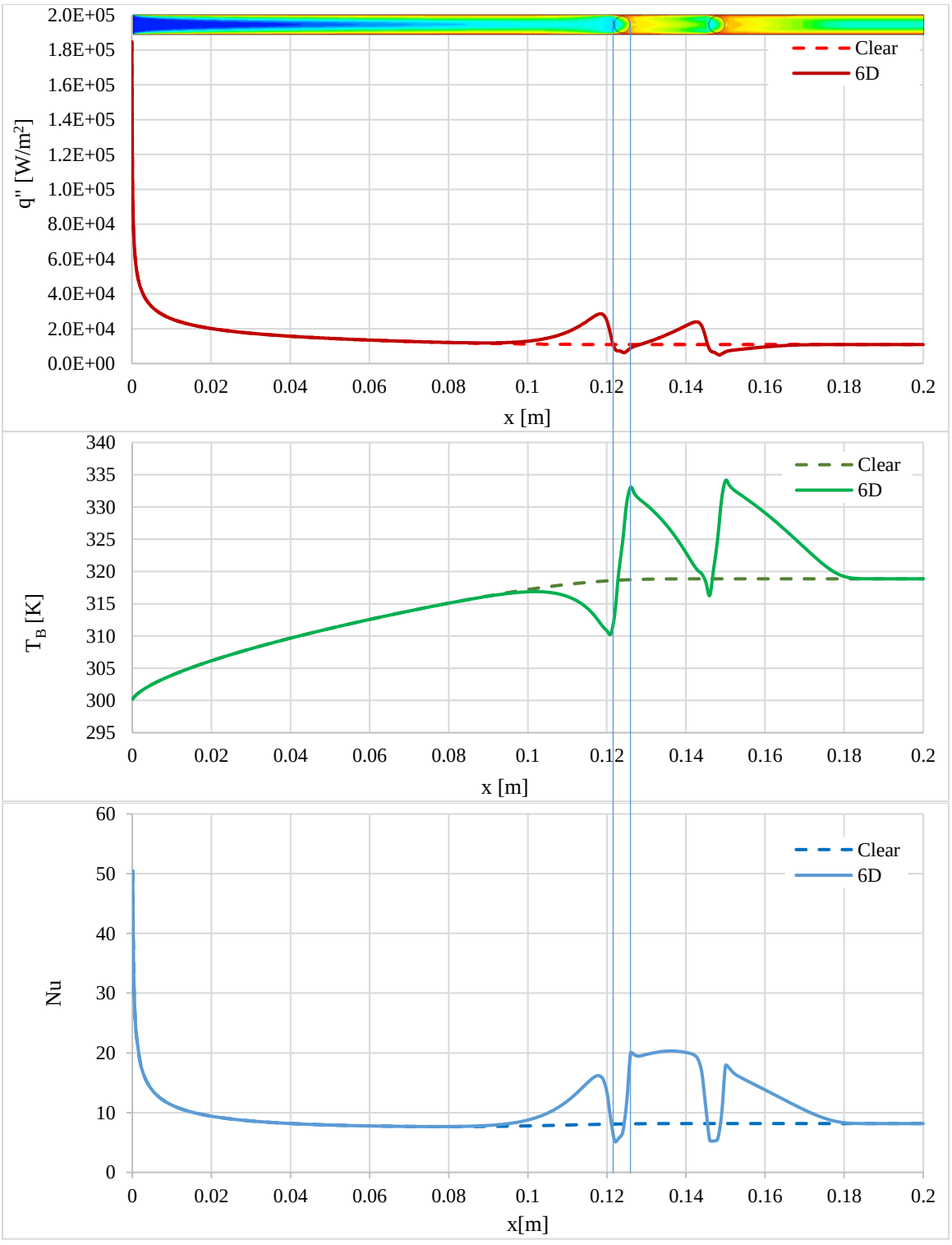

Fig. 3.18 Heat flux (top), bulk temperature (middle), and Nusselt number (bottom) graphs for the entire channel length at 10 s for the 6D and clear cases

Figure 3.19 presents curves for η_{Nu} versus time for all cases shown in figure 3.16, from start up to 10 s. Notice the cases with large distances between particles have a much larger increase in Nusselt number compared to the cases with small distances. This is due to the dragging and squeezing effects of the particles. The 12 mm and 24 mm (3D) case and the 48 mm and 60 mm ($3D^{+}$) case have the same distance between particles, and as seen in figure 3.19 and figure 3.20, the position of particles in the channel with the same distance between them yield the same convective effects. This is confirmed by the corresponding curves of figure 3.19.

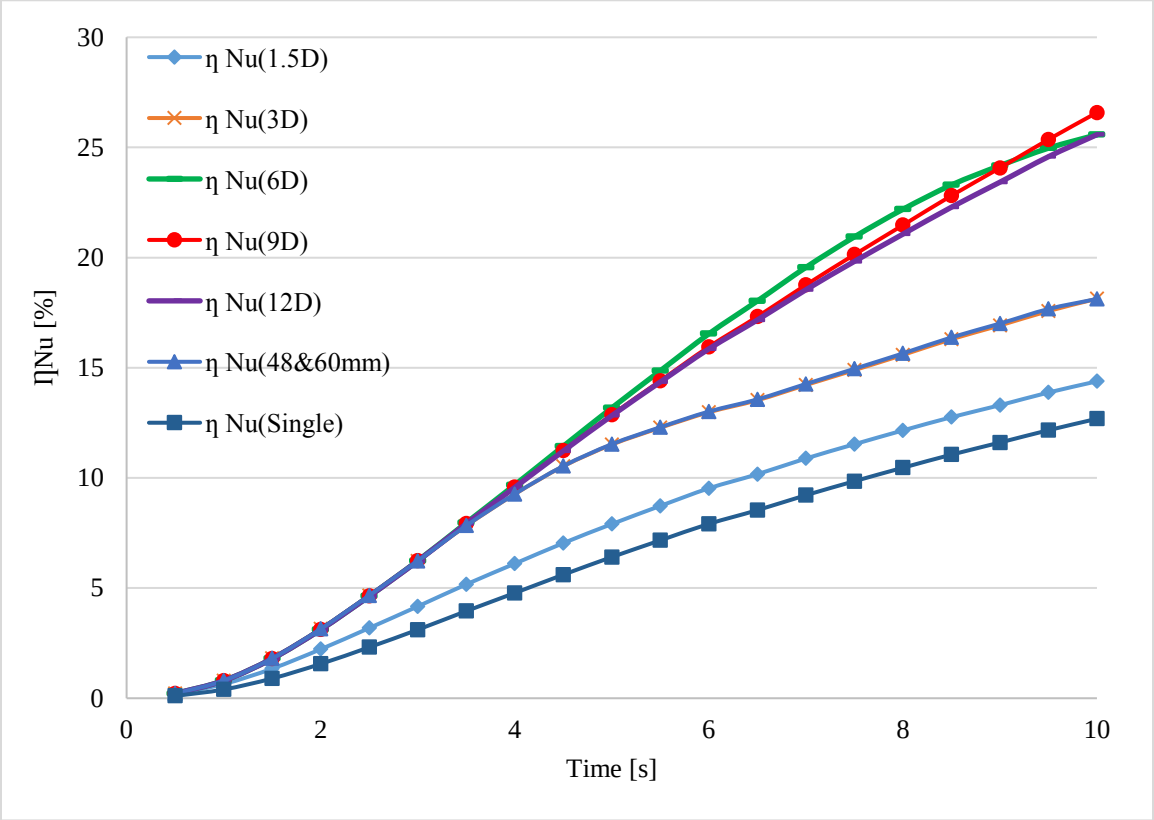

Fig. 3.19 Overall heat transfer improvement in time, in relation to the clear fluid case, for the single and two-particle cases

Figure 3.20 presents η_{HF} for all cases shown in figure 3.16 versus time from start up to 10s. Notice that the graph for Nu continues increasing while the heat flux increases, then peaks and begins to decrease. This aspect shows that as time gets closer to 10 s the temperature difference between the channel surface and the fluid decreases causing the surface averaged Nusselt number to continuously increase in time even though the heat flux is decreasing. In this figure the 9D case and the 12D case have identical surface averaged heat flux. This shows that as the distance between the particles increases past the optimal distance of 6D the convective effects remain about the same or plateaus.

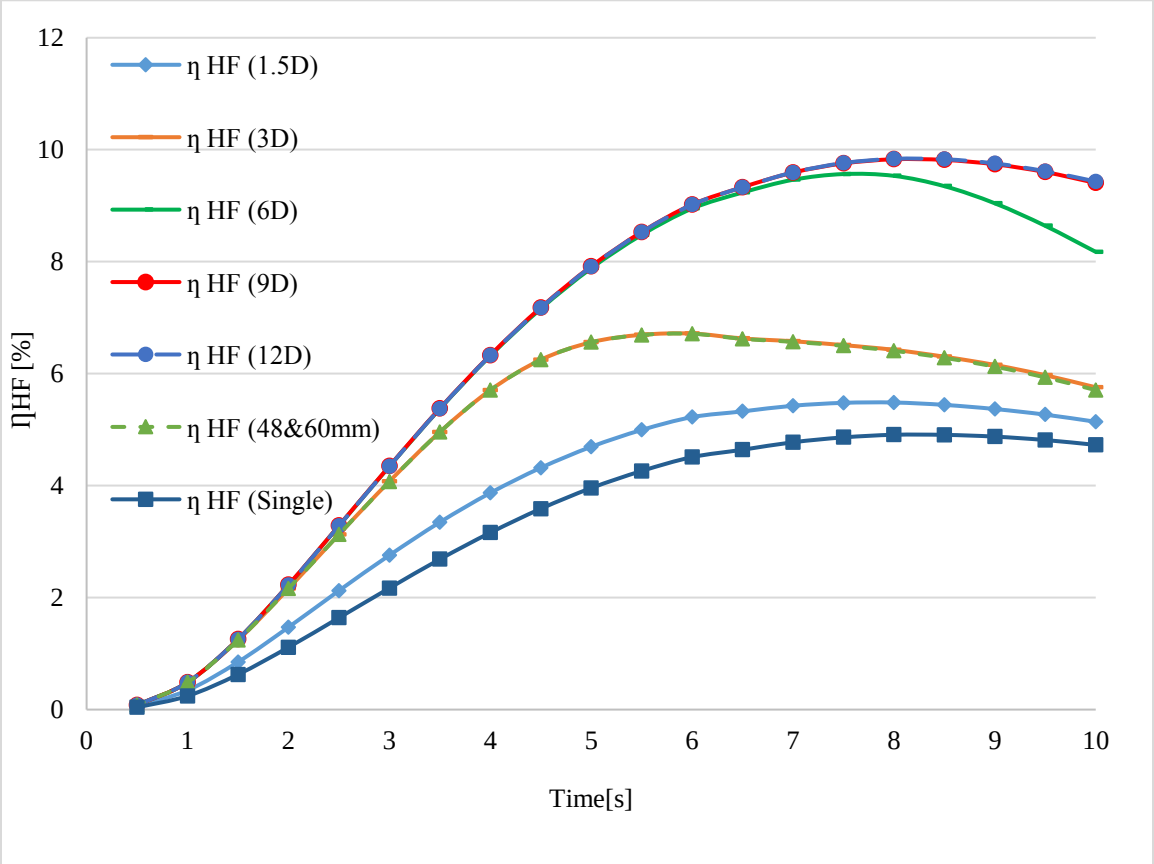

Fig. 3.20 Overall Heat Flux improvement in time, in relation to the clear fluid case, for the single and two-particle cases

3.4.3. Summary and conclusions

In the third configuration considered here, numerical simulations of flow of water along a straight heated channel with two solid circular particles flowing with the fluid are performed. The particles have a diameter slightly smaller than the channel cross section dimension. The results indicate a very strong effect on the heat transfer process around the particles, with enhanced heat transfer between the two particles. The graph of Π_{Nu} confirms that for the two-particle cases the large distance between the particles yields more efficient heat transfer, this effect flattening out when the distance increases past 6D. The results also show that the particle location within the channel at the start up has no effect on the heat transfer, if the distance between particles remains the same. These results show the existence of the sweeping convection effect by flowing solid particles during the start-up convection process in a channel even when two particles are present in the channel, indicating there is likely an optimal distance between particles for the most efficient heat transfer within the channel. The results indicate an enhancement of the average Nusselt number along the channel of almost 30% and an increase in the average heat flux of almost 10% when the particles are present. Also, it seems the distance between the particles correlates with the sweeping convection efficiency: as the distance between the particles increases the convection increases as well, up to an optimal distance between the particles beyond which no further increases take place. This optimal distance between particles happens to be 6 times the diameter of the particle in the present study. The results also indicate the initial location of the particles in the channel, with the same distance between them, has no apparent effect on the heat transfer process.

3.5. A model with partially heated channel and initialization based on steady state results

All three configurations discussed in this chapter so far simulate a startup process in which initially the particle(s) is(are) at rest within a fluid field with zero velocity and uniform temperature. In these cases, thermal boundary layer starts to grow, and the particle sweeps this growing layer. While the study of startup processes has its own importance, it is necessary to consider another scenario to address steady state conditions existing in many thermal systems such as heat exchangers. These conditions are more akin of practical experimental condition as well. In the configuration considered in this section, one of the main differences is to apply the results of a steady state clear flow case as the initial conditions for a transient particle flow case with the same boundary conditions. In other words, when a transient case with current configuration begins, the particles would like to be released in a flow field which has already achieved a steady state condition in another case. This leads to an appropriate comparison between the steady state clear flow case and the transient particle flow case and highlight the potential improvement that can be introduced to an existing steady state thermal system by using particulate flow and sweeping convection.

Observe in figure 3.21 temperature contours along the channel for 0, 1, 3 and 5 seconds are presented for two cases (in pairs) with a single particle flowing through the channel. The only difference between two cases is their initial conditions. For the startup case, the initial temperature and velocity in the entire channel are 300 K and zero, respectively, while for the steady case, steady state results of a clear flow case (obtained previously) are used as the initial conditions. It is important to mention the word “steady”

here is used to highlight the initial flow conditions; notwithstanding, both cases are solved in transient form. At time equal to zero which marks the starting of the simulation, the difference between the two initial temperatures can be observed in figure 3.21.

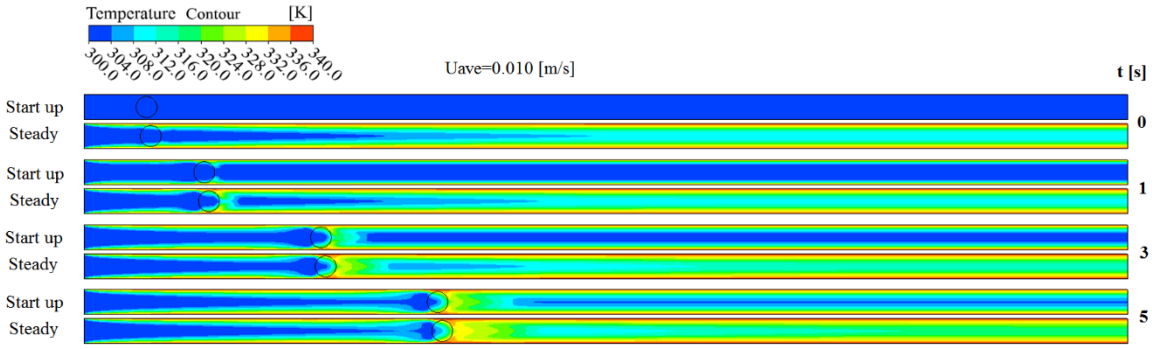

Fig. 3.21 Temperature contour samples within the channel with single particle for start-up and steady conditions

The particle has a small jump to the front in the steady case due to non-zero initial velocity of the fluid. As expected, the particle reaches the same terminal speed in both cases, reaching it a little faster in the steady case because of the non-zero starting flow conditions. It should not be surprising to see a larger amount of warm fluid collected in front of the particle in the steady case as the particle moves through a thicker (developed) thermal boundary layer rather than a thin growing one in the startup case. This leads to a better performance of the sweeping convection in the steady conditions rather than startup.

In this section, a new and more practical model is presented, as the geometry, and boundary conditions differ from those used in the three previous configurations. For instance, the previous channel length of 20 cm is now replaced with a longer 45 cm channel. Also, the new channel is split into an initial nonheated section L_u = 10 cm, a heated section L = 25 cm, and another nonheated section L_d =10 cm. This new configuration provides undisturbed upstream and downstream conditions for the heated section alleviating the

effects of imposing inlet and outlet boundary conditions affecting the heated section of the channel. The current simulations use, as initial conditions, the steady results obtained for a clear flow simulation with the same heat flux and inlet conditions. The effect of sweeping convection is then investigated by comparing four cases, namely: clear, single particle, two particles and three particles flowing with inlet velocity of 10, 20 and 40 mm/s.

3.5.1. Problem description and modeling

The present work expands on the previous three configurations by investigating the effect of adding more particles to the flow in the channel and considering the effect of steady state condition on the convection process. The basic configuration considered here is that of a straight, finite length channel, heated uniformly along a section of length L, distant L_u units from the channel inlet. An initial condition of a hydrodynamically and thermally steady fluid flow is imposed in the channel (this condition is obtained by running a clear flow case within the same boundary conditions, until steady state is achieved). Up to three particles can be positioned upstream of the heated section at distances L_1, L_2 and L_3 from the channel inlet, figure 3.22.

The Immersed Solids method is used here for the transient simulations involving rigid solid particle(s) which can move through the fluid domain. The current model involves the use of one, two or three immersed solid domains that are placed inside the fluid domain. The basic continuity, momentum and energy equations for a Newtonian fluid with constant and uniform properties, and the energy equation for the particles are the same as the ones in section 3.3. Hexahedral stationary mesh with 225,000 fluid cells for the clear case and 9801 cells for each particle are used, for being determined to offer a good

compromise between required computational time for convergence and grid independence. Time step size was chosen to be 0.01 s based on time step independency studies.

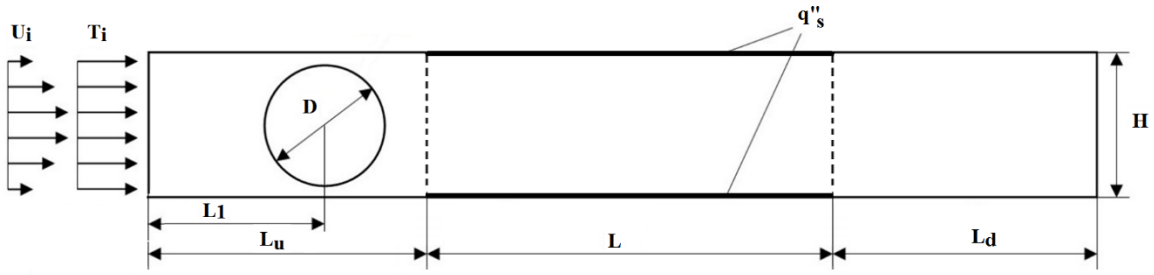

Fig. 3.22 Schematic view of the long channel with central heated surfaces (with the length of L), cooled by a flowing fluid with and without particle(s)

In this section a total of twelve cases are considered, for clear flow, and particulate flow with one, two and three particles, and three different average inlet speeds. Total channel length, as indicated previously, is 450 mm, with $L_u = L_d = 100$ mm, and L = 250 mm. When particles are present, their initial distances from inlet are $L_1 = 12$ mm, $L_2 = 48$ mm and $L_3 = 84$ mm. The channel height is H = 6.32 mm, and the particle diameter is chosen as D = 5.88 mm - note this diameter allows for only 0.22 mm spacing gap between the centered particles and the channel surfaces. Guided by the results from section 3.3 with two particles in use, the initial distance between particles is set as 36 mm, about six times the particle diameter, as to yield a high efficiency heat transfer of the particulate flow. Observe the flow speed and geometric dimensions of particles and channel can affect the optimum distance between particles for best heat transfer performance.

The initial temperature for the clear flow case is $T_i = 300$ K. This case evolves eventually to a steady state (when all results change by less than one percent), which is then used as initial condition for the cases with particles. The inlet fluid velocity for all

cases is a fully developed profile, with averaged inlet fluid velocities, $U_{ave,}$ equal to 10, 20 and 40 mm/s. Considering water as the flowing fluid at 23 °C, the corresponding Reynolds number, defined in respect to the channel height H and three average velocities U_{ave}, would be 141, 282 and 564, respectively. Notice these low Re suggest the flow regime remains laminar for the clear flow case. However, the flow can reach a transient or turbulent state at the gap between the particle and the surfaces of the channel when particles are present, depending of the gap size. Prandtl number remains constant for all cases as Pr = 6.13. At the channel outlet, the pressure is set as P = 0 while the thermal boundary condition is set as zero gradient condition ($\partial T/\partial x = 0$). A uniform wall heat flux applied along the channel top and bottom surfaces in the heated section is $q''_s = 8$ kW/m^2.

The simulations with particles are performed until a particle reaches the outlet section of the channel. Observe in cases with multiple particles the unheated downstream section is long enough to guarantee that all particles exit the heated section before a particle arrives to the outlet of the channel. The inclusion of upstream and downstream sections allows for identifying the process of particles entering and exiting the heated section of the channel.

The Nusselt number, Nu, for evaluating the convection performance of the channel, needs to be evaluated along the heated section of the channel. A Nu value on a specific cross section of the channel requires the bulk temperature of that section, which needs two integrations per equation 3.5. The results from previous configurations indicate the Nu value along the channel can change sharply specifically at locations close to a particle. To provide a smooth Nu curve with potential sharp variations, Nu needs to be calculated over cross sections close to each other. For the current setup, 251 cross sections with 1 mm

increments were used to provide a high-resolution Nu curve along the heated section of the channel. To reduce the post-processing time of the results for each case, a code was developed to calculate Nu value for all cross sections and return the result in a spreadsheet for further calculations.

3.5.2. Results

Temperature contours along the channel at times 0, 16 and 32 seconds are presented in figure 3.23 for the three-particle configuration with average velocity 10 mm/s and flow from left to right of the channel. From top to bottom, the first contour shows the start of the process when three particles in the upstream of the heated section are released to move in an already thermally and hydrodynamically developed flow. Observe in the upstream unheated region the temperature is uniform at 300 K because this region suffers no influence from the heated section. The middle contour, for time equal to 16 seconds, shows all three particles inside the heated section of the channel, while the last contour for time 32 seconds shows the moment the last particle leaves the heated section of the channel now occupying the downstream unheated section.

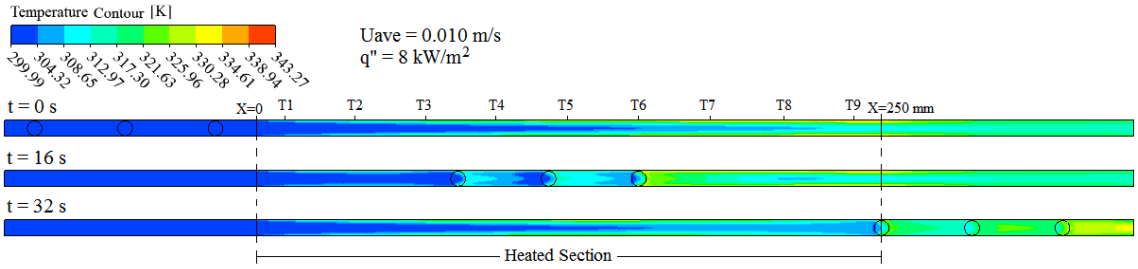

Fig. 3.23 Temperature contours sample within the channel with three particles, at 0, 16 and 32 s

The effects by the particle can be observed comparing the contour at 0 s to the other two contours. The dragging effect by the particles is noticeable at times 16 s and 32 s via the temperature contours upstream of the particles, even for the leftmost particle. It can be observed also from figure 3.23 that warm fluid is accumulated in front of the particles, making the fluid temperature at the center of the channel right in front of the particles to be higher than the adjacent channel surface temperatures – this is one of the particle's effects on the initially steady boundary layer, which was undisturbed at the beginning of the simulations. Upstream of the particles, dragged cool fluid has been accumulated which instantaneously reduces the channel surface temperature to drive the uniform heat flux to the fluid.

As shown in figure 3.23, nine points are distributed uniformly along upper surface of the heated section to monitor the surface temperature during the process. The locations considered for these nine points, T1, T2…, T9, are matching nine thermocouples' location placed on the outer surface of the heated channel in the experimental setup which is discussed in the next chapter. Figure 3.24 presents the surface temperature curves for these points versus time for the three-particle case with U_{ave} = 10 mm/s. Observe each curve has exactly three crests and troughs showing the moments that each one of the three particles pass through the corresponding point along the channel.

The highest temperature drop for each curve happens during the passage of the first particle, or the rightmost particle in the particle train. When this particle approaches a specific location, the wall temperature at that location increases slightly due to effect of warm fluid accumulation by the particle sweeping effect downstream of the particle. This hinders the heat transfer and the surface temperature increases to be able to transfer the

same amount of the heat flux, now to the fluid with higher mean temperature. As soon as the particle passes through that location, the surface temperature drops significantly as now the channel surface transfers the heat flux to a cooler fluid flowing upstream of the particle, with lower mean temperature.

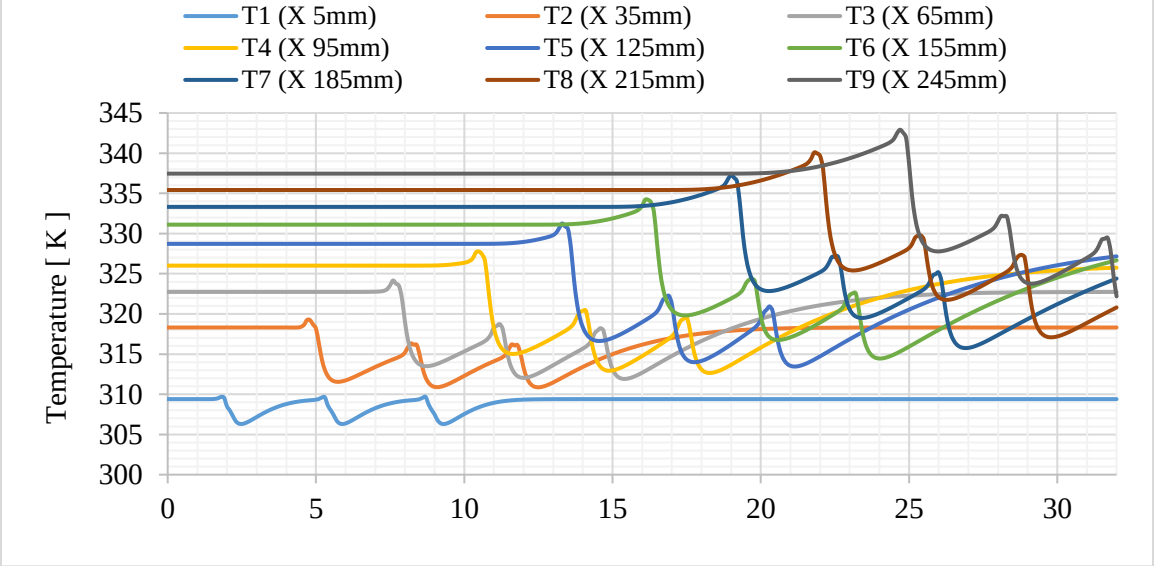

Fig 3.24 Temperature curves of nine points in upper wall of the heated section versus time for three-particle case run with U_{ave} = 10 mm/s

These changes in the surface temperature get more pronounced the farther the particles locations get from the inlet, along the heated section. For instance, T1 curve, which presents the surface temperature at the leftmost location in the heated section, has insignificant rises and very slight drops. For this curve, after each drop, the temperature rises to its previous steady value. On the other hand, the T9 curve, which is related to the rightmost location monitored, both rises and drops are significant with not enough time for the surface temperature to rise back to the previous steady value in this case. This suggests that at the last quarter time of the simulation (i.e. t = 24-32 s) the entire heated section is

under a more uniform and lower surface temperature due to the sweeping effect of the particles.

To study the effect of the number of particles present at the same time in the channel, results for three cases with different number of the particles are now considered. Figure 3.25 presents two sets of temperature contours, comparing one, two and three particles cases captured at 16 and 32 seconds along the channel. When more than one particle is used, the additional particles are placed downstream of the single particle. At 16 s, all particles are within the heated section of the channel, while at 32 s they are in the unheated downstream zone. Observe the temperature distribution upstream of the leftmost particle is almost identical in all three cases, due to growth of the new thermal boundary layer in the absence of the particles. Also, the temperature distribution between the two leftmost particles is again almost identical for the cases of two and three particles. Finally, there is a clear buildup of warm fluid downstream of the rightmost particles at 16 s for all three cases. However, the fluid downstream of the rightmost particle in the three-particle case is warmer than the two-particle case, which is warmer than the fluid in the one particle case. The reason is, at the same time of the simulation for each of the three cases, the rightmost particle in the three-particle case is in a channel section with a thicker thermal boundary layer and higher mean temperature. The same is not the observed for the 32 s results because the particles are then in the unheated zone where the thermal boundary has dissipated. In this zone, the temperature distribution between the two leftmost particles is also different for the cases of two and three particles due to the lack of the heating from the channel surfaces.

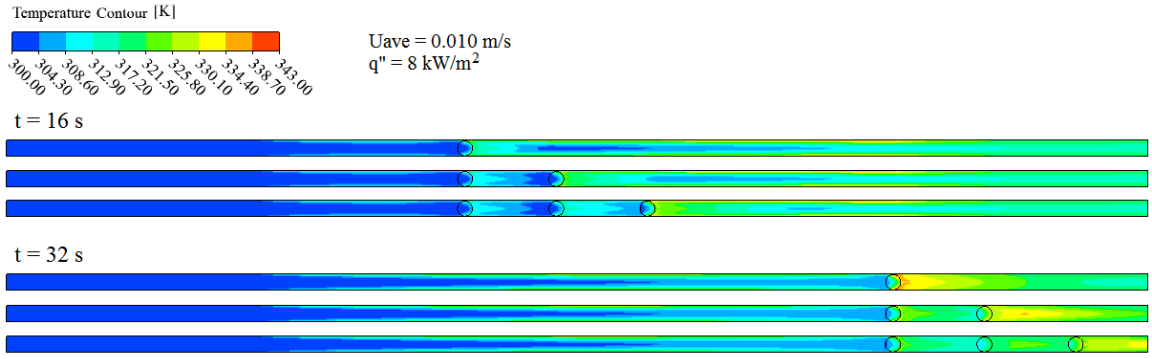

Fig 3.25 Temperature contours at two different times for the same configuration but with one, two and three particles

To investigate the effect of the inlet average velocity, U_{ave}, the results of three similar three-particle cases with different U_{ave} are considered. Figure 3.26 shows temperature curves of nine points in upper surface of the heated section versus time for three-particle cases with U_{ave} = 10, 20 and 40 mm/s, shown in top, middle and bottom charts respectively.

The vertical axes used in the three charts have the same scale to better show the differences between the cases. As expected, surface temperatures decrease by increasing the inlet velocity due to increased convection. Comparing the results for the three velocities, it can be observed the effect of the particles to drop the wall temperature is much stronger when the fluid speed is low. Observe on can compare the times when each thermocouple reaches its peak temperature for each different inlet velocity, with the result suggesting the particle velocity changes almost linearly with inlet velocity, as expected. For instance, the T9 first peak occurs at times 25 s, 13 s and 6.5 s for 10, 20 and 40 mm/s inlet velocities respectively.

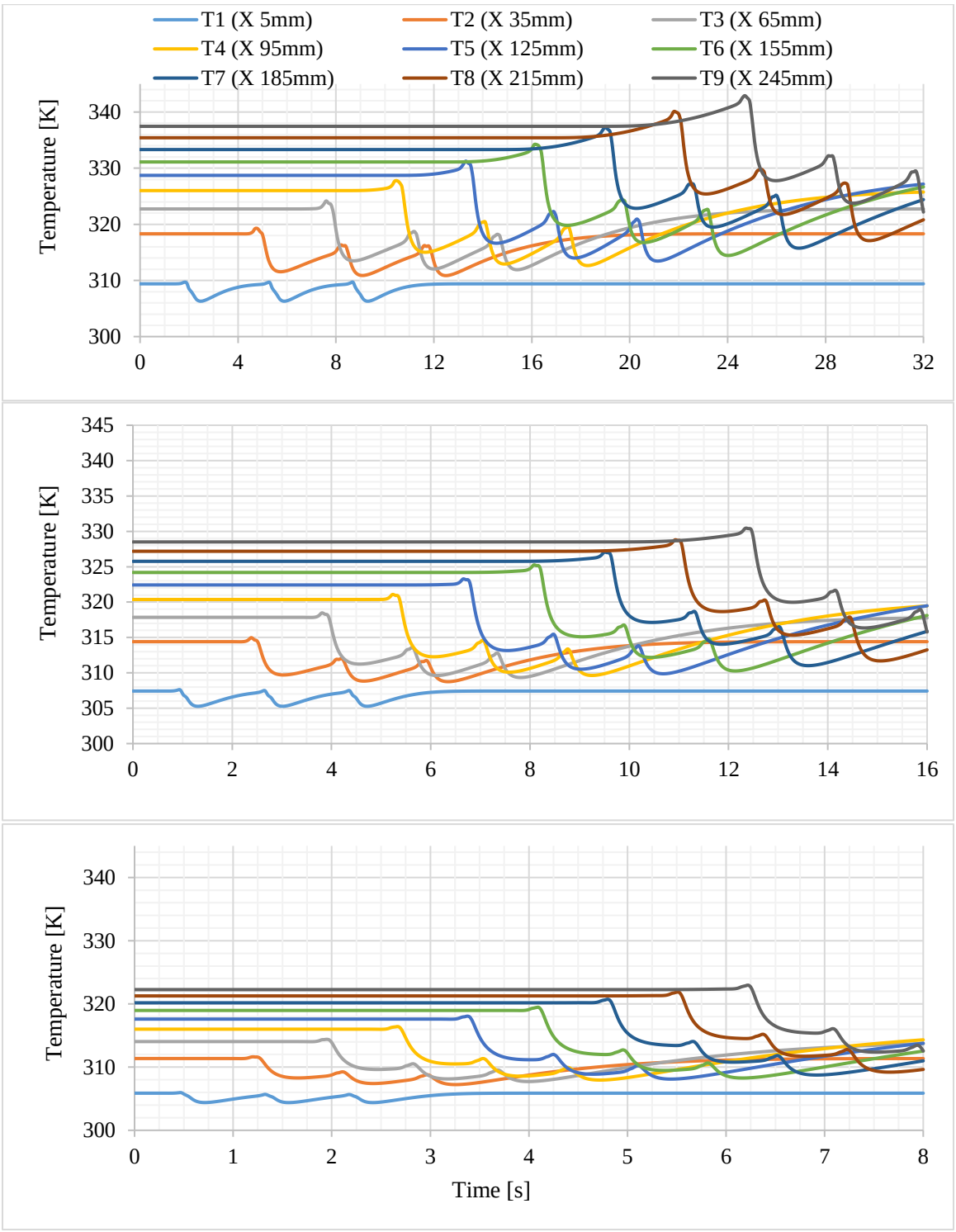

Fig 3.26 Temperature curves of nine points in upper wall of the heated section versus time for three-particle cases run with U_{ave} = 10 mm/s for top plot, 20 mm/s for middle plot and 40 mm/s for bottom plot

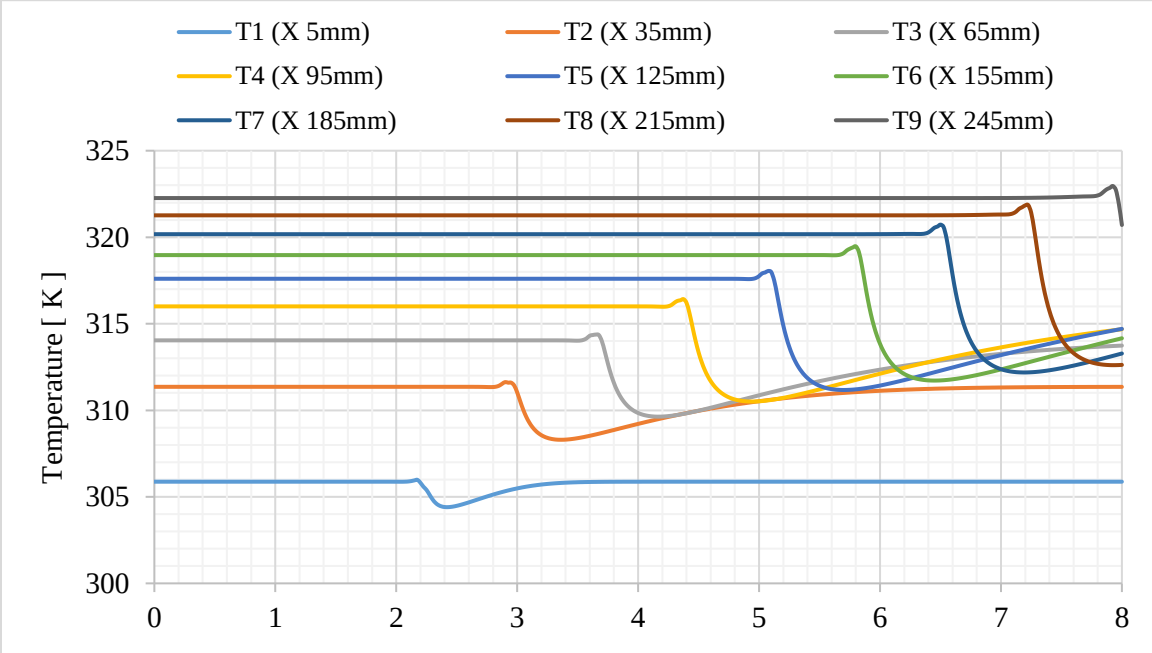

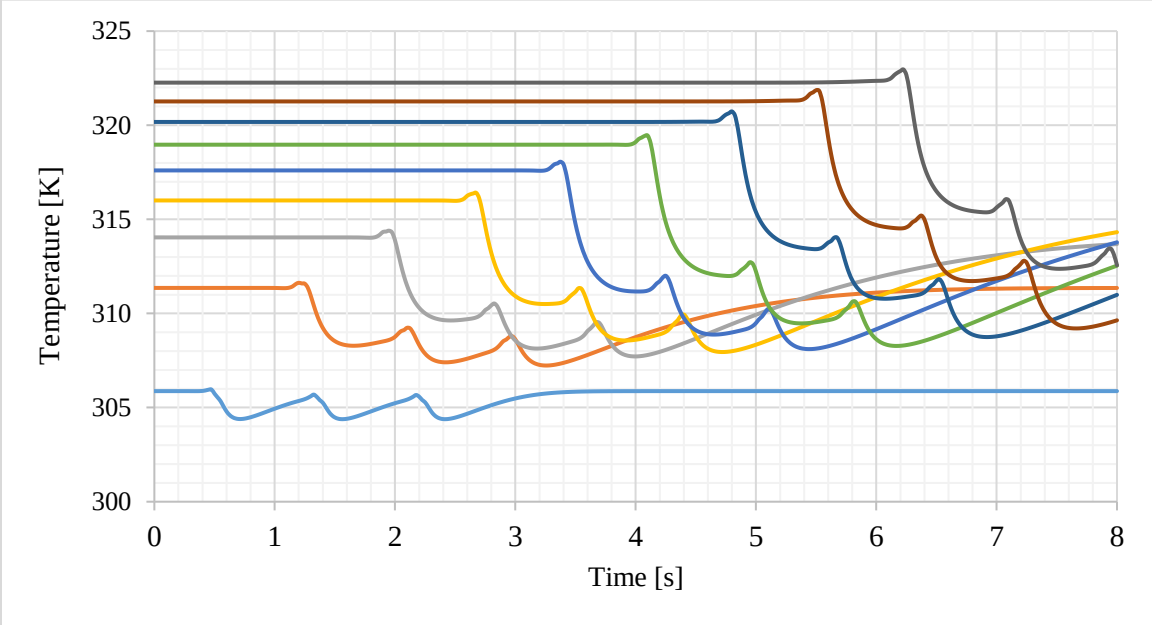

Fig 3.27 Temperature curves of nine points in upper wall of the heated section versus time for single particle case (upper plot) and three-particle case (lower plot) run with U_{ave} = 40 mm/s

To study the effect of number of the particles on heat transfer, wall temperature charts for the cases with one and three particles are shown in figure 3.27. The inlet velocity for both cases is equal to 40 mm/s. Note the first peaks for each location in the single

particle case (upper plot) occurs almost at the exact time of the third peak for each location in the case with three particles; this is due to the position of the particle(s) in the model, shown in figure 3.27. Consider T7 location, for instance, where the maximum temperature drop for the single particle is 9 ºC vs 12 ºC for three-particle case. While the highest temperature drop is due to the rightmost particle in both cases, the effect of including extra particles on the surface temperature drop can be observed in the case with three particles (lower plot) where the effect of the second and the third particles seems to be almost the same. This suggests including more particles is effective in causing a drop in the surface temperature (better convection heat transfer). Moreover, in a circulation system where particles would sweep the channel continuously, an oscillating wall temperature with lower mean (in comparison to the clear flow case) can be achieved. The amplitude of the surface oscillation in this case should depend on the flow conditions as well as the average distance between the particles.

Figure 3.28 shows the surface and bulk temperatures (left vertical axis) and Nusselt number (right vertical axis) along the heated section for one (upper graph), two (middle graph) and three (lower graph) particles, with U_{ave} = 10 mm/s and at time 24, 20 and 16 s, respectively. Steady clear flow results are presented with dash lines for reference. This figure clearly depicts the effect of changing the number of flowing particles on the bulk and surface temperatures along the channel. The right most particle in all cases has the most impact on the bulk temperature distribution and, as expected, the peak temperature around this particle shows almost identical values for all three cases. Notice the first (right most) trough present in the surface temperature distribution is a direct result of the sweeping convection.

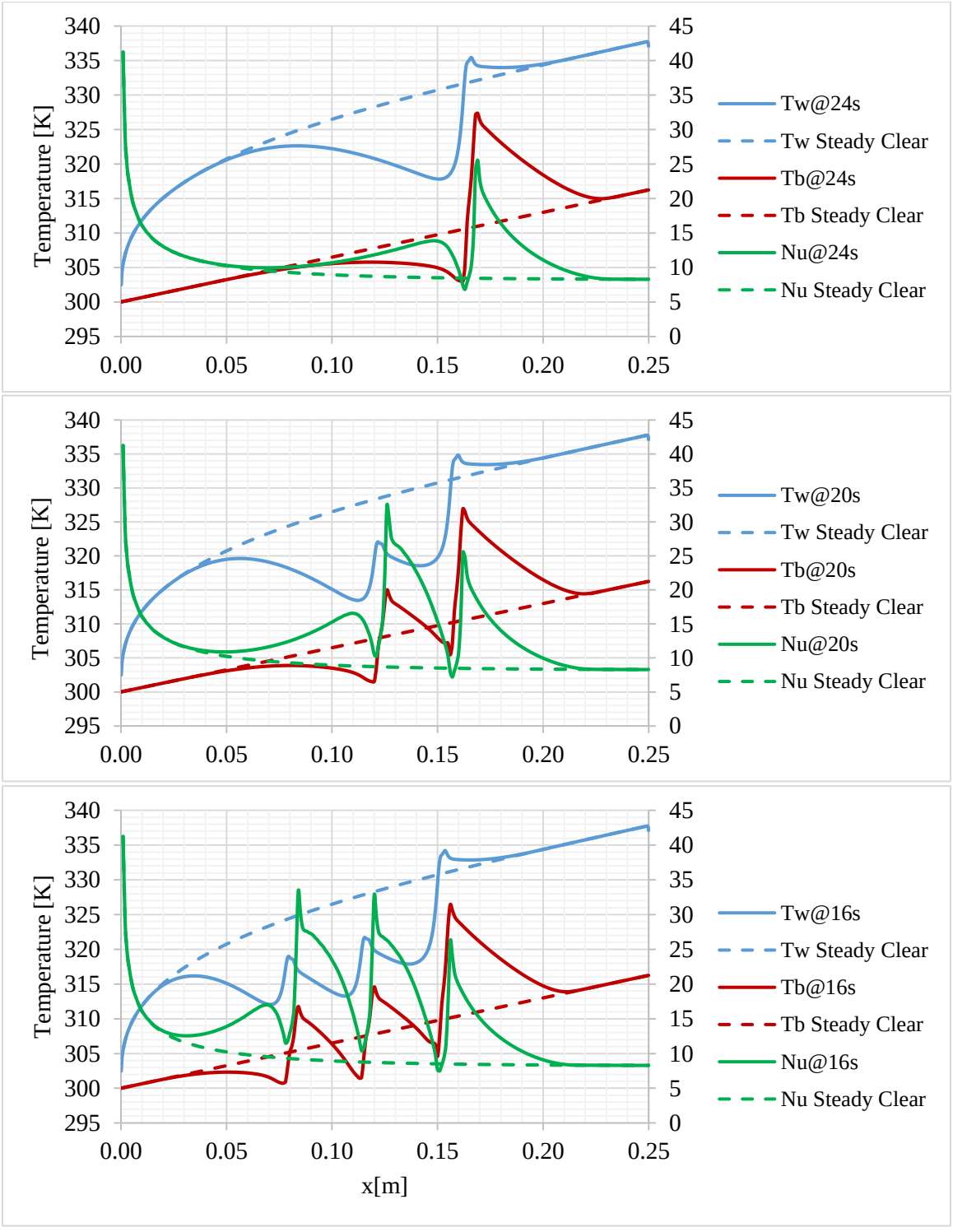

Fig. 3.28 Surface and bulk temperatures (left vertical axis) and Nusselt number (right vertical axis) along the heated section for one (upper graph), two (middle graph) and three (lower graph) particles with U_{ave} = 10 mm/s

In fact, every T_b trough is followed by a T_w trough in T_w, a desirable characteristic of particle flow in uniform and constant heat flux problem. Observe the second and the third particles cause other troughs of T_w with lower values in comparison to the trough caused by the lead particle. The T_w deviation from the clear fluid case increases by adding more particles and this deviation occurs in a longer length of the channel. Another interesting observation from this figure is the physical meaning of the Nusselt number: at any location where T_b and T_w get close, Nu value rises indicating a more effective convection process being attained (i.e., the fluid is transferring the same heat flux with a smaller surface-bulk temperature difference). Figure 3.28 shows that the addition of more particles, in this case, has a direct positive effect on the Nu deviation (increase) from the clear flow Nu.

Figure 3.29 shows the surface and bulk temperatures (left vertical axis) and Nusselt number (right vertical axis) along the heated section for with U_{ave} = 10 mm/s (upper graph), 20 mm/s (middle graph) and 40 mm/s (bottom graph) at time 16, 8 and 4 s respectively. Steady clear results are also here presented with dash lines for reference. It is well known in steady clear flow the increase of the fluid velocity in the channel enhances the convection heat transfer, increasing the Nu number along the channel. Observe in figure 3.29 the difference between the clear flow T_w and T_b decreases when the fluid speed increases, yielding a higher Nu. The relative (in relation to the clear fluid case) effectiveness of particulate flow then decays as the flow speed increases - note all three graphs have almost the same Nu curve without no significant difference. This behavior is expected when one considers the effect of increasing the fluid speed: a longer entrance length is obtained, with a less pronounced boundary layer effect, reducing the sweeping effect of the particles.

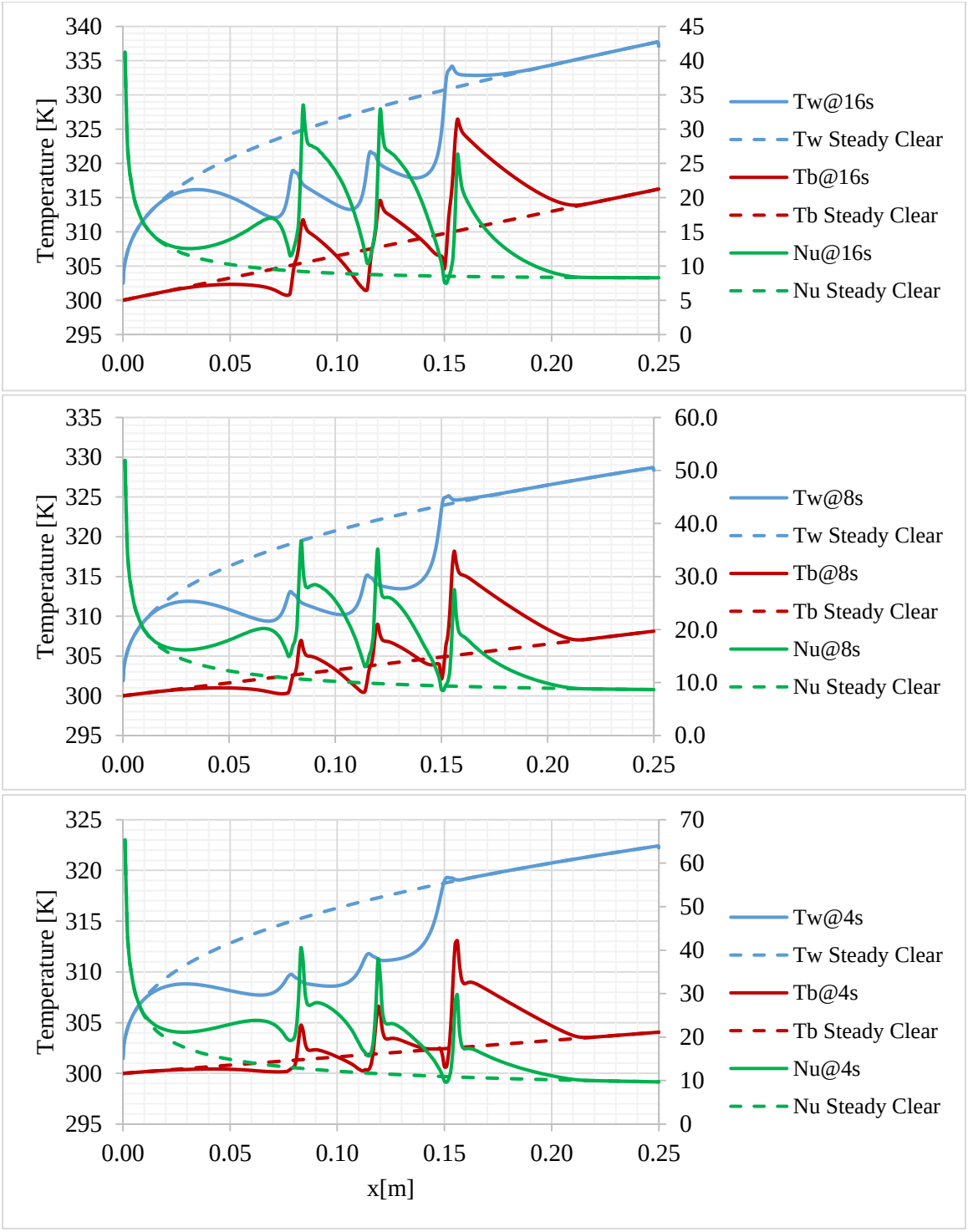

Fig 3.29 Surface and bulk temperatures (left vertical axis) and Nusselt number (right vertical axis) along the heated section for runs with U_{ave} = 10 mm/s (upper graph), 20 mm/s (middle graph) and 40 mm/s (bottom graph)

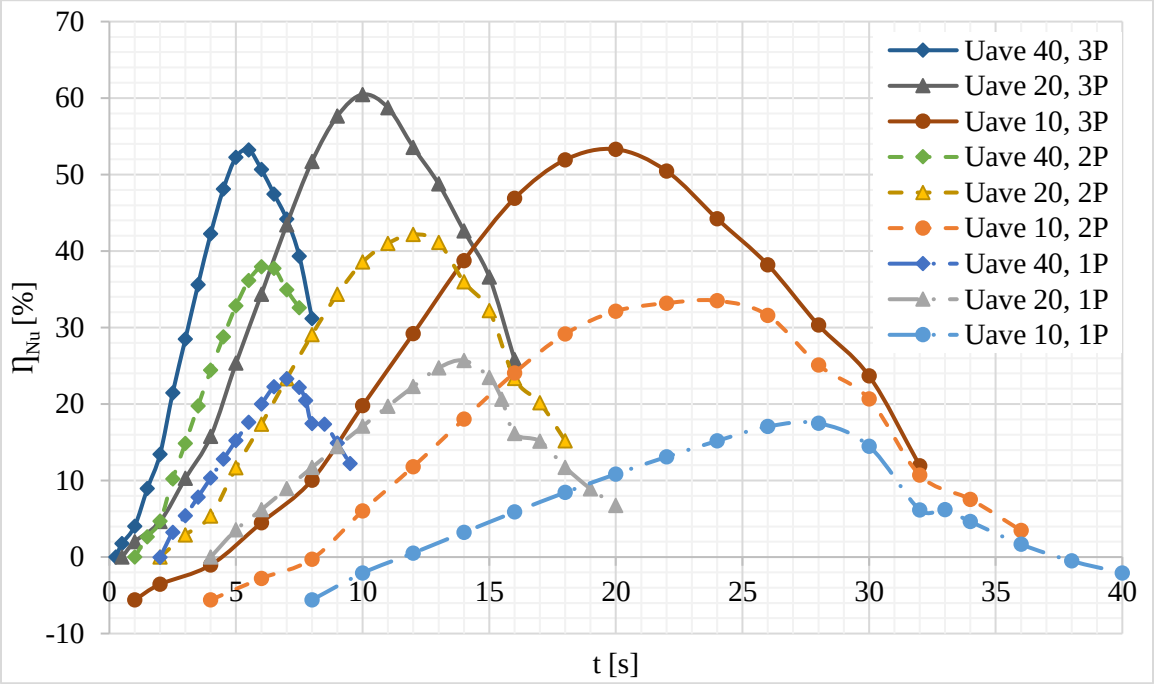

Fig. 3.30 Nusselt efficiency, η_{Nu}, for nine particle cases with one, two or three particles and U_{ave} equal to 40, 20 and 10 mm/s

Figure 3.30 presents nine curves for the Nusselt efficiency, η_{Nu}, versus time for all twelve cases, i.e., nine particle and three clear cases, considered in this section. Due to the use of three different U_{ave} values and different number of particles, the running time of the simulations were not the same. In the three-particle cases with U_{ave} equal to 40, 20 and 10 mm/s, the running times were 8, 16 and 32 s respectively. In the two-particle cases these times increased to 9, 18 and 36 s and for the single particle cases to 10, 20 and 40 s, respectively. The η_{Nu} is calculated using equation 3.7 to compare Nusselt values of each particle case with the corresponding steady state clear case. All the curves in this figure have a similar pattern, increasing in time to a maximum value and then decreasing. The peak value occurs when the rightmost particle approaches to end of the heating section. Observe by increasing the number of particles, the Nusselt efficiency increases. The greatest value among all peaks is 60 % for three-particle case with U_{ave} of 20 mm/s. Among

the two-particle cases, the same U_{ave} has the highest peak value of 42 % and for the single particle cases, the peak value happens again for the same U_{ave} being equal to 26 %.

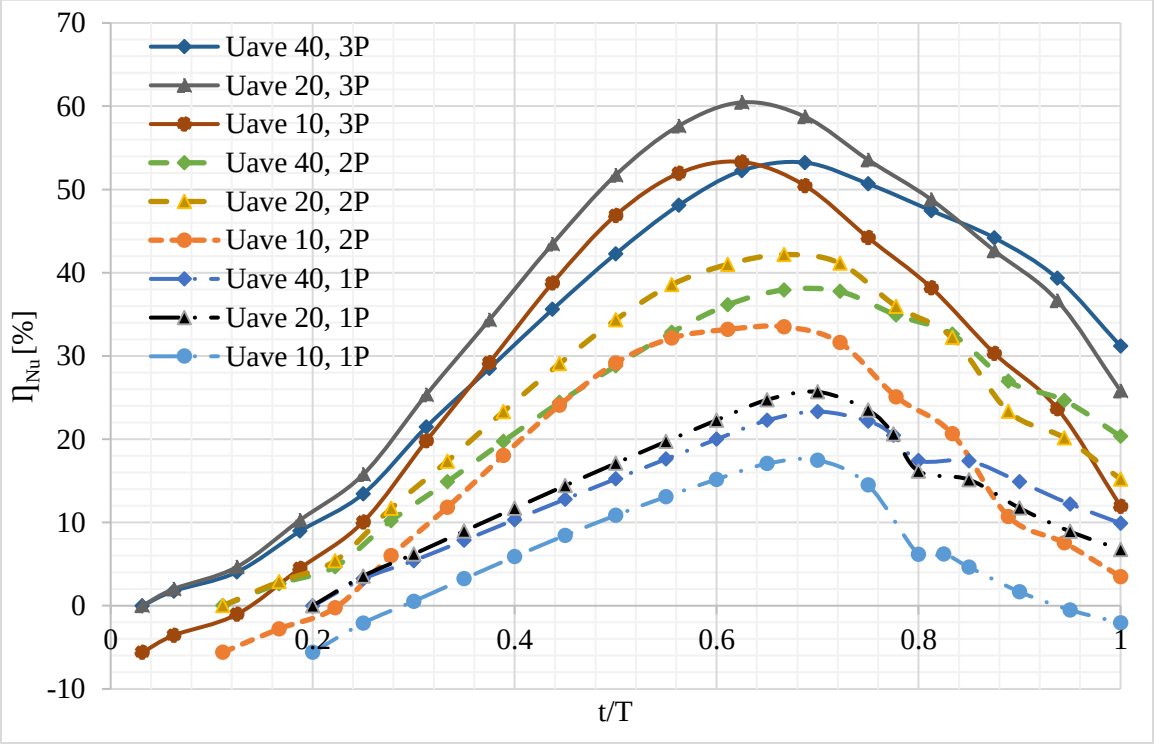

Fig. 3.31 Nusselt efficiency, η_{Nu}, versus nondimensional time for nine particle cases with one, two or three particles and U_{ave} equal to 40, 20 and 10 mm/s

To study all nine particle cases with different U_{ave}, Nusselt efficiency curves are re-plotted versus a nondimensional time, which is obtained by dividing time by the total simulation time of each case. For instance, in the three-particle case with U_{ave} of 40 mm/s, the time during the entire process is divided by 8 s, which is the total simulation time for this case. Consequently, all nine curves can be plotted in a single graph with the nondimensional time spanning from 0 to 1, as shown in figure 3.31. Interestingly, cases with the same number of particles now show close to each other with similar values, pattern and peak locations. Cases with U_{ave} of 20 mm/s, for all number of particles, present the

highest peak values; hence, this speed yields the most efficient sweeping process among the speeds tested here, namely 10, 20 and 40 mm/s. The beneficial effect of adding more particles can be observed clearly in this figure as there are significant increases in the Nusselt efficiency from using one, two and three particles – observe the peaks jump from approximately 26 to 42 to 60 %, respectively.

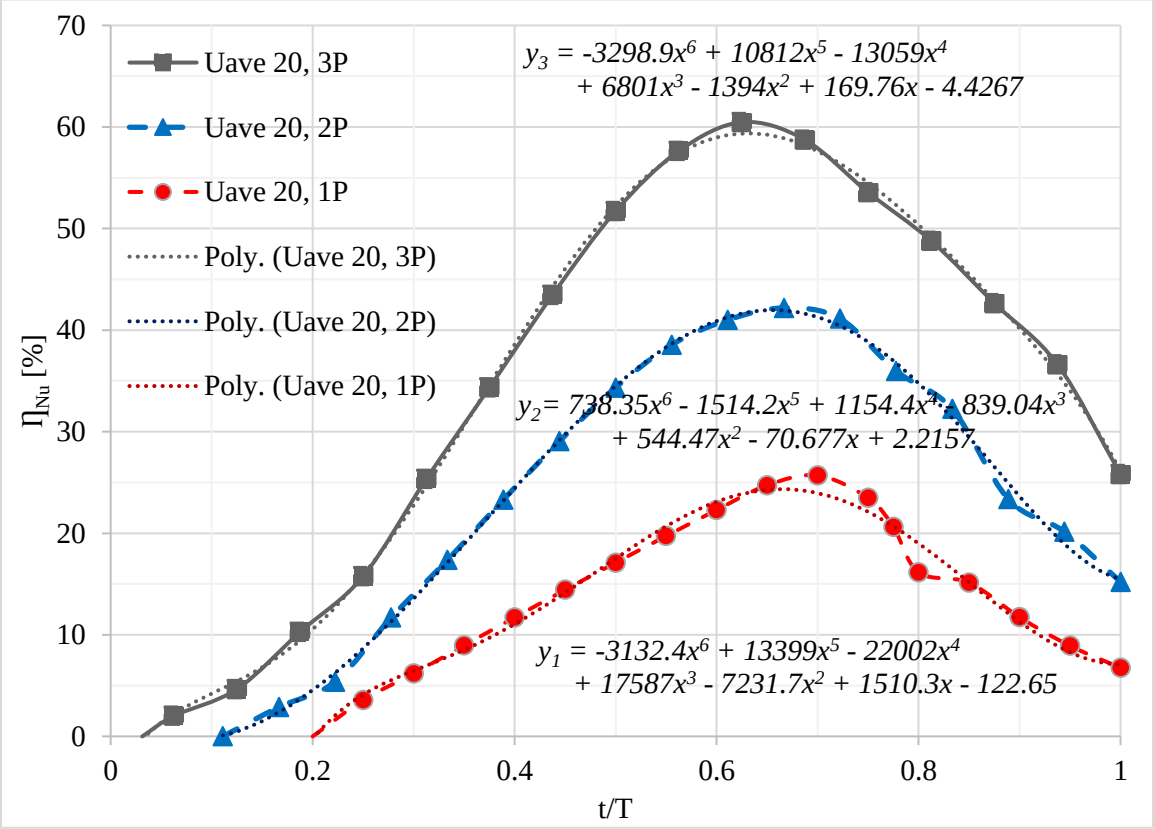

Fig. 3.32 Nusselt efficiency, ηNu, versus nondimensional time for three particle cases with one, two or three particles and U_{ave} equal to 20 mm/s

Figure 3.32 single out the η_{Nu} curves of figure 3.31 for the case of U_{ave} of 20 mm/s, which yields the highest peak values for the efficiency. For each curve, a sixth degree polynomial trendline was fitted and the average value of η_{Nu} was calculated by integration of the trendline equation over the interval [0,1] of the nondimensional time. The average

values obtained are 35 %, 22.6 % and 11.8 % for the three, two and single particle cases respectively. Hence, the three-particle case with U_{ave} of 20 mm/s, is 35 % more efficient than a steady clear flow case with the same conditions, which is a significant improvement in heat transfer efficiency.

3.5.3. Summary and conclusions

In this section, a new computational model was presented with geometry and boundary conditions different from those used in the three previous configurations. This new model is believed to be more akin to practical configurations. The changes include an upstream and a downstream adiabatic channel section, bounding the heated channel section, to allow the observation of the particles entering and leaving the heated section and to alleviate the effect on imposed inlet and outlet boundary conditions in the simulating results of the heating process. Also, the initial condition for the simulation is now that of steady velocity and temperature distributions. This initial condition is aligned with a situation in which fluid flows steadily in a heated channel and then a particle (or more than one) comes and flows through the heated section with the fluid. Again, this more practical configuration is similar to some experimental tests done subsequently and reported in the next chapter. A total of twelve cases were considered here, for clear flow, and particulate flow with one, two and three particles, and three different average inlet speeds. The results indicate an enhancement of the average Nusselt number along the channel of up to 35 % and maximum local Nusselt number of 60 %, obtained using three particles.

3.6. Velocity profile in particle flow

The main purpose of having large (in relation to the channel size) particles flowing with a fluid in a channel, in terms of the convection heat transfer process, is to force a change in the fluid velocity profile. Of course, for this change to be effective in increasing the convection heat transfer, the particles should yield a larger fluid speed near the channel surfaces, larger than the speed otherwise registered when the fluid flows without particles in it. Two important aspects evolve from the aforementioned, namely: (1) the particle surface must be close to the channel surface, and (2) the fluid velocity near the surface should be small. The first aspect argues for particles that are large in relation to the channel dimension, so their surface will be close to the channel surface. One needs to be careful with this though: as the distance between a moving particle and a stationary channel surface decreases, the shear stress between the two increases. This will inevitably lead to higher pump power to sustain the particle flow. The second aspect indicates the presence of particles to be more effective in laminar flow, when the fluid speed is relatively small near a relatively large distance from the channel surface, as compared to turbulent flow. In fact, the ideal case would likely be laminar and fully developed flow, in which case the boundary layer occupies the entire channel cross section. In this case, any particle capable of yielding a high fluid speed near the channel surface would cause an enhanced convection heat transfer process.

As an example, figure 3.33 shows a series of fluid velocity profiles on different cross sections along a flow channel, for a Newtonian and incompressible fluid (constant and uniform properties) flowing steadily. The profiles are upstream, downstream and

around the position of a circular solid and impermeable particle that flows with the fluid, with same density as the fluid density. All these profiles are drawn at the same time. This figure is built as if one had taken a single shot of the flow, identifying the fluid velocity profile at different locations along the channel. Notice this configuration is one in which the fluid has a fully developed profile upstream and downstream of the particle. Observe the leftmost and rightmost fluid velocity profiles in figure 3.33 are parabolic, and don't seem affected by the particle.

The average longitudinal fluid speed in this case is U_{ave} = 0.010 m/s and the maximum velocity is U_{max} = 0.015 m/s, which occurs at the center of the channel when the flow is in the fully developed condition. As one progresses visually in figure 3.33 from upstream to downstream of the particle, the fluid velocity profiles change because of the presence of the particle in the flow. From upstream (left hand side) of the particle, the fully developed (parabolic) flow profile flattens in the center of the channel as one approaches the particle. With the fluid speed getting slower in the center channel region, the fluid must speed up closer to the channel surfaces to maintain mass conservation in every cross section of the channel (steady flow and incompressible fluid), and this is observed with a slight deformation in the velocity distribution of the 3rd profile (from the left).

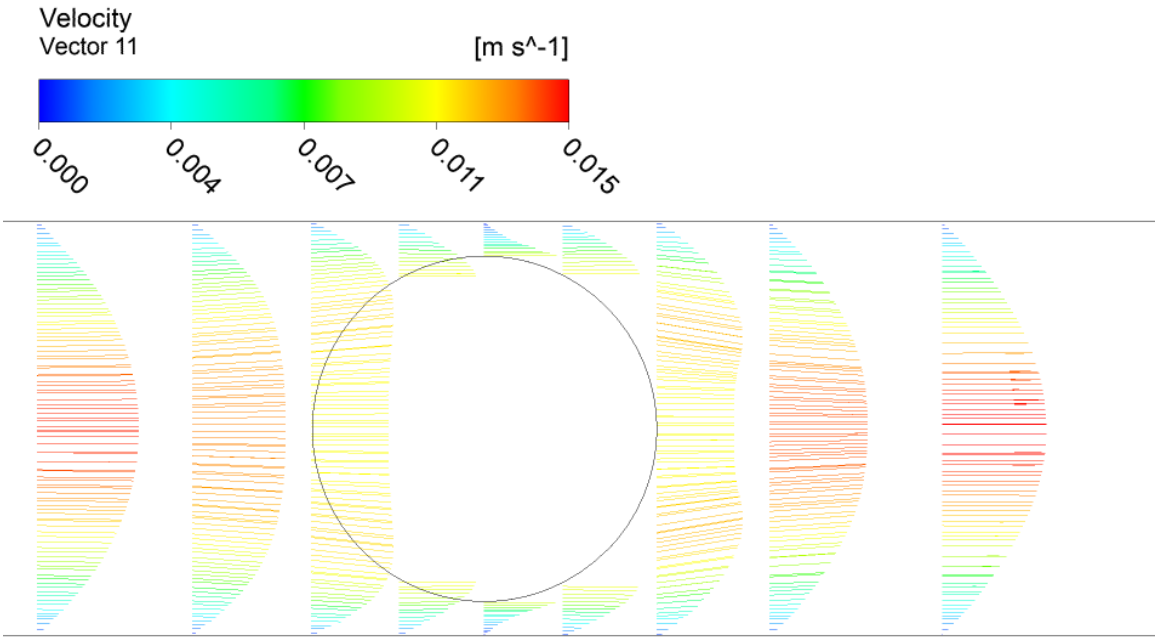

Fig. 3.33 Velocity profiles on different cross sections located upstream, downstream and at the particle location at a specific time

The third profile from the left demarcates the last profile outside the particle from upstream. The next profile to the right does not show the velocity distribution in the region occupied by the particle, because that region has a uniform speed – the particle speed. Observe, nevertheless, how the flow velocity distribution within the gap formed by the channel surface and the particle surface (4^{th}, 5^{th} and 6^{th} profiles) increases as we move to the right in the figure. At the 5^{th} profile, the small gap for fluid to flow shows very high fluid speed (because the gap is at its smallest section). From that section on, the velocity profiles rebuild themselves all to way to the fully developed profile, achieved at the right most 9^{th} profile in the figure. One final observation: see how the profile tangential to the particle upstream (3^{rd} profile) and downstream (7^{th} profile) show the fluid flow (velocity) opening (upstream) and closing (downstream) around the particle. These profiles are

directed toward and away from the channel surfaces, what should definitely affect the convection process in the gap region.

3.6.1. Velocity profile in the gap

The analytical prediction of the fluid velocity at the gap is essential not only for establishing the sweeping effect of the particle but also for gaining confidence on the numerical results reported here. Consider then, for simplicity, the case of a Newtonian and incompressible fluid flowing through a regular parallel plates channel, with the plates H units apart, with cross section averaged fluid speed U_{ave}, and having a square solid particle with side length L_s flowing with it, as shown in figure 3.34. Keep in mind the particle is smaller than the flow channel, maintaining a gap δ from the channel surfaces.

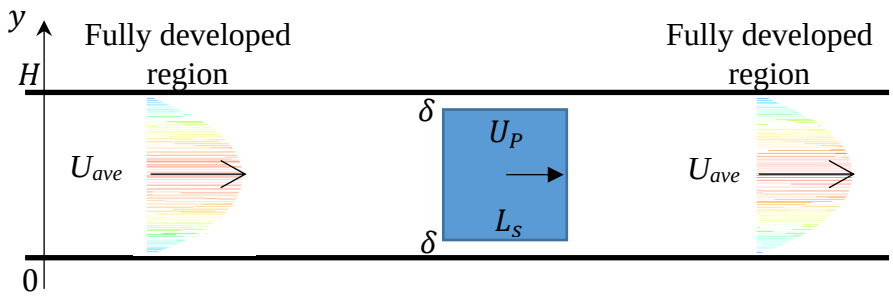

Fig. 3.34 Channel flow of a fluid with solid particle

As shown in figure 3.33, upstream and downstream of the particle the flow is considered steady, laminar and fully developed. In this case, the velocity profile is parabolic, as shown in figure 3.34, namely:

$$u(y) = \frac{6U_{ave}}{H^2} y(H - y) \tag{3.9}$$

Notice the maximum fluid speed in this case, happening at the center of the channel, equals $3U_{ave}/2$. Now, from equation (3.9), one can infer the fluid velocity at a distance δ from the channel surface as

$$u(\delta) = 6U_{ave}\frac{\delta^2}{H^2}\left(\frac{H}{\delta} - 1\right) \tag{3.10}$$

The flow distribution in the gap region, $u(y)$, is similar to the classical Couette flow, as the solid particle moves in relation to the stationary channel surfaces with speed U_P. However, the velocity profile there must satisfy the conservation of mass at any cross section along the channel. In a cross section where the particle is located the speed outside the gap region equals the solid particle speed. Considering the density of the solid particle equal to the density of the flowing fluid, also for simplicity, and the half-channel symmetry, the conservation of mass at a cross section where the particle is located then requires:

$$U_{ave} = \frac{1}{(H/2)}\left[\int_0^{\delta} u(y)dy + \int_{\delta}^{H/2} U_P dy\right] \tag{3.11}$$

Considering the parabolic profile of $u(y)$, i.e., assuming steady, fully developed flow in the gap, together with equation (3.11), and imposing no-slip condition $u(y) = 0$ at $y = 0$ and $u(y) = U_P$ at $y = \delta$, the velocity profile at the gap can be shown to be of the form

$$u(y) = \left[\frac{-3U_P}{\delta^2} + \frac{3H}{\delta^3}(U_P - U_{ave})\right]y^2 + \left[\frac{4U_P}{\delta} - \frac{3H}{\delta^2}(U_P - U_{ave})\right]y \tag{3.12}$$

From equation (3.12), one can deduce the shear stress acting on the solid particle surface, namely

$$\tau_L = \mu\frac{du(y)}{dy}\Big|_{y=\delta} = \mu\left\{2\delta\left[\frac{-3U_P}{\delta^2} + \frac{3H}{\delta^3}(U_P - U_{ave})\right] + \left[\frac{4U_P}{\delta} - \frac{3H}{\delta^2}(U_P - U_{ave})\right]\right\} \tag{3.13}$$

Now, a force balance in the longitudinal flow direction on the solid particle yields:

$$\Delta p A_p = 2\tau_L A_s \tag{3.14}$$

where ΔP is the difference between upstream and downstream pressures acting of the face of the solid particle area $A_p = (H - 2\delta)z$, and the surface area where the shear stress acts is the particle surface $A_s = L_s z$. Re-writing equation (3.14) using $\Delta P/L_s = -dp/dx = 12\mu U_{ave}/H^2$,

$$\frac{12\mu U_{ave}}{H^2} = \frac{2\tau_L}{(H-2\delta)} \tag{3.15}$$

Combining equations (3.13) and (3.15),

$$\left[\frac{6(H-2\delta)}{H^2} + \frac{3H}{\delta^2}\right] U_{ave} = \left(\frac{3H}{\delta^2} - \frac{2}{\delta}\right) U_P \tag{3.16}$$

Now, consider again the numerical results obtained in relation to figure 3.33, for which $H = 0.0048$ m, $\delta = 0.0004$ m, and $U_{ave} = 0.010$ m/s, then the particle speed must equal $U_P = 1.071 U_{ave} = 0.01071$ m/s.

Figure 3.35 shows a zoomed in version of figure 3.33, focusing on the fluid velocity distribution at the gap between the particle and the upper channel surface. Indicated in the figure, by the downward arrow, is the fluid speed at the fluid-particle interface, that is $u(\delta) = 0.01113$ m/s. Per the no-slip condition, this must also be the particle speed. Observe the difference between the numeric $u(\delta)$ value of the particle speed and the analytically predicted particle speed U_P is a mere 3.8 %, which is remarkable, and it helps validate the numerical predictions.

Now, included also in figure 3.35, overlapping the numerically obtained fluid profile at the gap, is the fully developed fluid velocity profile – the profile that would exist

there if the particle where not present. Using the velocity distribution for fully developed flow, equation (3.9), one obtains the fluid speed at a distance δ from the channel surface as $u(\delta) = 0.00458$ m/s, indicated in the figure by the upward arrow. Then, the particle speed, or the maximum speed at the gap, is a whopping 2.43 times greater than the fluid speed at the same location if the particle were not there. This is an example of the quantitative effect of the particle flowing with the fluid – this is the sweeping effect!

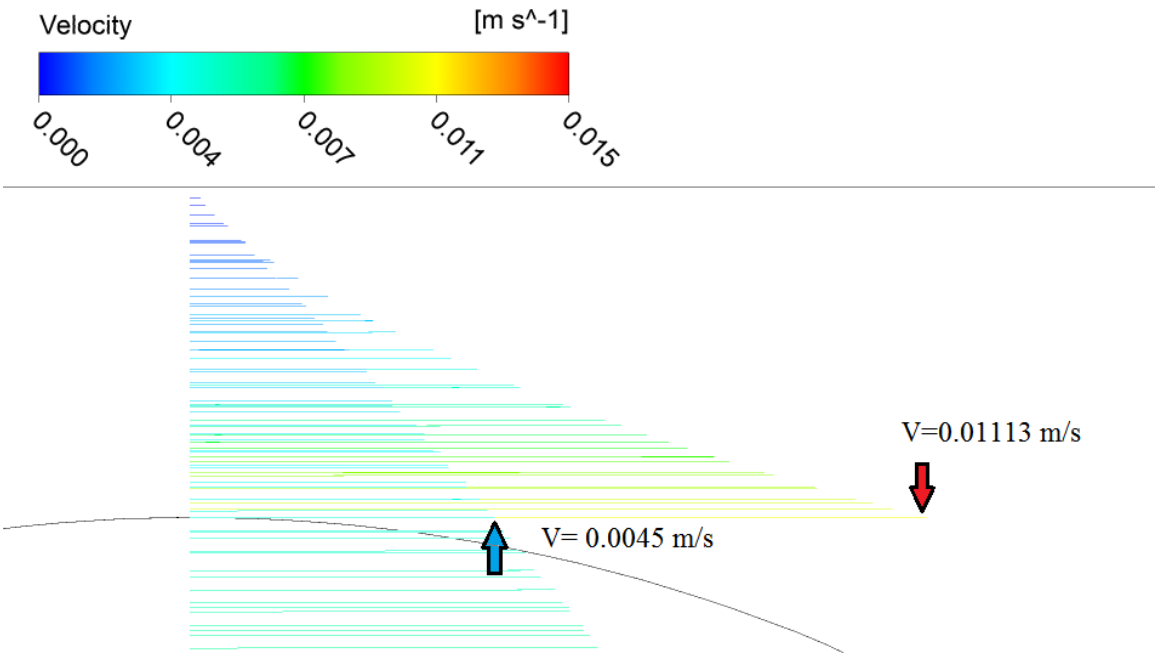

Fig. 3.35 Overlap of the fully developed profile and the velocity profile at the gap between the particle and the channel upper surface

An additional validation of the numerical results is presented in figure 3.36 for the same cross section, at the middle of the particle, and the same flow conditions. The circles denote numerical results obtained with the moving-mesh method. Overlapping these results is a continuous line, representing the results obtained via immersed-solid method (in which case the simulation resolves the solid speed as well). The matching between the

two results is noteworthy. Finally, the triangles show superimposed in the figure the fully developed velocity profile obtained numerically, and the continuous line shows the analytical prediction of the fully developed profile.

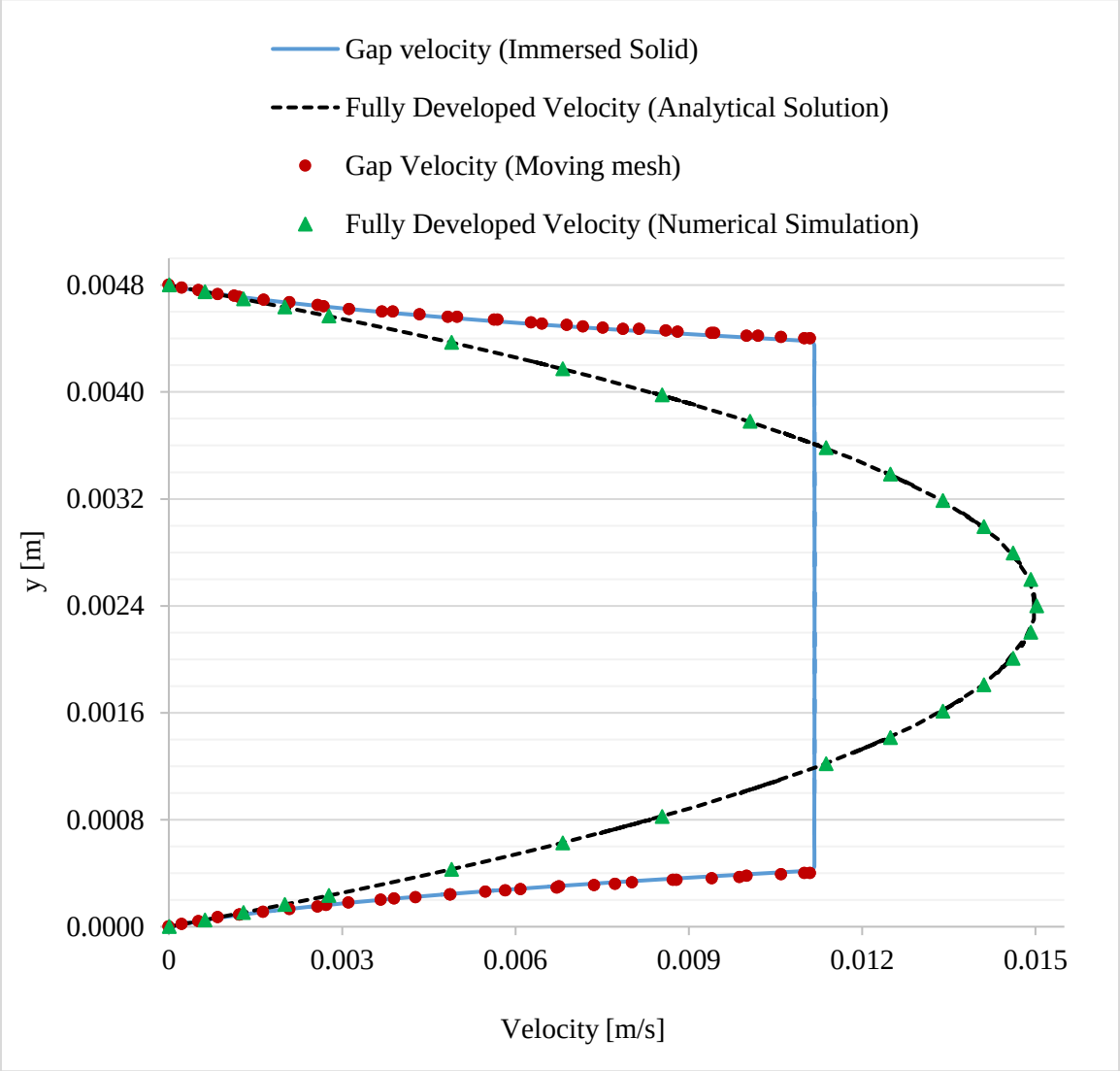

Fig. 3.36 Velocity profiles at a same cross section derived from different methods

One final note about the sweeping effect: the increase in fluid speed at the gap caused by the particle not only leads to an increase in the local heat transfer coefficient, but also to an increase in the local friction coefficient due to the increase in the velocity gradient

at the channel surface. This increase, however, for being localized at the gap does not affect the total pressure drop along the channel, as shown previously by the numerical results. This aspect is key to the sweeping convection: convection enhancement at a minimum cost.

3.6.2. Combined speed and temperature sweeping effects

Figure 3.37 shows a time-series of the particle flow, now indicating to the left of the figure the combined velocity and temperature effects, as the particle passes through a selected imaginary cross section of the channel. The thermal effect is clear: the trailing cold fluid behind (upstream) of the particle is the dragging effect. Ahead (downstream) of the particle, the hot fluid swept away by the particle accumulates as it is pushed forward. Observe also, in the velocity profiles, the "jets" ahead of the particle, emanating from the gap by the fluid, are inclined toward the center of the channel, where the hot fluid tends to be driven. The rebuilding of the boundary layer seems clear after the particle moves past the selected cross section. The velocity evolution caused by the particle, shown in detail to the right of the figure, shows precisely all the deformation undergone by the fluid velocity profile: from fully developed profile, to gap profile, and back to the fully developed profile. The squeezing of the flow as it passes through the gap, with the consequent fluid velocity increase, is also evident once more.

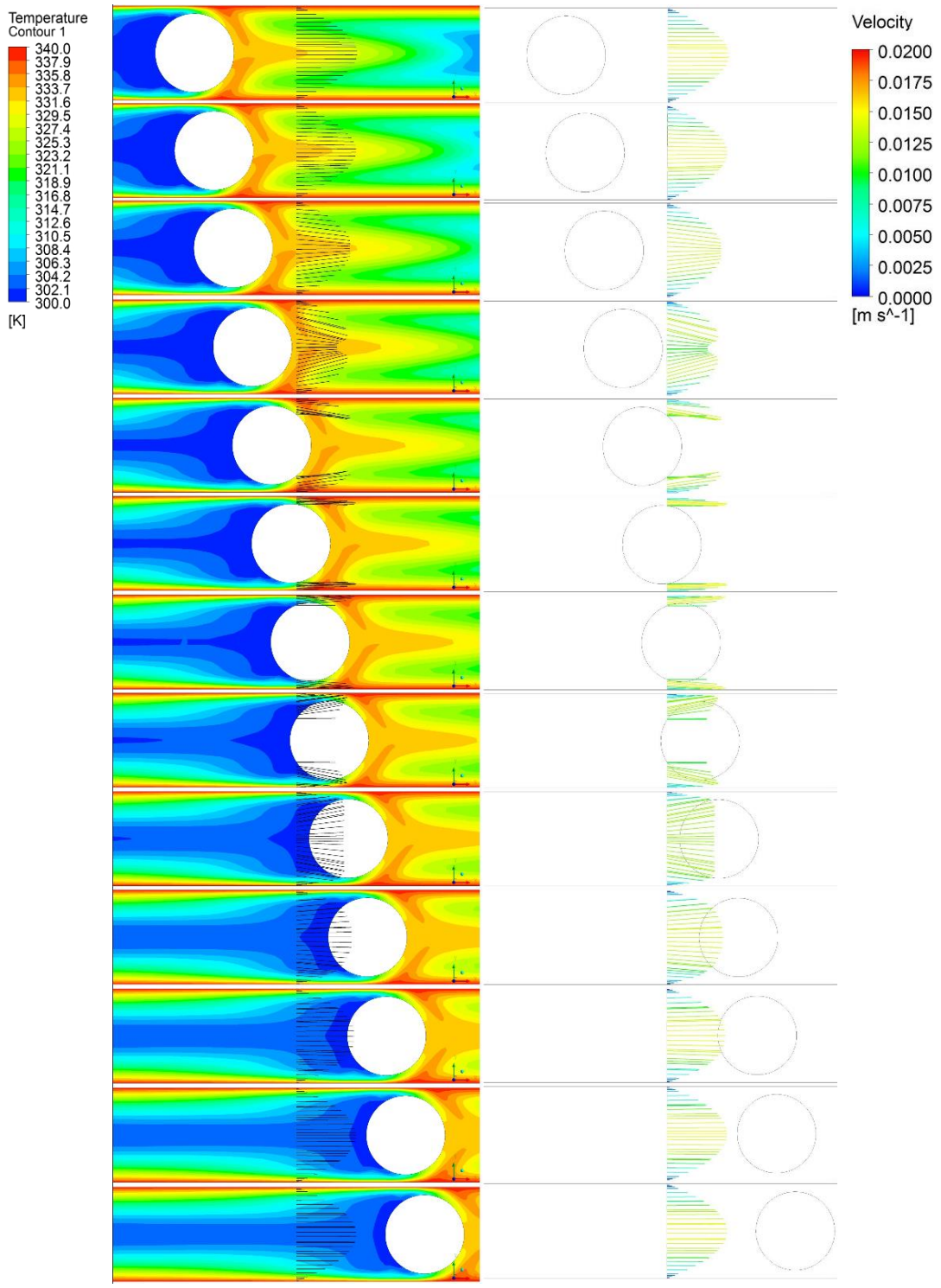

Fig. 3.37 A time series of the particle flow through a channel with temperature contour shown on the left and velocity profiles shown individually on the right

3.7. Non-dimensional study of the sweeping convection

Nondimensionalization is the transformation of a dimensional quantity, having values related to a measuring system, into an equivalent quantity with no related dimension. This transformation is usually obtained by dividing the original quantities by scales, or fixed (usually known) quantities, having the same units of the original quantity. In differential equations, including their boundary and initial conditions, the nondimensionalization process yields not only variables that are nondimensional, but also a reduced set of ruling parameters formed by the combination of the scaling factors used for the nondimensionalization. These parameters present themselves as coefficients of the terms in the differential equations, usually carrying physical meaning. That is, their values usually help predict the relative strength of the terms in the differential equations, allowing one to predict the physical behavior of the modeled system. The combination of the original quantities into a smaller number of coefficients affecting the mathematical results, effectively reduces the number of degrees of freedom one needs to be concerned with. Because the scaling of the original dimensional quantities tends to limit their variability, nondimensionalization can also be advantageous in performing numerical simulations of the differential equations for avoiding the handling of quantities having very diverse values, which can compromise the accuracy and even the convergence of the numerical simulations.

3.7.1. Problem description and modeling

In this section a procedure to obtain a nondimensional model based on the configurations discussed in section 3.2 is presented, with dimensionless form of the governing equations, initial and boundary conditions. Recall the configuration in section

3.2 involves a fully developed flow entering the channel with a constant temperature T_i = 300 K. The velocity profile is parabolic at the inlet, resulting in a maximum velocity of 1.5 U_{ave}. The channel is 200 mm long and 4.8 mm wide, with surfaces subjected to a constant and uniform temperature T_w = 340 K. The particle is adiabatic, and the no-slip boundary condition is applied on its surface as well as the channel surfaces, while zero-Neumann boundary conditions for both velocity and temperature at the outlet are imposed ($\partial u/\partial x = 0$, $\partial T/\partial x = 0$). As initial conditions, at time equal to zero, the entire domain temperature is set to 300 K and the fluid and particle speeds are set to zero.

The dimensionless unsteady incompressible continuity, momentum (for Newtonian fluid) and energy equations, with constant and uniform properties, are then:

$$\nabla .\ \mathbf{u}^* = 0 \tag{3.17}$$

$$\frac{\partial \mathbf{u}^*}{\partial t^*} + (\mathbf{u}^* . \nabla)\ \mathbf{u}^* = -\nabla \mathrm{P}^* + \frac{1}{Re} \nabla^2 \mathbf{u}^* \tag{3.18}$$

$$\frac{\partial \mathrm{T}^*}{\partial t^*} + (\mathbf{u}^* . \nabla)\ \mathrm{T}^* = \frac{1}{Re . Pr} \nabla^2 \mathrm{T}^* \tag{3.19}$$

The nondimensional length and speed in equations (3.17)-(3.19) are based on the channel width, H, and cross section averaged velocity, U_{ave} (so, $\mathbf{x}^* = \frac{\mathbf{x}}{H}$ and $\mathbf{u}^* = \frac{\mathbf{u}}{U_{ave}}$). In equation (3.19), the non-dimensional temperature, T*, is defined as $T^* = \frac{\mathrm{T} - T_i}{T_w - T_i}$, where T is the temperature, T_i in is the inlet bulk temperature and T_w is temperature of the channel surface. Other non-dimensional variables are $\mathrm{P}^* = \frac{\mathrm{P}}{\rho U_{ave}^2}$ and $t^* = \frac{t U_{ave}}{H}$, where ρ is the density of the fluid, P is the pressure and t is the time.

In this nondimensional form, the Reynolds number is based on the channel width and averaged velocity ($Re = \frac{U_{ave}(2H)}{\nu}$). Notice Re = 200 in all simulations reported in this section, while the Prandtl number ($Pr = \frac{\nu}{\alpha}$) is varied between 0.1 and 10. A fully developed (parabolic longitudinal velocity profile) flow with constant temperature, $T_i^* = 0$ enters the channel from the left. The nondimensional channel width and length are set to 1 and 40, respectively. The channel upper and lower surfaces are subjected to constant and uniform temperature $T^* = 1$ while the particle is adiabatic. No-slip boundary conditions are considered on the channel and particle surface, and zero-Neumann boundary conditions for both velocity and temperature at the outlet are set $\frac{\partial \mathbf{u}^*}{\partial \mathbf{x}^*} = 0$ and $\frac{\partial \mathrm{T}^*}{\partial \mathbf{x}^*} = 0$. The nondimensional initial conditions become zero temperature and velocity within the entire domain.

The solution of the new governing equations in non-dimensional form by the same code is easily achieved by matching the coefficients of the corresponding terms between the dimensional and nondimensional sets of balance equation, namely equations (3.1)-(3.3) and equations (3.17)-(3.19), as follows:

$$\mathbf{x}^* = \frac{\mathbf{x}}{H}, H = 1 \rightarrow \mathbf{x}^* = \mathbf{x} \tag{3.20}$$

$$\mathbf{u}^* = \frac{\mathbf{u}}{U_{ave}}, U_{ave} = 1 \rightarrow \mathbf{u}^* = \mathbf{u} \tag{3.21}$$

$$\mathrm{P}^* = \frac{\mathrm{P}}{\rho U_{ave}^2}, U_{ave} = 1, \rho = 1 \rightarrow \mathrm{P}^* = \mathrm{P} \tag{3.22}$$

$$\mathrm{T}^* = \frac{\mathrm{T} - T_i}{T_w - T_i}, T_i = 0,\ T_w = 1 \rightarrow \mathrm{T}^* = \mathrm{T} \tag{3.23}$$

$$t^* = \frac{tU_{ave}}{H}, U_{ave} = 1, H = 1 \rightarrow \mathrm{t}^* = \mathrm{t} \tag{3.24}$$

$$Re = \frac{U_{ave}(2H)}{\nu}, \nu = 0.01 \rightarrow Re = 200 \tag{3.25}$$

$$Pr = \frac{\nu}{\alpha}, \nu = \alpha = 0.01 \rightarrow Pr = 1 \quad (3.26)$$

$$\alpha = \frac{k}{\rho c_p} = 0.01, \rho = 1 \rightarrow \frac{k}{c_p} = 0.01 \quad (3.27)$$

$$q''^{*} = \frac{q''(2H)}{k(T_w - T_i)} = 1 \quad (3.28)$$

Equations 3.20-3.28 convert the dimensional solution into a non-dimensional one. For instance, for a case with desired Re = 200 and Pr = 1, one needs to input H = 1 m, U_{ave} = 1 m/s, ρ = 1 kg/m^3, ν = 0.01 m^2/s, T_i = 0 and T_w = 1 K, α = 1 m^2/s (by keeping the ratio of k, thermal conductivity, and c_p, specific heat capacity, as unity).

3.7.2. Results

Figure 3.38 shows the time evolution of the convection process for the particle and clear flow cases with Re = 200 and Pr = 0.1, 1 and 10. Keep in mind the particle is the same large particle used previously. It is well known a decrease in Pr yields a thicker thermal boundary layer, and consequently a shorter entrance length. For an isothermal channel, this means the fluid temperature reaches the surface temperature within a short distance from the inlet, from this point on the heat transfer process ceases. Hence, the sweeping convection would become increasingly ineffective as Pr increases because most of the fluid in the channel would quickly reach thermal equilibrium with the channel surfaces. The most a particle could do in this case would be to drag cold fluid deeper into the channel, and even this effect is likely restricted to a short distance. These observations are corroborated by the graphs shown in figure 3.38, where the sweeping effect by the particle is clear in the case of Pr = 10, but not so much for Pr = 1, and almost non-observable when Pr = 0.1.

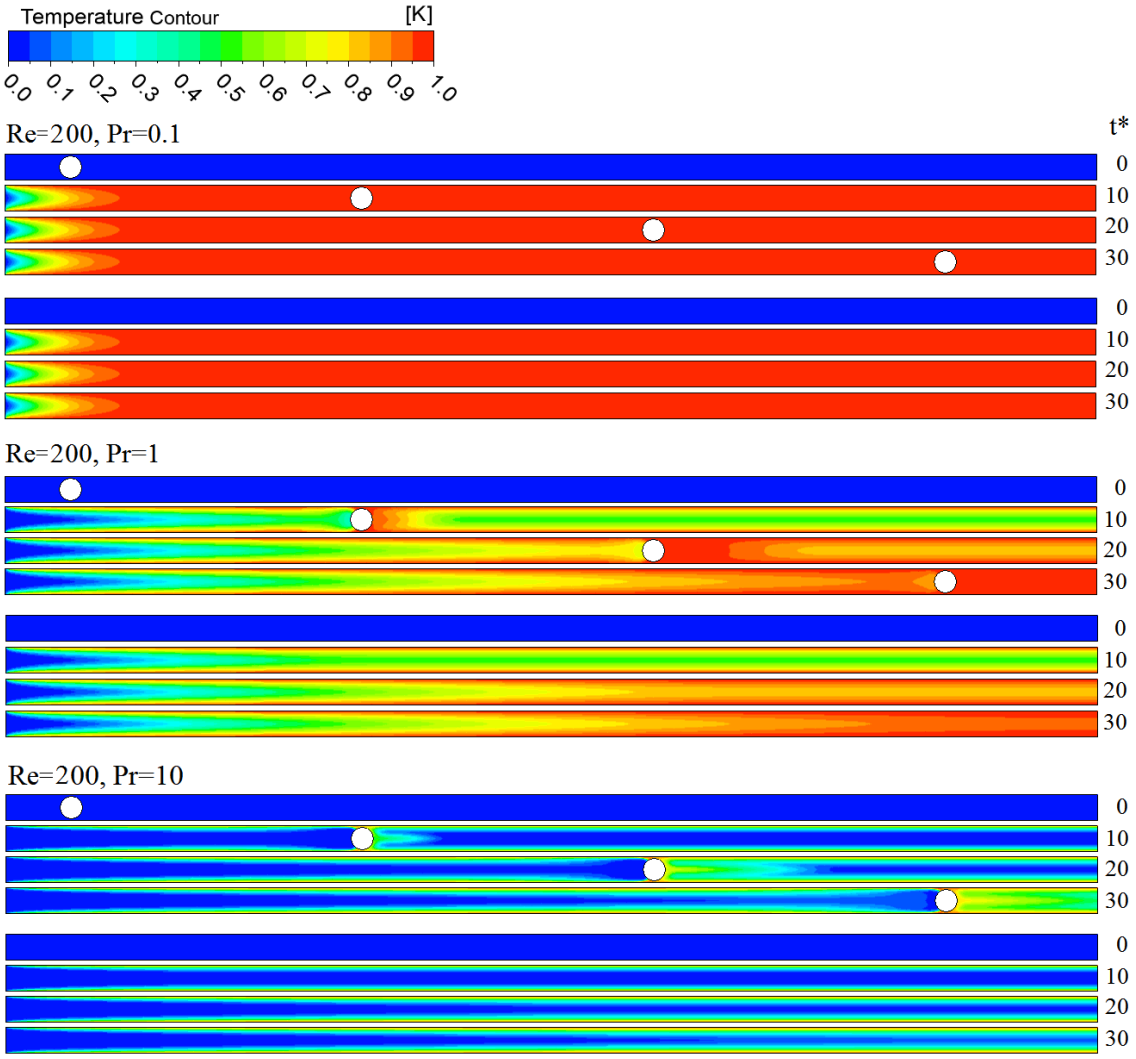

Fig. 3.38 Time evolution of convection by fluid with large particle for non-dimensional cases with Re = 200 and Pr = 0.1, 1 and 10

As expected, the effect of the particle on sweeping thermal boundary layer in non-dimensional terms is the same as in dimensional terms, suggesting the heat transfer improvement observed in previous dimensional results is not limited to the specific flow conditions used in the dimensional simulations.

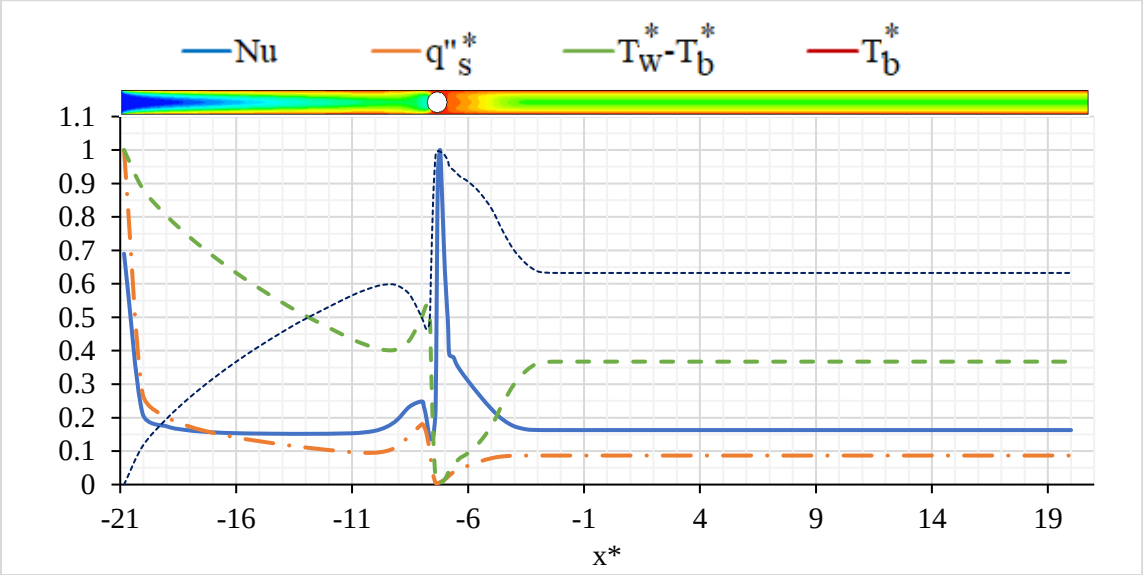

Fig. 3.39 Normalized values of heat flux, bulk temperature, wall and bulk temperature difference and Nusselt number plots along the channel length at t* = 10

Figure 3.39 depicts curves of Nusselt number, surface heat flux, bulk temperature and difference between bulk and surface temperature along the channel with Re = 200 and Pr = 1 at t* = 10. Nusselt and heat flux curves are scaled by dividing the values by their maxima (respectively, 49.82 and 17.19) to show all curves within the same vertical range. The sharp peak of the Nusselt curve at the particle location is due to a very small difference between bulk and surface temperature at the gap between the particle and the heated surface. Recall for an adiabatic particle a higher T_b ensues at a cross section where the flow gap is small, yielding a sharp Nu. These sharp peaks have been eliminated in the previous dimensional cases to facilitate the reading of the graphical results (see section 3.4 and 3.5). Another important observation for the isothermal channel case is the heat flux represent the heat transfer improvement better than Nu. In figure 3.39, note the Nu curve has two peaks, one upstream and another downstream of the particle while the heat flux curve has one peak upstream and a trough downstream of the particle. Consequently,

integrating the Nu curve along the channel shows a stronger convection improvement when compared to integrating the heat flux curve (i.e. $\Gamma_{Nu} > \Gamma_{HF}$). Recall the main purpose in a heat transfer improvement by the particles in the isothermal channel case is to increase the heat flux crossing the channel surfaces (and transported by the fluid) with the same surface temperature as compared to the clear flow case.

The local, instantaneous effect of the flowing particle is shown in figure 3.40, where the calculated non-dimensional heat flux from the channel surfaces is plotted along the channel at 4 different times for Re = 200 and Pr = 1. For this flow condition it can be observed the heat flux increases upstream of the particle, decaying as time goes by, while the negative effect of the particle on the heat flux, due to warm fluid collection in front of the particle, reduces in intensity but it spreads out in length.

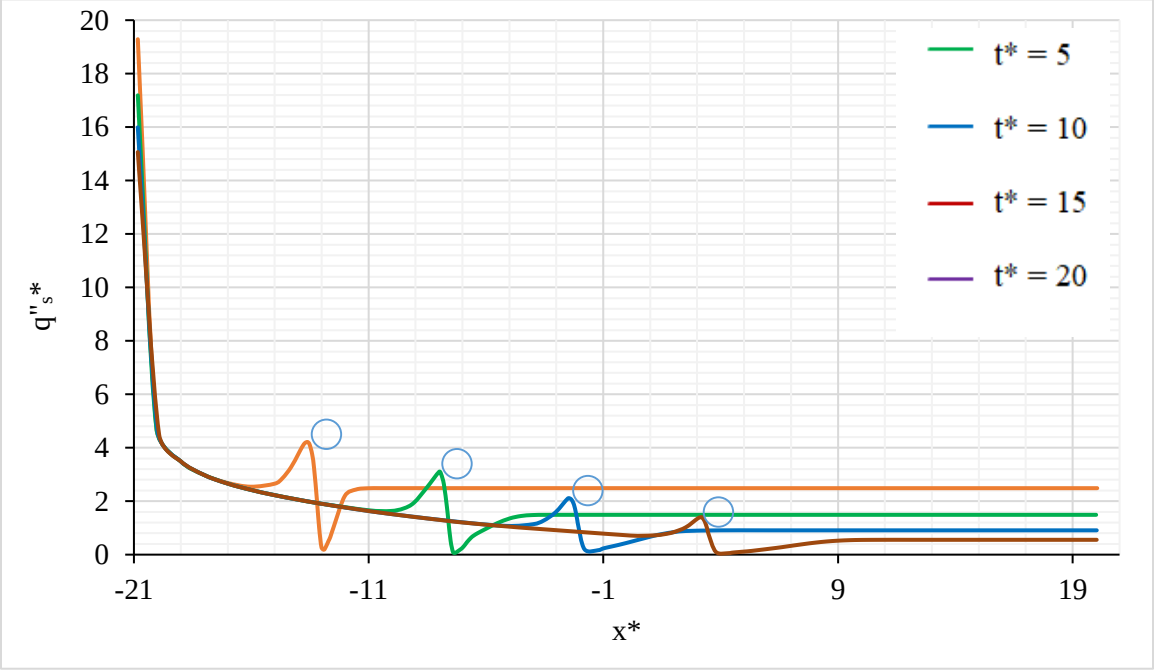

Fig. 3.40 Non-dimensional heat flux curves along the channel for different times

Figure 3.41 presents Nu curves along the channel through time. Observe the positive effect of the particle is reflected in Nu increasing in time, with the increase occurring upstream and downstream of the particle. The apparent anomaly shown in the Nu results is due to the smaller difference between T_w and T_b downstream of the particle.

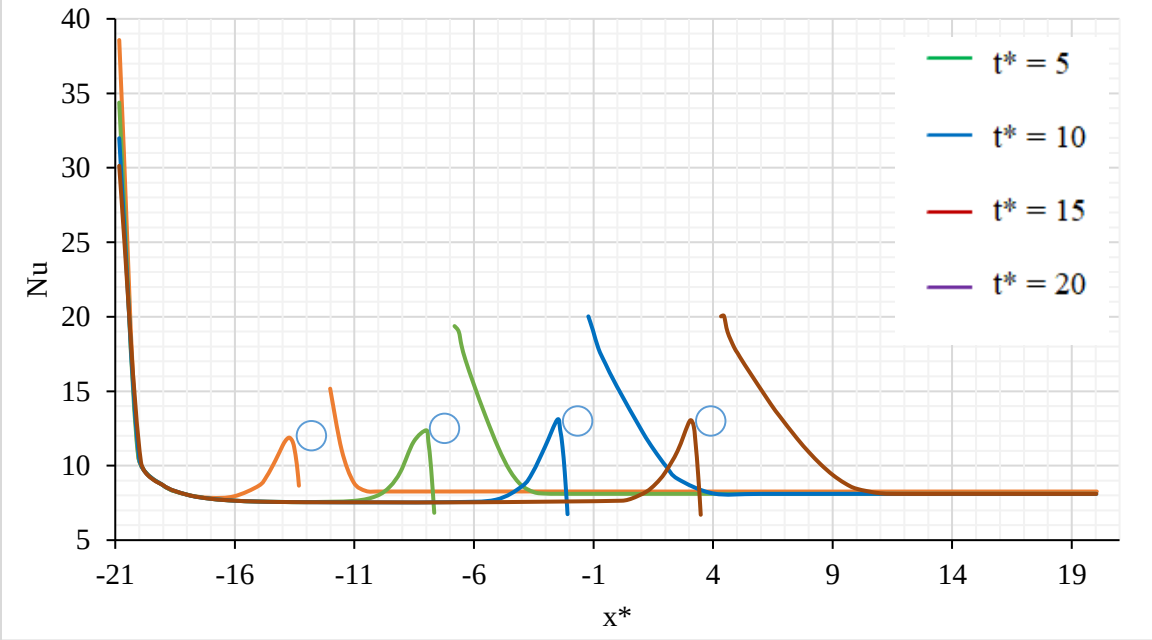

Fig. 3.41 Nusselt number curves along the channel for different times

3.7.3. Summary and conclusions

In this section a procedure to obtain a nondimensional model based on the configuration discussed in section 3.2, with non-dimensional governing equations, initial and boundary conditions, is presented. The main purpose is to broaden the applicability of the code for simulating the sweeping process, and to show indeed the nondimensional results are equivalent to the dimensional results. Also, additional results for the case of varying the fluid Pr are presented and the effect on the sweeping convection and on surface heat flux and Nu discussed.

3.8. Conclusions

The numerical simulations conducted in this project were discussed in this chapter. The strategy behind the numerical simulation part of this research was to begin with the simplest configuration possible, develop the corresponding numerical model, overcome programming difficulties and obtain reliable simulations to then pursue more complicated configurations. Simulations included particle flow and clear flow in a straight heated channel with constant surface temperature or heat flux. Two different methods were utilized to simulate the flow of the particle with the fluid, namely: moving mesh and immersed solid. In all cases the main objectives were first to understand the effect of particle motion within the fluid on heat transfer, and second to provide a tool to quantify the heat transfer improvement as compared to the clear flow case. Although the majority of the simulations were done in dimensional form, a simple case was included and modeled and solved in nondimensional form.

Based on the results from different cases, the three-particle case with U_{ave} of 20 mm/s (Re = 282, Pr = 6.13), is 35 % more efficient than a clear flow case with the same conditions, which is a significant improvement in heat transfer efficiency, all with minimum pressure drop. This shows the potential practical application of sweeping convection.

Chapter 4

EXPERIMENTAL STUDY

4.1. Introduction

As stated in the previous chapters, a flow of particles with a cooling fluid through a heated channel is considered in this study. It is worth mentioning, the transport of particles is not the main objective of the transport process. The particles are included in the flow to enhance the convective energy transport of the fluid by sweeping the thermal boundary layer along the flow channel, which is achieved by the solid particles providing higher velocity adjacent to the channel surfaces. The heat transfer improvement by sweeping convection, and other nuances, were discussed in chapter 3 using results obtained via numerical simulations. While the focus of the present study is on numerical simulation results, an experimental attempt to simulate sweeping convection is presented and discussed here. An experimental setup and its utilization was pursued for two main reasons: first, to verify, at least qualitatively, the numerical simulation results; and, second, to investigate the suitability and effectiveness of the sweeping convection idea in a heat exchanger. Hence, this chapter provides a detailed description of the experimental setup development for a particulate flow circulation system, its main characterizations and challenges, as well as obtained results and their comparison with results obtained

numerically. A very important outcome of this chapter (and of the experimental effort) is to show the sweeping convection idea to be not only a theoretical concept but also, and more importantly, an idea of practical relevance to many areas of engineering where heat exchange by convection via liquid flow is of importance.

4.2. Vortex pump-reservoir system development

There are three important technical challenges that are relatively difficult to resolve when attempting to build a liquid flow system with large particles (in respect to the flow channel) included in it. The first challenge is related to particle clogging along the flow system, a common phenomenon observed particularly around channel constrictions (e.g., at the inlet of a pump or at the transition from a reservoir to a narrow channel). The clogging is caused primarily by the competition between particles trying to enter the constriction section at the same time. The second challenge has to do with the settling of particles in the flow system, due to gravity, particularly in large regions where the flow speed tends to weaken because of the large available area (e.g., reservoirs). The settling issue becomes more dramatic as the density of the particles increase in relation to the density of the flowing fluid. Observe these two challenges have one common characteristic: the agglomeration of particles in the flow. The third and last technical challenge is the pumping of the fluid-particles medium through the flow system. The utilization of regular pumps (e.g., centrifugal pump) is problematic in this case as the pump impeller and casing can not only be damaged by, but can also damage the particles.

Previous preliminary attempts, by our research group, to operate a flow system with a liquid flowing with large particles have led to an ingenious solution, Hassanipour and Lage [26], to overcome the clogging, settling and pumping challenges. The solution

is based on using an impeller inside a reservoir to generate a vortex directed to a suction line of the flow system. The vortex creates a low pressure at the center, sucking the fluid and the particles toward it. Notice the particles need not to flow through the impeller, which is protected by a net permeable to the fluid only. Avoiding contact between the particles and the moving impeller resolves the pumping issue. The same vortex created by the impeller forces the particles to maintain a relatively uniform distribution in the available flow region, avoiding at the same time the settling and the clogging issues. Finally, the flow rate of the fluid-particle medium can be controlled easily by changing the impeller rotational speed.

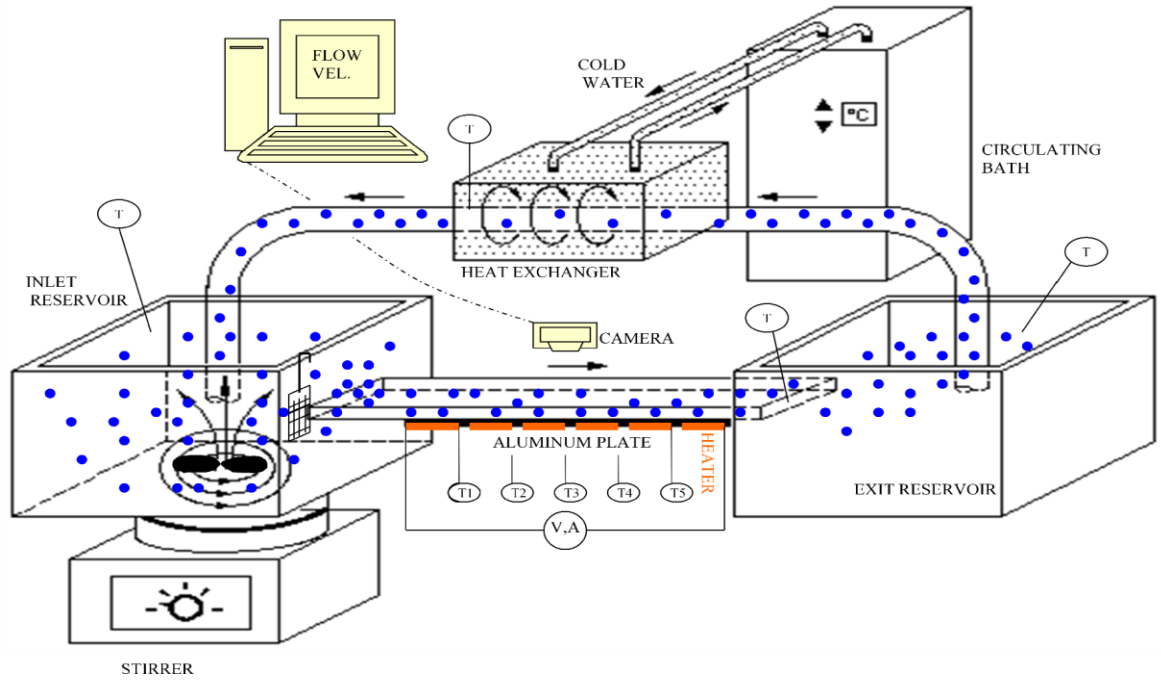

Fig. 4.1 Sketch of the original experimental set-up [26]

Although successful in hindering the clogging, settling and pumping issues, the previous flow system had a few limitations. Generating the circular vortex inside a

rectangular reservoir (figure 4.1, left) limited the strength of the induced flow rate through the test channel. Another limitation was caused by the magnetic coupling mechanism chosen to transfer rotational motion from an external magnetic motor to the impeller inside the reservoir. This inductive power transmission required the impeller to sit flush with the bottom of the reservoir, limiting not only the type of impeller to be used but also the strength of the resulting flow (the resulting flow near the impeller in this scenario was radial).

The flow design of figure 4.1 provided a robust flow system to study the sweeping effect of several particles flowing with a liquid through a rectangular (parallel plates) wide channel. Although the gap between the top and bottom surfaces of the rectangular channel was only slightly larger than the particles diameter, providing for a snug particle flow through the channel, the wide characteristic of the channel hindered a very strong sweeping effect by each particle. Restricting the particles to sweep only a very small portion of the existing boundary layers in the channel, this design is not useful for investigating the full sweeping effect that would otherwise result from a single particle (or train of particles) flowing through a circular channel. Furthermore, the rectangular wide channel allows the particles to flow freely not only in the longitudinal direction of the channel but also in the perpendicular direction to the flow. Hence, particles could align themselves side-by-side in the direction perpendicular to the flow, possibly affecting (competing) with each other's sweeping mechanism. Notice, on the other hand, the wide rectangular channel was a good choice when considering the relatively weak flow strength generated by the vortex because of the small pressure-drop imposed along this channel.

In an attempt to improve the experimental investigation of sweep convection, a new flow circulation system was conceived. The main objective was to improve the design discussed earlier and to resolve some of its main issues. The first consideration was to have the wide rectangular channel, where the heating test took place, replaced by a circular tube, dimensioned to provide a snug fitting all around the passing particles. The circular channel does not allow the particles to flow side-by-side, avoiding any possible competing effect. Also, the proximity of the particles to the channel surface all around their circumference should yield a much stronger sweeping effect. On the other hand, a circular channel is expected to yield increased frictional resistance (i.e., pressure-drop) inside the channel. The second consideration was then to design a more effective pumping mechanism, i.e., a new way to generate a strong vortex with a significant pressure difference capable of maintaining the fluid-particles flow through the system. To this end, the previous inductive power transmission design was replaced with a direct torque transmission from an AC motor to the impeller via a shaft. To expedite the development process, an AC motor and mechanical parts of a commercial blender was used. The third consideration was to replace the rectangular container, where the vortex was created, by a cylindrical reservoir designed to better accommodate the generated (circular) vortex reducing the flow resistance imposed by the reservoir geometry. This reservoir was then placed on top of the new rotary impeller system. Finally, the exit reservoir was eliminated in the present design, as the circular pipe channel allows for a direct recirculating system. The resulting experimental apparatus is presented next.

4.3. Experimental setup

The main component of the experimental set-up is the test section, which in the present design is a straight circular copper tube, as shown in figure 4.2. The 26 ± 0.1 cm long and 6.3±0.1 mm diameter (length about 46 D) tube, is covered by a 25 ± 0.1 cm long flexible electric heater (Minco HK5167R264L12) with resistance of 276 ± 1 Ω. The heater is tightly attached to the surface of the copper tube to provide a heat flux as uniform as possible. A one-inch fiber insulation layer is placed around the heater to reduce heat loss (the maximum heat loss through the insulation was estimated analytically at less than 8% of the dissipated heat). The maximum available heat flux through the tube wall is 9,000 ± 100 W/m^2 which can be adjusted by varying the voltage of the heater with a powerstat (Superelectric-116B) variable transformer. Nine type-E thermocouples, with 0.05 mm diameter, were uniformly distributed along the length of the heated tube surface, (30 ± 0.2 mm apart) placed as close as possible to the inner tube surface of the channel to monitor the surface temperature. The first thermocouple (T1) was placed 5 mm from the inlet of the heating tube, while the last (T9) was placed 24.5 cm from it. Two additional type-E thermocouples are placed at the inlet and outlet of the tube to estimate the fluid inlet and outlet temperatures.

Fig. 4.2 Sketch of test channel (heated section) with flowing particles

Spherical plastic particles with 5.9 ± 0.1 mm diameter and 1,100 ± 50 kg/m^3 density, flow with water through the test tube. Notice the particle diameter was slightly less than the tube diameter leading to a very small gap of only 0.2 mm between the particles surface and the tube internal surface. The test copper tube connects to the pumping component of the flow system, as shown in figure 4.3, via transparent flexible tubes of same diameter. The pumping component is made of a basic impeller centered at the bottom of a cylindrical reservoir, with 33 mm diameter and 8 mm height. When rotating, the impeller creates a large primary vortex that fills the entire circular reservoir. At the top of the impeller a flexible tube brings the water and particles into the reservoir via the suction produced by the depression inside the vortex. Once flowing downwards through the center of the main vortex, the flow reaches the bottom of the reservoir, where the water and the particles are pushed radially to engage in a secondary vortex (similar to Taylor vortices), circulate along and up the reservoir wall, eventually reaching the outlet side opening, which leads to the heated test section (the copper tube).

Preliminary flow tests were conducted without particles added to the flow of water. A paddle flow meter was placed into the flexible tube leading to the test section to measure the water flow rate. This flow rate was then correlated to the voltage applied to the motor linked to the impeller. This approach provided an estimate of the flow rate obtained by the impeller, once the voltage to the impeller motor is known. Using a non-contact digital laser tachometer, the impeller rotational speed is also monitored during the tests to find a correlation between the impeller rotational speed, input voltage of the motor and the flow rate through the system. Although the addition of solid particles alters the flow, their presence is not expected to alter significantly the flow rate and impeller rotational speed

as per preliminary tests indicating the particles effect on the pressure-drop through the tube section to be negligible within the range tested here.

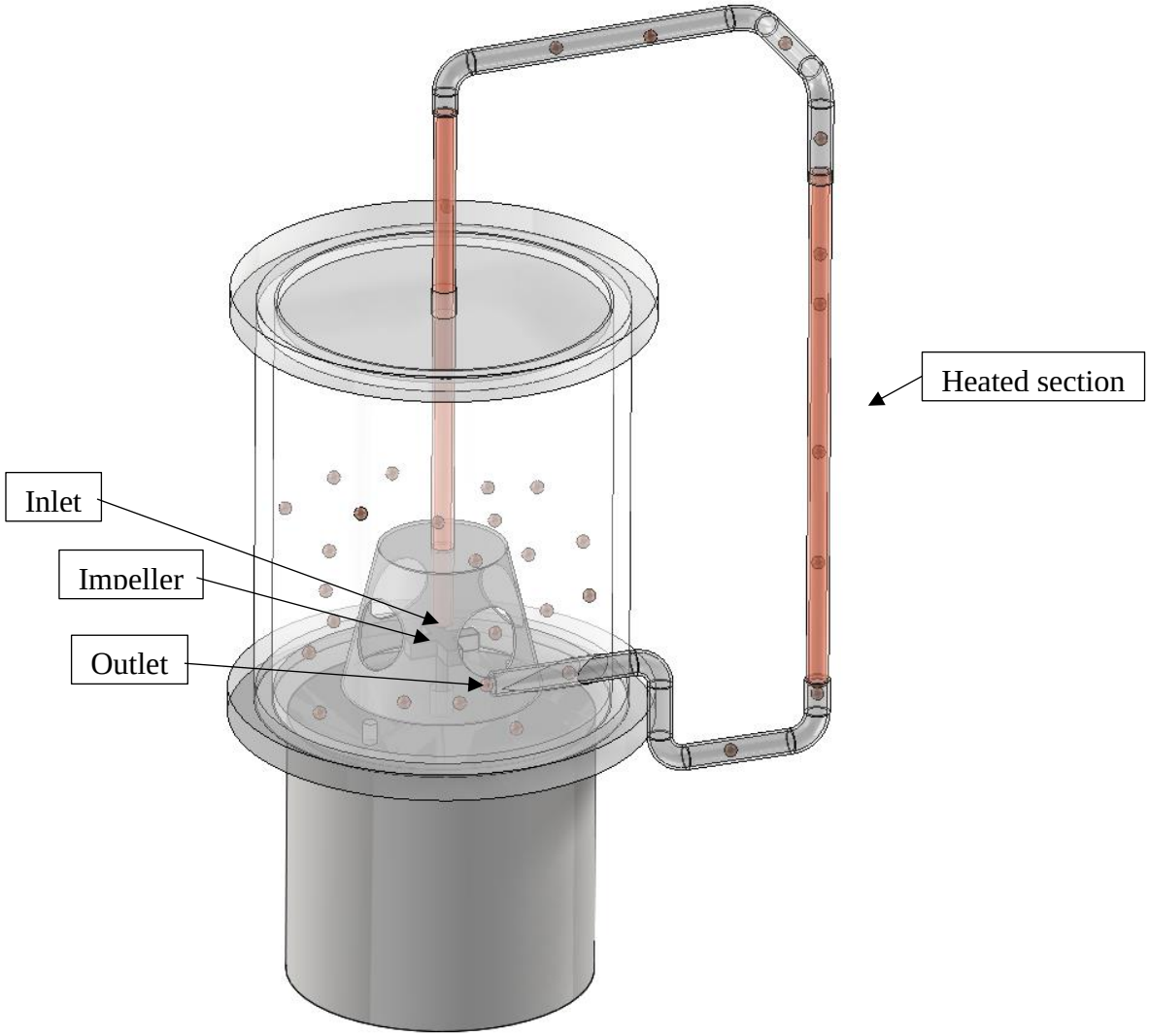

Fig. 4.3 Sketch of the circulation system including the vortex pump, heating section and circulating particles along with the flow

Because of the circulating character of the flow system, a cooling arrangement is designed and added to the system using a circulating bath and a helical copper tube placed in the circular reservoir to keep the temperature of the water being fed to the testing tube constant during the experiment. Figure 4.4 shows a sketch of the helical cooling tube and its position inside the reservoir. The cooling coil is placed close to the reservoir lateral surface, and the coil pitch and diameter selected as to minimize any possible trapping of solid particles within it. The helical tube is connected to the circulating bath device (not shown in the figure 4.4). For the experimental tests described here the circulating bath temperature was set as equal to the room (ambient) temperature.

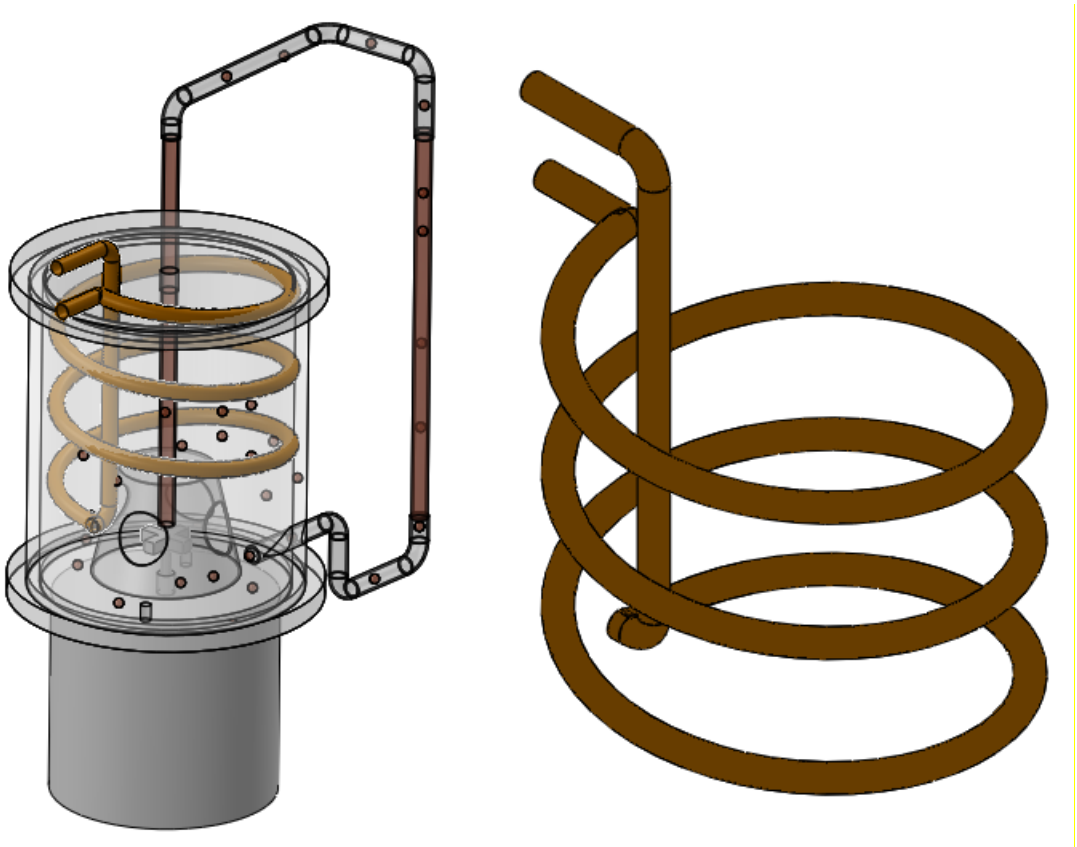

Fig. 4.4 Sketch of helical cooling tube and its position inside the reservoir

To control the number of the particles in the channel and the distance between them, a particle feeder mechanism was designed and built to selectively "feed" particles at the outlet of the reservoir with the minimal distortion in the vortex flow. This feeder is used to introduce a few particles in the steady circulation of the clear flow to investigate thermal boundary layer sweeping by them.

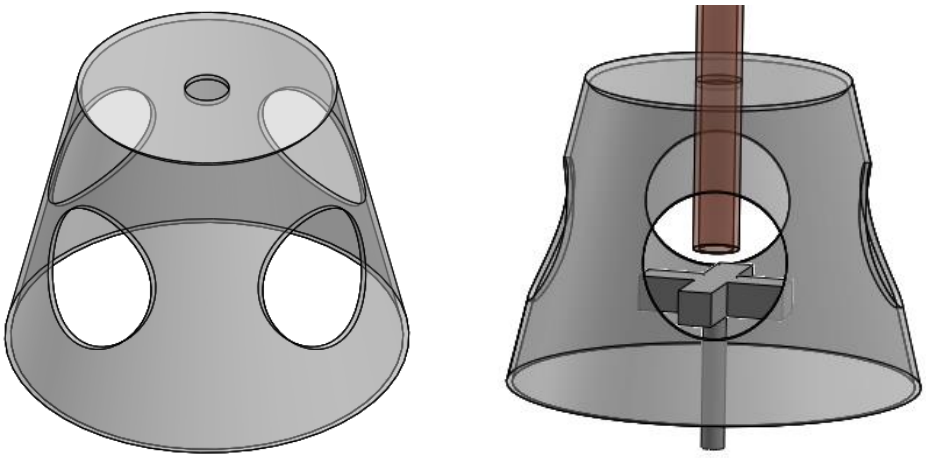

Fig. 4.5 Sketch of the cup shape part with and without the inlet pipe and impeller

The new impeller system design provides a very strong vortex, and by consequence a large pressure difference, inside the circular container. As a result, the new vortex pump is able to sustain a high flow rate, as much as 2 L/min through the flow system.

A few unexpected issues were inherent to the new vortex pump system. One was the need to manage the shape of the funnel generated by the vortex. For high rotational speed the funnel shape would become too sharp, with a free surface of water developing all the way to the impeller, causing air bubbles to mix with the flowing water decreasing the suction by the system significantly. A plastic cup-shape part was designed with several large holes on the side wall to cover the impeller region, as shown in figure 4.5. Notice

the tubing bringing the water-particles medium into the reservoir was placed inside this cup, right above the impeller.

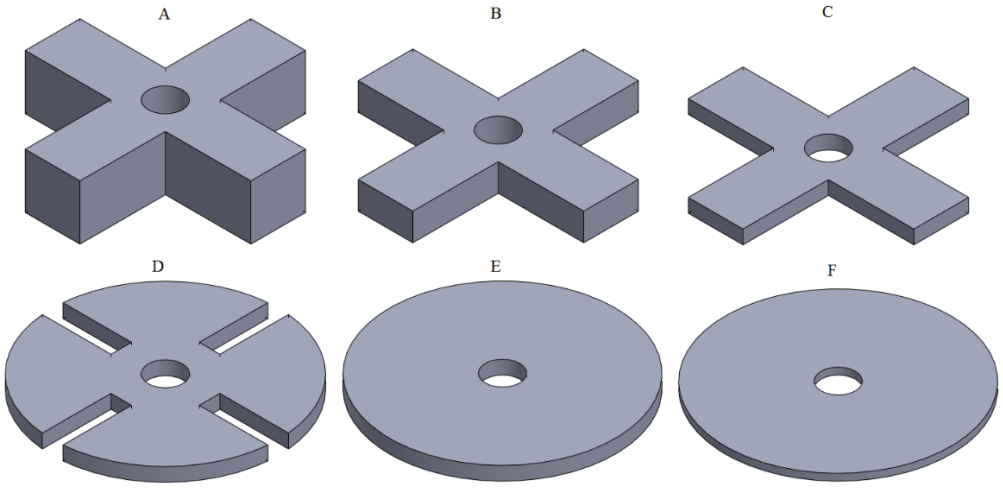

Fig. 4.6 Sketch of the several impellers used for the experiments

One of the important control parameters of the flow system is the flow rate. Low flow rates cause low particle speed inside the flow loop, including the heated channel. Low particle speeds provide long residence time of the particles inside the heated section of the flow system. Keep in mind low flow rates also lead to short developing length in the heated channel, particularly for laminar flow. The combination of long particle residence time and short developing length at low flow rate allows the effect of the individual particles in the heated tube to be more easily observed, particularly when particles flow in and out at a low rate. The objective to achieve stable low flow rate with particles in the test section led to the testing of several different impellers (figure 4.6). Propeller A, which is a flat four-blade impeller with 8 mm thickness and 33 mm diameter, for instance, yielded strong suction generating a circulation with high flow rate even with relatively slow impeller rotation. As the electric motor linked to the impeller was steadier at high rotational speed, as opposed to low speeds, propeller F, which is a thin disk with 1

mm thickness and 33 mm diameter, is the best for achieving steady low flowrates with high motor speed. In conclusion, the propellers in figure 4.6 were found to provide a very broad range of motor rotational speed and flow rate combinations suitable for the testing. It is worth mentioning the replacement of the AC motor in the current pump system by a servo or stepper motor would likely improve the stability of the vortex pump, resulting in steadier flow rates even at low motor speed.

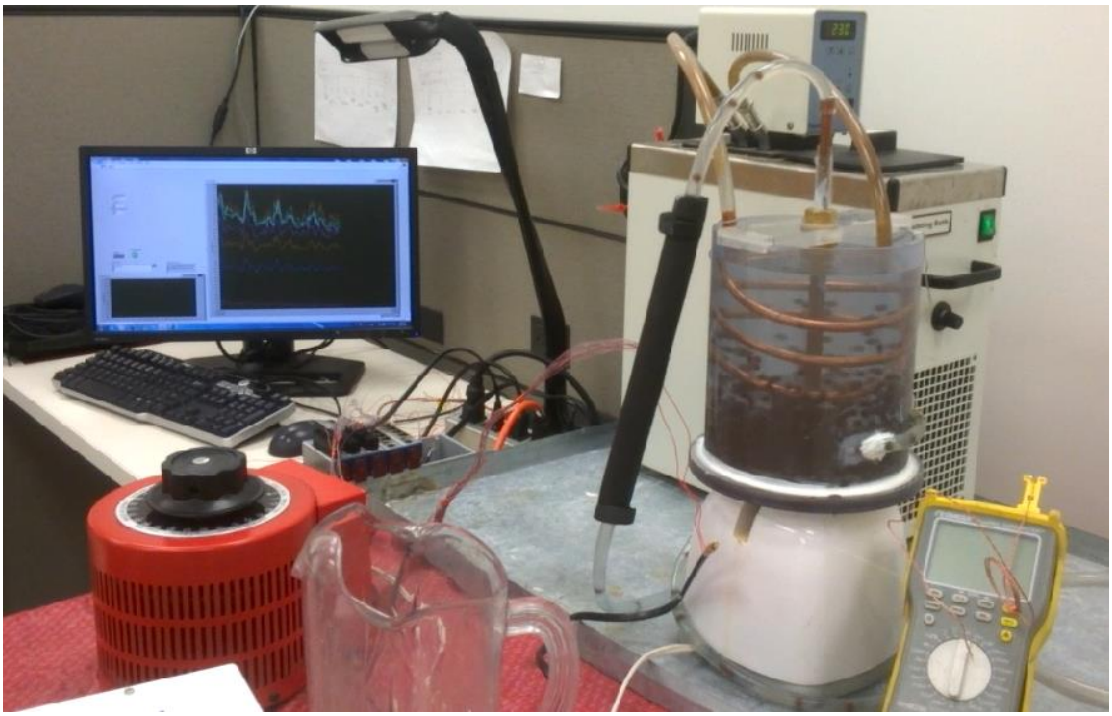

Fig. 4.7 Final version of the experimental setup, with particles running through it

Another important challenge in the experimental setup was sealing the entire system to avoid water and air leakages, particularly the motor-propeller connection at the base of the main fluid reservoir. Water leakage out of the system would reduce the mass flow rate of the fluid affecting the steady-state condition sought at the reservoir. Also, if the setup is not completely sealed, air could easily enter the loop causing bubbles to affect the heat transfer and the temperature distribution along the test section.

Figure 4.7 shows the final version of the experimental setup. Notice the test tube section is to the left of the circular reservoir. Also, visible in the figure is the chiller (behind the reservoir) used, connected to the cooling coil placed inside the reservoir.

4.4. Experimental procedure

To investigate the effect of the particles in the flow on the heat transfer efficiency inside the test section, two types of experimental procedures are considered: (1) the Local Effect Study (LES), which focuses on a single or only a few particles circulating in the test section; and, (2) the Overall Effect Study (OES), which investigates the effect of a large number of particles placed in the circulation system.

4.4.1. Local Effect Study

In the LES tests, the circulating system is set to run initially without particles at a certain flow rate while a pre-determined heat flux is applied to the testing section until a steady-state is reached. By then, either a single or a few particles are fed manually to the circulation system (past the outlet of the reservoir) to flow through the heated section. Using the particle feeder described previously, it is possible to control the number of particles and the distance between them while passing through the channel. This method provides results comparable to the simulation results presented in chapter 3.

Figure 4.8 presents the temperatures read by all nine thermocouples (T1-T9) placed along the heated section, under steady-state, with flow rate of $(2.2 \pm 0.1) \times 10^{-6}$ m^3/s (Re = 610) and maximum available heat flux equal to $9{,}000 \pm 100$ W/m^2. As expected for an isoflux channel surface case, the variation of the surface temperature T_s along the channel decreases gradually from channel inlet to the outlet, tending to a constant when the flow becomes fully developed (dT_s/dx = constant). One can observe,

from the temperature differences of figure 4.8, the flow is developing within most of the channel. Keep in mind by changing the flow rate the developing length and the range between temperatures T1 and T9 could be altered. The thermal entry length (for a fully developed momentum) flow in a circular pipe can be estimated as equal to 0.05×D×Re×Pr, which in the present configuration with D = 0.0063 m, Re = 610 and Pr = 4.82, for water at 35 ºC, turns out to be 0.93 m for the 0.26 m long channel.

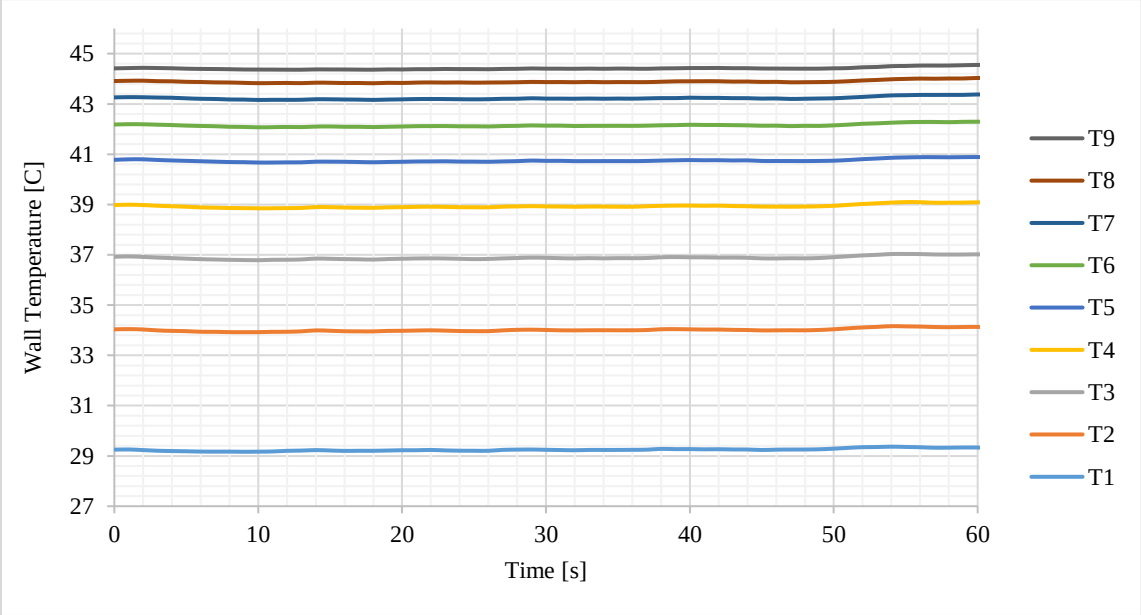

Fig. 4.8 Steady channel surface temperature recorded for 9 locations in the heated channel

Once the steady-state was determined, a single particle was then deployed in the flow. The resulting effect of this single particle flowing through the heated section of the flow system is observed in the surface temperatures shown in figure 4.9. Noticeable is the surface temperatures by all thermocouples show a slight increase followed by a significant decrease, of around 1.5 ºC (close to a 10 % reduction in delta-T when compared to the 16 ºC range between T1 and T9 under flow of water only), before recovering to the previous

steady values as the particle passes through the test section. It can be observed the surface temperature drop caused by the particle gradually increases until reaching a maximum drop at T9, the closest location to the channel outlet. This can be explained by considering the developing aspect of the flow (mentioned in conjunction with figure 4.8), which would indicate a thin boundary layer near the entrance section of the copper tube. As the particle flows downstream the tube, it encounters progressively thicker boundary layers, making its sweeping effect more pronounced along the channel. When crossing a location with thicker boundary layers, the particle induces a change in the fluid velocity distribution, increasing the velocity near the surface of the tube, which in turn should enhance the convective heat transfer process. For a uniform and constant heat flux at the surface, higher convection heat transfer coefficient is known to lead to a lower surface temperature, and this is exactly what is observed in figure 4.9.

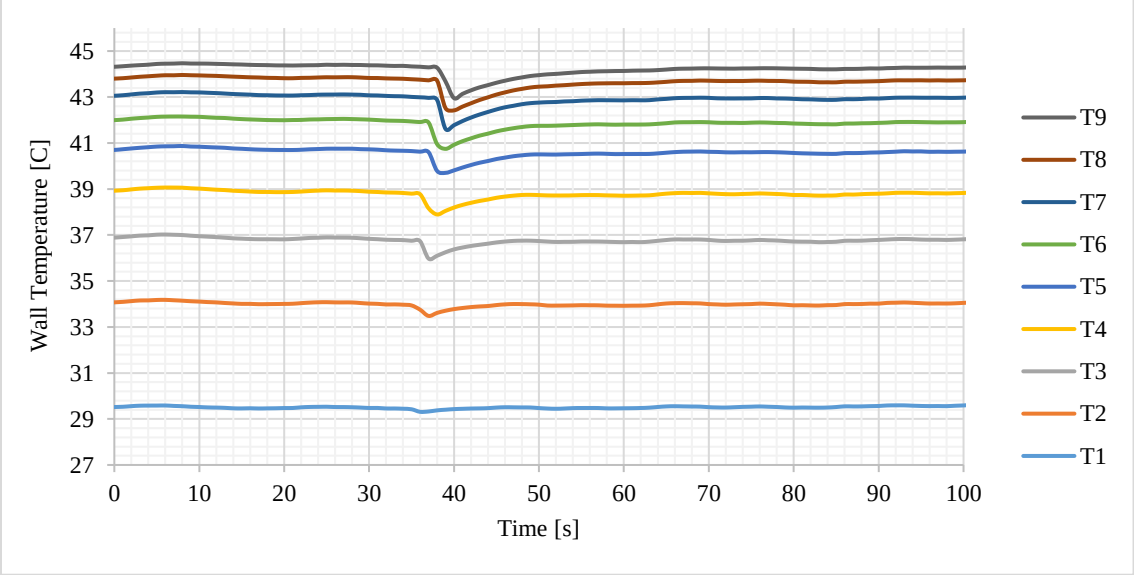

Fig. 4.9 The effect on tube surface temperature by a single particle

Another interesting observation from figure 4.9 is the evolution in time of the temperature effect of the particle at each thermocouple location. With a known distance between the thermocouple locations, it is possible to predict the particle velocity in the channel by dividing the distance between any two thermocouples and the difference in time of the temperature change in each thermocouple from figure 4.9. For instance, using T4 and T9, distant by 0.15 m, and estimating the time difference from figure 4.9 between the two effects as 2 s, the particle speed should be approximately 0.075 m/s.

Figure 4.10 shows a similar surface temperature pattern for the case of multiple particles flowing through the testing channel, one after the other. Observe the distance between said particles is large enough to allow for the flow to recover the steady surface temperature after the passing of each particle. The top graph in figure 4.10 shows the effect of passing two consecutive particles, while the bottom graph shows the effect of three consecutive particles through the channel. It worth mentioning for the experiments which their results are presented in this section, heat flux remained constant while the flow rate had slight changes from case to case.

Now, if the distance between consecutive particles is reduced, the particles will flow through the channel in a train-like pattern. In this case, their sweeping effect would eventually add up, with the flow not having enough time to re-establish the steady temperature in between particles passing. Consequently, the surface temperatures should continuously decrease in steps, as each particle flows through the thermocouple location pushes the temperature a little lower. This prediction is confirmed by the graphs shown in figure 4.11 where (from top to bottom) 2, 4 and 6 particles are set to flow through the channel maintaining a short distance from each other. Observe the maximum temperature

drop observed from these cases is around 3 ºC for 4 and 6 particles, which is about a 25% drop of the range between T1 and T9 (about 12 ºC).

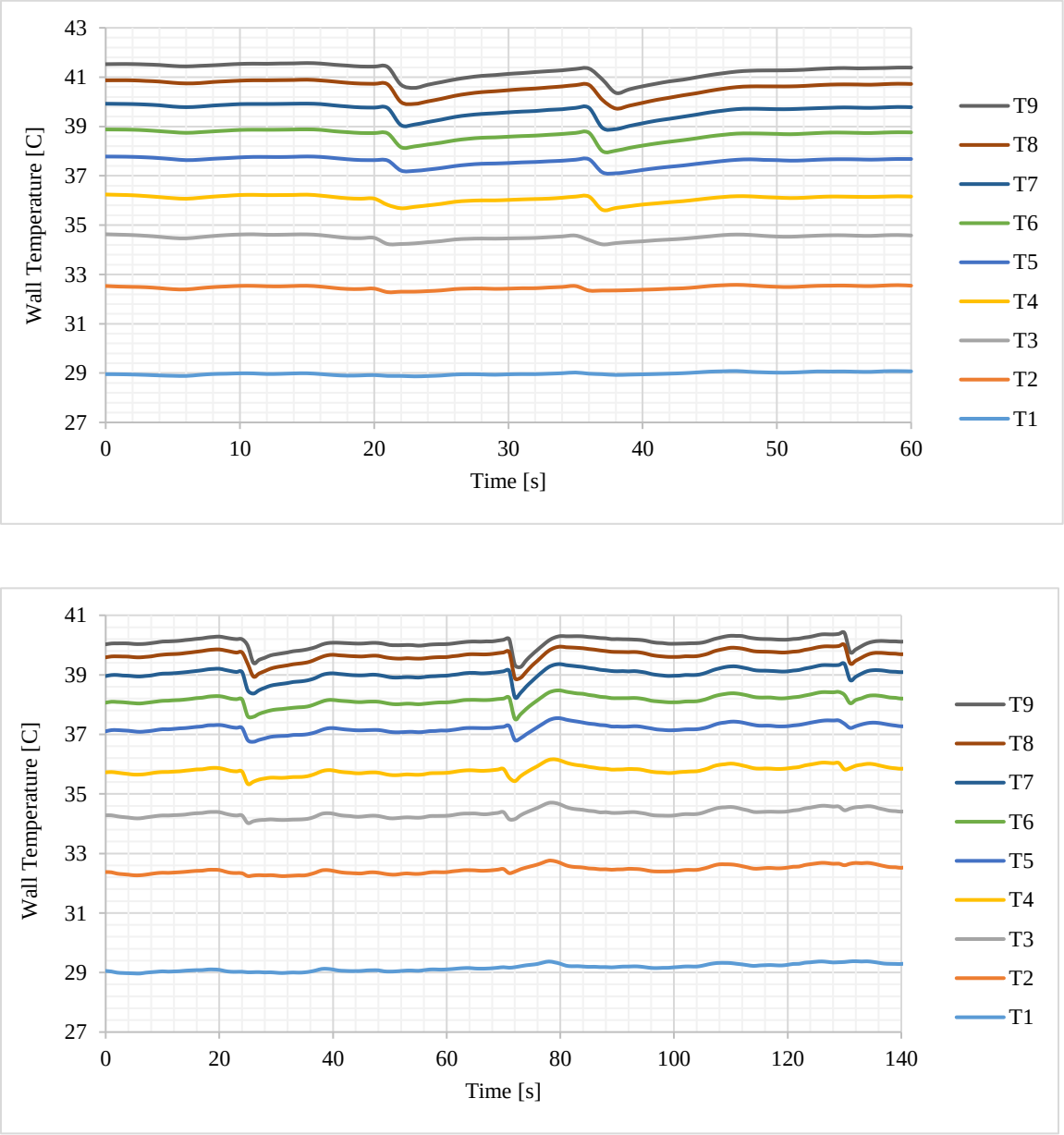

Fig. 4.10 The effect of passing two (upper plot) and three (lower plot) particles, with relatively large distances, through the channel on the wall temperatures

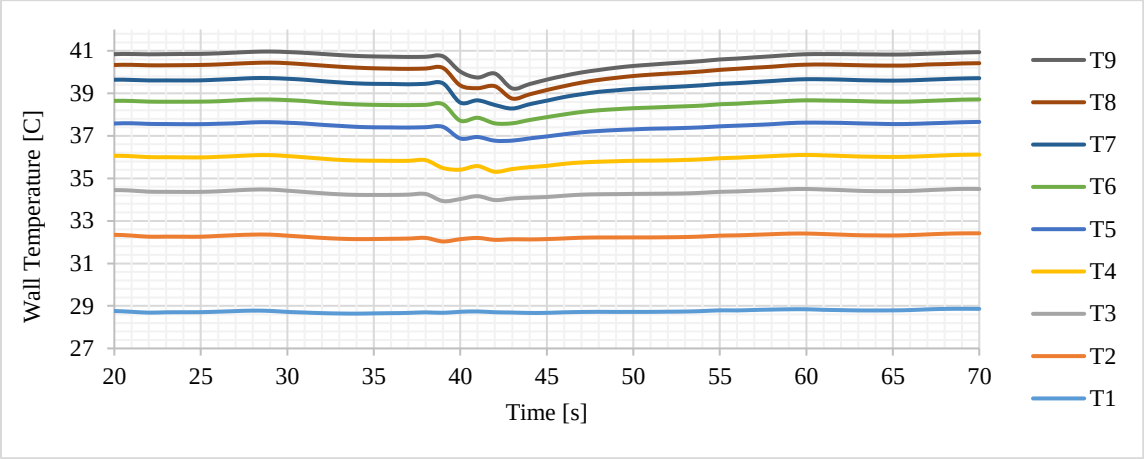

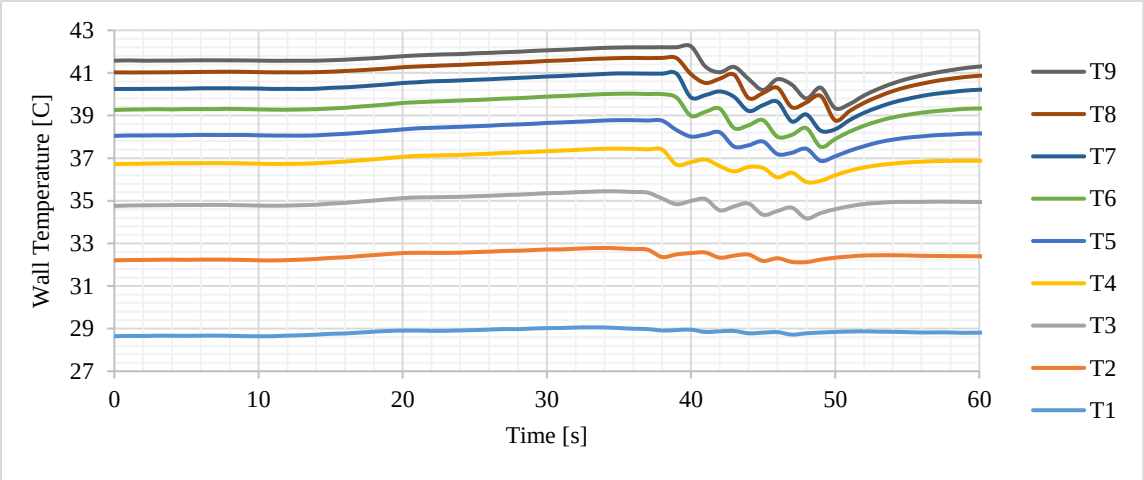

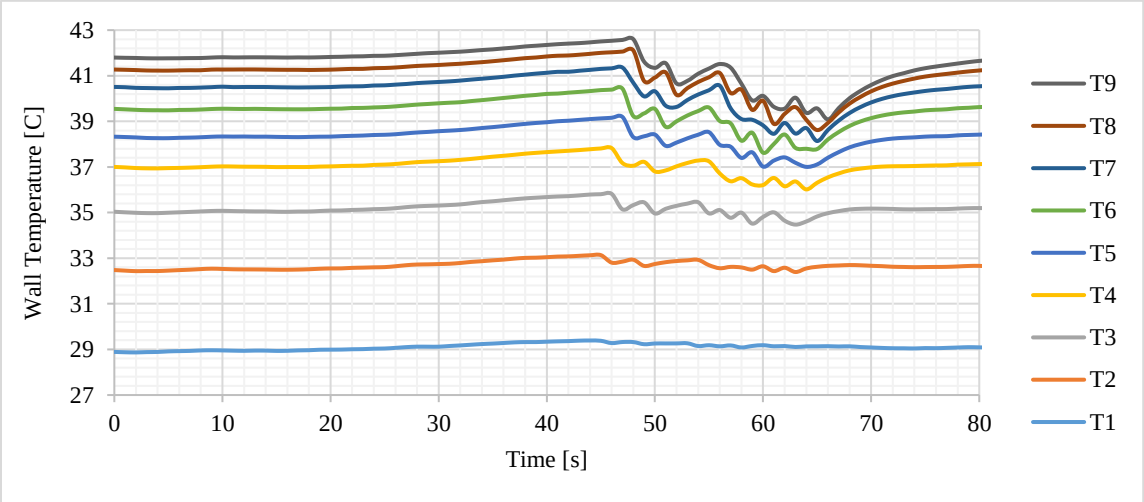

Fig. 4.11 The effect of passing two (upper plot), four (middle plot) and six (lower plot) particles, with relatively small distances, through the channel on the wall temperatures

Adding more than four particles in the train-like pattern makes it harder to have the particles equidistant from each other – see in figure 4.11 how the temperature evolution of T9, for instance, for six particles (bottom graph) is not as regular as the one shown for four particles (middle graph). The more particles added to the train-like flow, the more difficult it is to track their individual sweeping effects graphically.

Notwithstanding, the overall effect on T1 through T9 is observed to become ever more significant, as seen in figure 4.12. In this case, with several particles flowing through the channel, the maximum temperature drop observed is over 5 ºC, or 38% of the T1-T9 range (about 12 ºC).

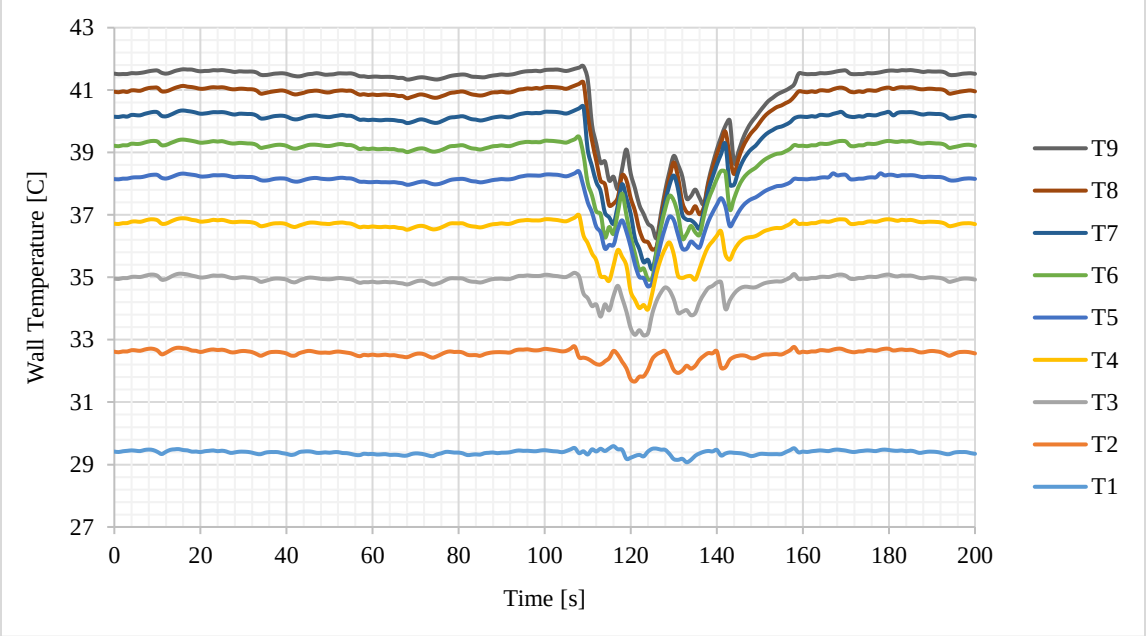

Fig. 4.12 Train of several particles with different distances

4.4.2. Overall Effect Study

The second procedure in the current experimental study is an observation of OES of many particles circulating with the fluid in the flow system. At first step, the clear (without particles) flow runs with a constant flow rate and heat flux, while water temperature in the reservoir and along the channel is monitored. Then, a specific number of particles is added to the flow system and allowed to circulate with the water, keeping the same heat flux, impeller rotational speed and water temperature inside the reservoir. Surface temperatures at the nine locations through the heated section are then recorded for comparison with the temperatures of the clear flow case.

The main difference between OES and LES is the control on the number and distance of particles as they flow through the heated tube. In LES case, a particle feeder is used to precisely put a single or few particles in the circulation system to pass through the heated section once. In the OES, on the other hand, a large number of particles is placed in the reservoir for circulation. During the experiment, particles randomly enter the channel exiting the reservoir, and flow through the heated section before returning to the reservoir. Although with less control of the flow of particles through the heated section, this alternative is perhaps more attuned with a potential simple design for a particulate heat exchanger.

Figure 4.13 presents temperature results for a case with similar conditions as the clear steady flow case shown in figure 4.8, with addition of 100 particles into the reservoir. It can be observed the average temperature of the locations near the outlet are reduced significantly, from 44 ºC under clear flow to about 42 ºC with the particles, as the particles pass through the heated section. This clearly shows the potential practical impact of the

sweeping convection effect. Also observable from figure 4.13 is the temperature recovery when the distance between particles is large enough.

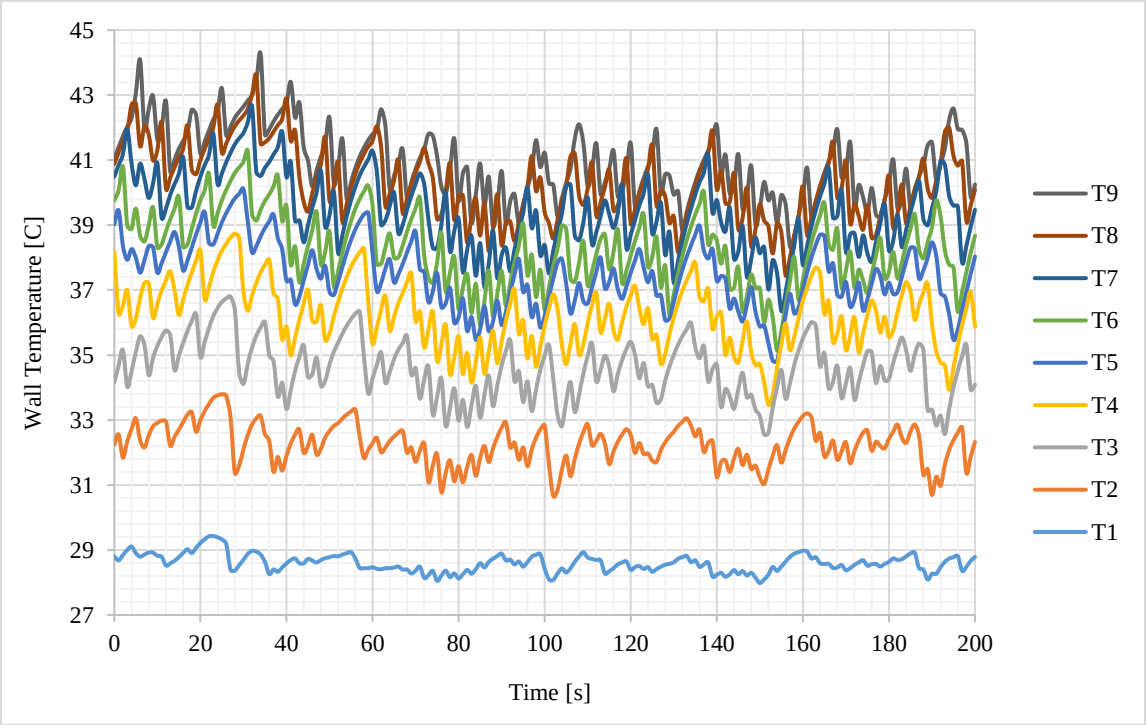

Fig. 4.13 Overall study case with 100 particles and low flow rate

Figure 4.14 shows a different OES experiment, with the same conditions and number of particles as those leading to figure 4.13 results, but with higher flow rate. In this case, it becomes even harder to observe the individual effects of each particle on T9 in comparison to the results for smaller flow rate shown in figure 4.13. As expect, higher flowrate reduces the range between T1 and T9, making it harder to verify the individual particle effects. As the flow reaches fully developed pattern and the temperature variation along the heated channel becomes smaller, the temperature variation of the thermocouples placed near the outlet of the channel (T5-T9) becomes less distinguishable.

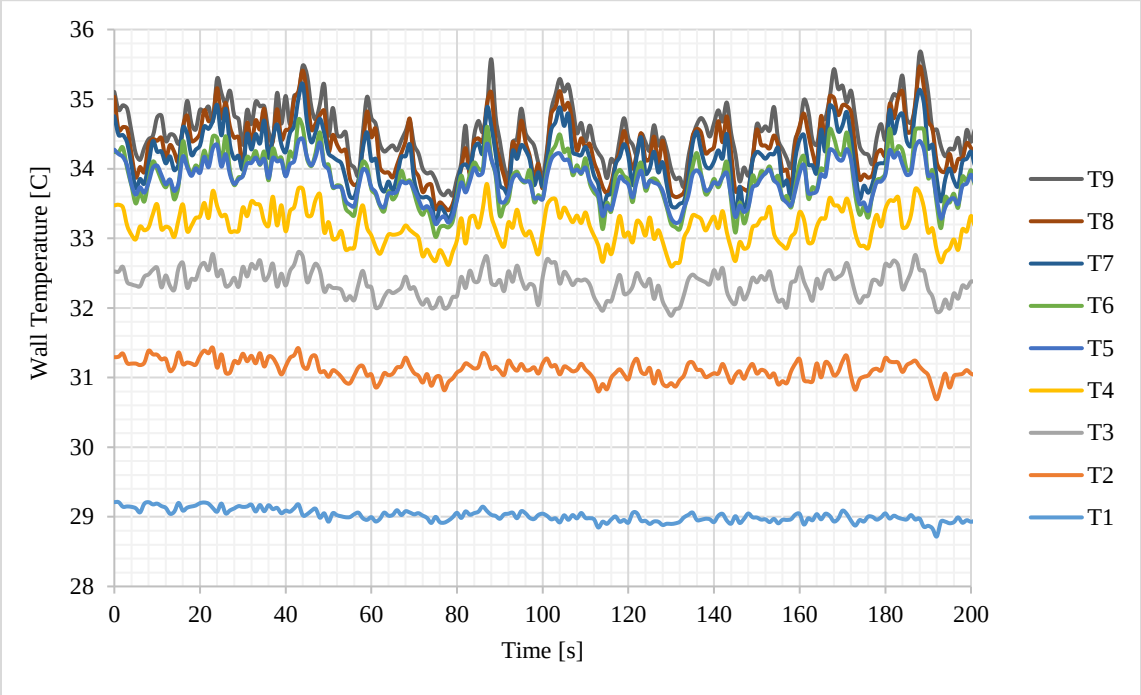

Fig. 4.14 Overall study case with 100 particles and high flow rate

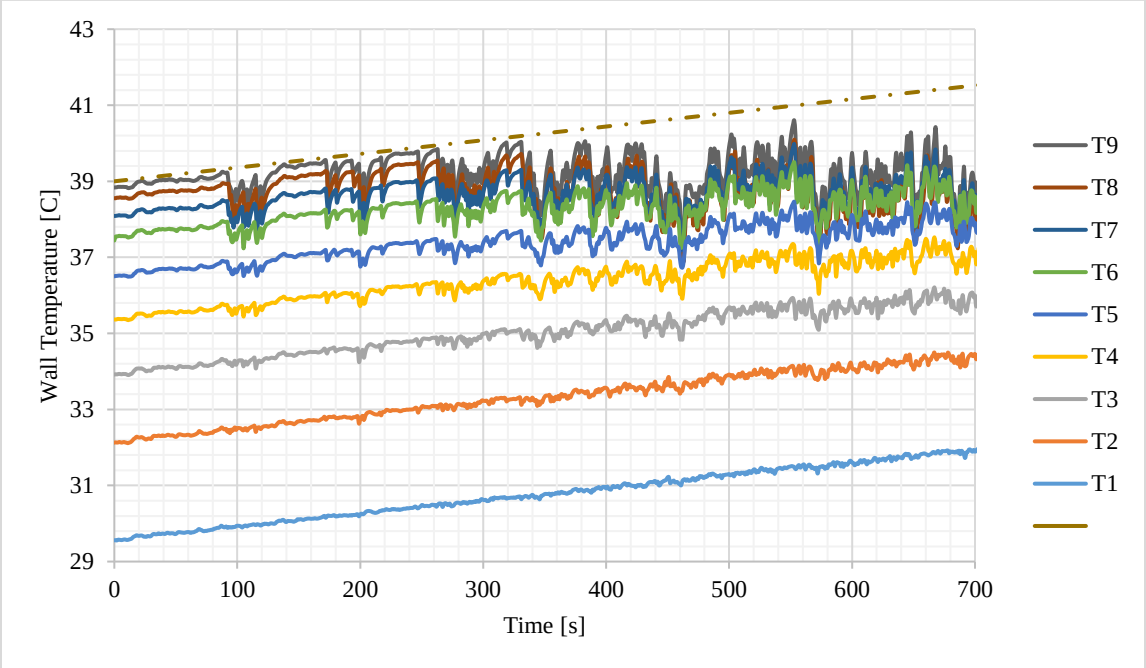

Fig. 4.15 Overall study case with 100 particles and high flow rate without cooling

Some OES experiments were performed without cooling, leading to a transient situation (the fluid temperature increases continuously in the system). Results, shown in figure 4.15, seem to indicate the rising the temperature of the system in time, in the absence of cooling, yields an even greater sweeping effect, particularly near the outlet of the heated channel. Notice the dashed line in figure 4.15 above T9, which is parallel to T1, represents approximately the expected temperature trend for T9 in the absence of particles. The result is about 4 ºC of temperature range difference by the particles (T1-T9 of about 5 ºC with particles versus about 9 ºC without particles).

4.5. Conclusions

In this chapter a new and improved experimental setup for a particulate flow circulation system was introduced, not only to provide a new tool to verify numerical simulations but also to study the possibility and applicability of sweeping convection. The new vortex pump system, flow container and heated channel resolved several issues observed with a previous design. The new design represents an evolution toward learning more about sweeping convection and making it more practical. The results of the conducted experimental tests support the qualitative findings of the numerical simulations, and provide venues for expanding this study in several directions and scales.

A comparison between the experimental results and the numerical simulation results presented in Chapter 3 require much care due to fundamental differences between numerical and experimental approaches and limitations in the experimental equipment. The experimental results are generated by recorded data from sensors placed in specific locations of the apparatus (e.g. thermocouples along the heated channel surface). The

numerical simulation results, on the other hand, are available at each node of the computational domain, providing a much greater definition. It is much easier to find data (e.g. pressure, temperature, velocity, etc.) to help understand the physics of the problem and study the results. This is an intrinsic advantage of numerical simulations.

There are some issues that can be addressed in yet a new design of the flow system. The current motor driving the impeller, for instance, could be replaced with a powerful stepper or servo motor to provide a more constant rotational speed, specifically when low flow rate is needed. A contactless flow meter would provide the ability to measure flow rates in both clear and particle flows more easily as well. Finally, different sizes and types of particles could be tested, including flexible particles, to gather their effects in the flow system.

Chapter 5

CONCLUSIONS AND FUTURE RESEARCH

5.1. Conclusions

The overall objective of the present research was to study numerically and experimentally a specific type of convective heat transfer due to a particle flow in narrow channels where the diameter of the particles is very close to the channel diameter or width. From a heat transfer point-of-view, the tight fitting between particles and the channel surfaces sets the particles acting like pistons as they flow downstream with the fluid, disrupting the velocity and temperature profiles that characterize the developed boundary layers in a heated (or cooled) straight, and long enough, channel. The sweeping of the boundary layers was expected to yield higher heat transfer coefficients, as compared to the heat transfer coefficient achieved when particles are not present.

All numerical study and simulations were presented in chapter 3 in the form of separate case studies with the focus on heat transfer improvement achieved in particulate flow over the clear (of particles) flow under the same flow conditions. The strategy behind the numerical simulation part of this research was to begin with the simplest configuration possible, develop the corresponding mathematical model, overcome numerical difficulties and obtain reliable simulations to then pursue more complicated configurations. This

strategy helped to progressively build a better understanding of the physical problem by increasing the level of detailed information obtained through the simulations, particularly on velocity and temperature fields. Each advanced configuration study was developed considering the results from prior configuration studies, by adding new features and/or removing simplifying assumptions from it. All case results reported here are valid for Newtonian fluids with constant and uniform properties, negligible body force and no viscous dissipation, solid and impermeable spherical particles with constant and uniform properties and negligible buoyancy in the fluid.

The first case considered was presented in section 3.2, where the start-up (where particle and fluid start moving from rest) sweeping convection effects of a single adiabatic particle in a straight isothermal channel with uniform inlet velocity and temperature conditions was introduced and discussed. Isotherms and surface heat flux were used primarily to identify the sweeping effects of the particle. Some important results were observed, such as the small effect of the particle when the particle diameter is small in comparison to the channel size, even though the particle moves at a higher speed than when the particle diameter is large. This is simply a result of the particle not being able to reach the region near the channel surfaces where heat transfer is initially taking place; a very small particle, flowing at the center of the channel, is less likely to reach this region. The effect of the entrance length on the sweeping convection was then found to be important as heat transfer improvement is negligible in the region of flow developing when the boundary layers are thin and restricted to a region close to the channel surfaces, far from the particle. This effect was more pronounced for higher inlet velocities because of the longer entrance length they yield. By the same token, the imposing of uniform

velocity inlet condition hinders the sweeping effect as compared to a fully developed inlet velocity profile when the momentum boundary layer is already developed. This hindrance was investigated further in subsequent simulations by replacing the uniform inlet velocity profile with a fully developed one. In summary, the first case indicated there should be a balance between the flowing speed of the particle and the speed of thermal boundary layer development in the channel for sweeping convection to be most effective. Another potential issue, anticipated by this initial case, was the need for an appropriate tool to quantitatively compare different cases when the channel surfaces are isoflux, as opposed to isothermal. Although isothermal contour plots, when seen near the channel surfaces, can provide a glance on the heat transfer effect of a particulate flow over the clear flow in the isothermal case, they are no longer so effective in the isoflux surface case. Also, when isothermal surface condition is considered, as in the initial case study, the resulting heat flux through the channel surfaces is an appropriate parameter to quantitatively compare the heat transfer performance of different cases. Of course, this is no longer the case when uniform surface heat flux is considered. Although the resulting surface temperature along the channel could be used for comparison, the integration of surface temperature along the channel does not provide a useful physical quantity, as the heat flux does in the isothermal case.

In section 3.3, results of flow of water along a straight isoflux heated channel with and without a single adiabatic spherical particle flowing with the fluid. This section focused on using the large particle of case 3.2. The results revealed the particle effect on the convection process to be localized and yet very significant, with the surface-averaged Nusselt number (introduced for quantifying the sweeping heat transfer effect of the isoflux

case) increased by up to 9%, and with negligible pressure drop effect across the channel. The results also indicated enhanced heat transfer upstream the particle location and hindered heat transfer downstream of the particle location, as compared to the results obtained for the clear fluid case. The net effect, however, is a considerable gain in heat transfer efficiency by the sweeping effect. Although the effect is limited to a flow region around the particle, it is nevertheless substantial considering only one particle is present in the channel at all times.

Observe the Moving Mesh numerical method was used in both, sections 3.2 and 3.3 cases. This method re-meshes the domain every time the particle changes location along the channel by stretching or compressing the existing cells, a process likely to affect the result quality. Results from sections 3.4 and 3.5 were obtained using the Immersed Solid numerical method as an alternative to the Moving Mesh method. For not requiring the remeshing of the domain during the simulation, the Immersed Solid method also expedites the numerical simulation. A potential drawback of this new method is when the particle is nonadiabatic, in which case an extra equation for heat transfer through the particle has to be resolved.

The case of section 3.4 returns to the isothermal surface configuration case of section 3.2, but now with fully developed inlet velocity and two (instead of only one) adiabatic particles in the channel. This case aimed at determining not only the effects of having two particles in the channel, but also the effect of changing the initial distance between the two particles on the sweeping of the thermal boundary layers that forms along the channel surfaces as the fluid and particles move. A Nusselt-efficiency parameter, η_{Nu}, introduced and used in section 3.3 for measuring the sweeping effect in relation to

convection by a clear (of particles) fluid, confirmed here for the two-particle cases the large distance between the particles yields more efficient heat transfer. This distancing test indicates how particles can detrimentally affect each other when flowing too close along the channel. This effect, however, is seen to flatten out when the distance between the particles increases past 6D for the studied configuration. The results also showed that the particle location within the channel at the start up has no effect on the heat transfer, as long as the distance between the particles remains the same throughout the channel.

All cases in sections 3.2, 3.3 and 3.4 simulated a startup process in which initially the particle(s) was (were) at rest within a fluid field with zero velocity and uniform temperature. In these cases, the thermal boundary layer starts to grow as the flow begins, and the particle(s) may sweeps this growing layer depending on its velocity and position in the channel. While the study of startup processes has its own merit, it was necessary to consider another scenario to address the steady state conditions existing often in many thermal systems, such as heat exchangers. These conditions are more akin of practical experimental condition as well.

In section 3.5, a new case study was presented with geometry and boundary conditions different from those used in the three previous configurations. The changes included an upstream and a downstream channel section with adiabatic surfaces, bounding the uniformly heated channel section, to allow the observation of the particles entering and leaving the heated section and to alleviate the effect on imposed inlet (fully developed velocity and uniform temperature) and outlet (zero gradient) boundary conditions in the simulating results of the heating process. Also, the initial condition for the simulations was the steady solution for velocity and temperature distributions in the entire channel,

without particles. This initial condition is aligned with a situation in which fluid flows steadily in a heated channel and then a particle (or more than one) comes and flows through the heated section with the fluid. Finally, this case includes the investigation of up to three particles flowing concurrently through the channel. The results indicated an enhancement on the average channel Nusselt number of up to 60% at a specific time in the process and up to 35% when time averaged during the entire process. More specifically, the three-particle case with U_{ave} of 20 mm/s (Re = 282, Pr = 6.13), is 35 % more efficient overall than a steady clear fluid case under the same conditions, which is a significant improvement in heat transfer efficiency.

The sweeping particle effect is now known to be centered in the gap, a region between the particle and the channel surfaces; after all, the "sweeping" pertains to the process of moving away the boundary layers that developed along the channel surfaces. Because convection is intrinsically a flow (motion) induced phenomenon, a decision was made to investigate more closely the velocity profile in particle flow, which was discussed in section 3.6. in it, a sample of the results show the particle speed, or the maximum speed at the gap, can be 2.43 times greater than the fluid speed at the same location if the particle were not there. This is an example of the quantitative effect of the particle flowing with the fluid. The increase in fluid speed at the gap caused by the particle not only leads to an increase in the local heat transfer coefficient, but also to an increase in the local friction coefficient due to the increase in the velocity gradient at the channel surface. This increase, however, for being localized at the gap, does not affect much the total pressure drop along the channel, as shown previously by the numerical results. This aspect is key to the sweeping convection: convection enhancement at a minimum cost. Also in section

3.6, a model was developed and presented, leading to an analytical prediction of the fluid velocity at the gap and for the particle speed. This analytical predictive tool turned out to be essential not only for better understanding the sweeping effect of the particle but also for gaining confidence on the numerical results, as the predicted particle speed matches well (within 4 %) the numerical results of a considered test case.

Section 3.7 shows a procedure to obtain a nondimensional model based on the configurations discussed in section 3.2, including the non-dimensional form of the governing equations, initial and boundary conditions. This effort also shows the procedure for solving the non-dimensional equations using the same code used for the dimensional equations. The non-dimensional results were compared to the dimensional results, showing their equivalency. Also included in this section is an investigation into the effect of the fluid Prandtl number on sweeping convection, indicating the limitations of sweeping convection induced by low Pr, particularly when isothermal channel surfaces are considered.

In Chapter 4 a new and improved experimental setup for a particulate flow circulation system was described in detail, not only to provide a new tool to verify numerical simulations but also to study the possibility and applicability of sweeping convection. A new vortex pump system, flow container and heated channel resolved several issues observed with previous designs developed by our research group. The new design represents an evolution toward learning more about sweeping convection and making it more practical. The results of the conducted experimental tests support the qualitative findings of the numerical simulations, and provide venues for expanding this study in several directions and scales. It is worth noting a direct comparison between the

experimental results and the numerical simulation results presented in Chapter 3 require much care due to fundamental differences between numerical and experimental approaches and limitations in the experimental equipment.

5.2. Future research

This study has provided a significant development on the sweeping convection idea in both, numerical simulation and experimental study. There are several opportunities to extend this study further in both directions.

5.2.1. Future research in numerical simulations

Chapter 3 reports on the evolution of the mathematical modeling and numerical simulations, beginning with a simple configuration (section 3.2), by considering different scenarios and applying more realistic conditions. This approach can be extended further toward a model and simulation capable to mimic particles entering and exiting the channel in sequence with any speed and any distance between them. The particle distances can be controlled by the time they enter the channel, being either a fixed value (for a constant distance between all particles) or a different value for varying distances. This can help leading the simulation closer to a real experimental setup specially by applying a random time difference between entering particles. This flexibility would also allow consideration pertaining to the control of a system using sweeping convection to achieve and maintain a certain channel surface temperature, or heat flux, of a device being cooled down or heated up by the convection process. Another extension would be the consideration of 3D effects, for instance using a two-way solid-fluid interaction model. This would also allow perhaps the modeling of flexible particles, which can become useful under certain flow conditions.

The relation between all parameters (e.g. particle material, shape and size, gap size, distance between particles, flow conditions) and average Nusselt number, as an indicator for heat transfer efficiency, should be studied further to finally provide an analytical model to optimize these parameters for an existing problem. To this end, the non-dimensional model effort can be a starting point in helping to investigate the effect of a vast range of fluid material and flow conditions in sweeping convection.

Considering phase change material inside the particles is not a new idea but still can be applied by extending the current model. Also, while the model was developed for heat transfer improvement, it may also be used to study mass transfer of gases in liquids (e.g. oxygen and drug delivery as well as carbon dioxide and waste removal from the blood in the capillary system) with some adjustments.

5.2.2. Future research on experimental setup

Designing and building a novel particulate system during this study was a challenge and a very successful effort in allowing the practical examination of sweeping convection. The system was also invaluable for confirming some of the fundamental observations from the numerical simulation results. As mentioned in chapter 4, the experimental approach was not without intricacies and a few issues could be addressed in yet a new design of the flow system. The current motor driving the impeller, for instance, could be replaced with a powerful stepper or servo motor to provide a more constant rotational speed, specifically when low flow rate is needed. A contactless flow meter would provide the ability to measure flow rates in both, clear and particle flows more easily as well. Different sizes and types of particles could be tested, including flexible

particles, to gather their effects in the flow system. The experimental study may be extended for micro channels by scaling down the circulation system. This should be investigated, as per the results gathered so far sweeping convection shows tremendous promise in improving laminar convection flows.

BIBLIOGRAPHIES

[1] Ali Beskok, Mehrdad Raisee, Bayram Celik, Bedri Yagiz, Mohsen Cheraghi "Heat transfer enhancement in a straight channel via a rotationally oscillating adiabatic cylinder" International Journal of Heat and Mass Transfer 58 (2012) 61–69

[2] Julian Marschewski, Raphael Brechbühler, Stefan Jung, Patrick Ruch, Bruno Michel, Dimos Poulikakos "Significant heat transfer enhancement in microchannels with herringbone-inspired microstructures" International Journal of Heat and Mass Transfer 95 (2016) 755–764

[3] Mark E Steinke, Satish G. Kandlikar "Review of single-phase heat transfer enhancement techniques for application in microchannels, mini-channels and microdevices" International Journal of Heat and Technology 22.2 (2004): 3-11

[4] Image from www.slideshare.net Author: the law of science

[5] Fatemeh Hassanipour, José L. Lage "Numerical simulation of capillary convection with encapsulated phase-change particles" Numerical Heat Transfer, Part A: Applications 55.10 (2009): 893-905

[6] Deniz Ulusarslan, Ismail Teke "An experimental investigation of the capsule velocity, concentration rate and the spacing between the capsules for spherical capsule train flow in a horizontal circular pipe" Powder technology 159.1 (2005): 27-34

[7] Deniz Ulusarslan, Ismail Teke "An experimental determination of pressure drops in the flow of low density spherical capsule train inside horizontal pipes" Experimental thermal and fluid science 30.3 (2006): 233-241

[8] Ismail Teke, Deniz Ulusarslan "Mathematical expression of pressure gradient in the flow of spherical capsules less dense than water" International journal of multiphase flow 33.6 (2007): 658-674

[9] Ali Merrikh, José L. Lage "Effect of Blood Flow on Gas Transport in a Pulmonary Capillary" ASME. *J Biomech Eng.* 2004;127(3):432-439

[10] A.E.P. Veldman "Boundary layers in fluid dynamics" Lecture Notes in Applied Mathematics, University of Groningen (2011)

[11] Ludwig Prandtl "Über Flüssigkeitsbewegung bei sehr kleiner Reibung" Verhandlungen des Dritten Internationalen Mathematiker-Kongresses in Heidelberg 1904, A. Krazer, ed., Teubner, Leipzig, 484–491

[12] Created using Microsoft Powerpoint, previously published: Weyburne, David (2018). "New thickness and shape parameters for describing the thermal boundary layer," arXiv:1704.01120 [physics.flu-dyn]

[13] Frank P. Incropera, David P. DeWitt, Theodore L. Bergman, Adrienne S. Lavine, "Introduction to Heat Transfer" 5th Ed. 2007

[14] https://www.wikizero.com/en/Heat_convection

[15] Adrian Bejan "Convection heat transfer" Hoboken, NJ: John Wiley & Sons, (2013)

[16] Reza M Sadri "Channel entrance flow" University of Western Ontario, 1999

[17] Yunus Cengel, Afshin Ghajar "Heat and mass transfer: Fundamentals & applications" New York: McGraw-Hill, (2015)

[18] Michelle E. Staben, Alexander Z. Zinchenko, Robert H. Davis "Motion of a particle between two parallel plane walls in low-Reynolds- umber Poiseuille flow" Physics of Fluids 15, 1711 (2003)

[19] S. Bhattacharya, J. Bławzdziewicz, E. Wajnryb "Hydrodynamic interactions of spherical particles in Poiseuille flow between two parallel walls" Physics of Fluids (1994-present) 18, 053301 (2006)

[20] James W. Swan and John F. Brady "Particle motion between parallel walls: Hydrodynamics and simulation" Phys. Fluids 22, 103301 (2010)

[21] R. B. Jones "Spherical particle in Poiseuille flow between planar walls" journal of chemical physics volume 121(1), 2004

[22] James W. Swan and John F. Brady "Simulation of hydrodynamically interacting particles near a no-slip boundary" Physics of Fluids 19, 113306 (2007)

[23] E. H. Dowell, K. C. Hall "Modeling of fluid-structure interaction" Annual review of fluid mechanics, 33(1), 445-490 (2001)

[24] Patrick Le Tallec, J. Mouro "Fluid structure interaction with large structural displacements. Computer methods in applied mechanics and engineering" 190 (24-25), 3039-3067, (2001)

[25] Ansys® CFX, Release 16.0, Help System, ANSYS CFX-Solver Modeling Guide, ANSYS, In

[26] Fatemeh Hassanipour, José L. Lage "Preliminary experimental study of a bio-inspired, phase-change particle capillary heat exchanger" International Journal of Heat and Mass Transfer, Volume 53, Issues 15–16, (2010) 3300-3307